Evaluating the effects of air pollution derived toxic nanoparticles on astrocyte reactivity and neurodegeneration

Beatrice Villani

40525463 / 40016574

June 2023

Supervisory Team:
Dr Fiona Kerr (Director of Studies)
Prof Gary R. Hutchison (Second Supervisor)
Dr Amy Poole (Second Supervisor)
Dr Eva Malone (Advisor)

This project was funded by the "**Derek and Maureen Moss Scholarship 2021**" and by the "**Edinburgh Napier Strategic Fund 2021/2022**".

"A thesis submitted in partial fulfilment of the requirements of Edinburgh Napier University, for the award of Master by Research".

Abstract

Particulate Matter is a toxicologically relevant air pollution component that has been shown to damage the cardiopulmonary system. Emission of ultrafine particulate matter – the most toxic type – is not regulated around the globe. Recent evidence from epidemiological studies, supported by a recent UK government COMEAP advisory report, states that exposure to these particles increases risk of dementia and cognitive decline. However, the variability in the design of public health studies, so-far, prevents confirmation of a causal link between specific types of air pollution associated particles and neurodegeneration, and few empirical analyses have assessed the effects of specific particles on brain derived cells. This research aimed to investigate the effects of ultrafine carbon black (UFCB), a surrogate air pollution derived nanoparticle, on primary cortical astrocyte reactivity and potential for subsequent neurotoxic or neuroprotective functions. Viability of primary human cortical astrocytes was measured, using the WST-1 assay, following exposure across a toxicologically relevant UFCB nanoparticle concentration range. qRT-PCR was used to investigate astrocyte reactivity, by via GFAP expression, and polarisation, by measuring expression of astrocyte genes linked to neurotoxic A1 (LCN2 and GBP2) or neuroprotective A2 (S100A10) states. Although not statistically significant, a trend to increased S100A10 expression, but no change in GBP2 or LCN2, was observed after UFCB exposure. Attempts were also made to measure levels of the astrocyte-specific pro-inflammatory marker LCN2 and the anti-inflammatory marker IL-6 in response to lethal and sub-lethal doses of UFCB. Lcn2 levels were below the limit of detection, but low levels of IL6 were measured in astrocyte conditioned media and were mainly unchanged by UFCB exposure. To further investigate the effects of UFCB exposure on neuronal toxicity, differentiated NT2 neuronal-like cells were treated with either UFCB-stimulated astrocyte conditioned media or direct UFCB and viability measured. Direct exposure to lethal and sub-lethal UFCB doses resulted to be toxic to differentiated NT2 neuronal-like cells, whereas conditioned media lead to negligible effects. These preliminary results indicate that acute exposure to UFCB leads to astrocytes adopting a more **neuroprotective** role and morphology, and that any toxic neuro-inflammatory responses to UFCB are not clearly astrocyte-mediated. Further research is required to confirm these findings.

Thesis Contents

1. Introduction 5

1.1 An Introduction to Air Pollution, Particulate Matter and Health 5

1.2 Air Pollution Explained 6

1.3 Global impact of Particulate Matter exposure: a brief statistical report 7

1.4 Particulate Matter and Mechanisms of Molecular and Cellular Pathophysiology 11

1.5 Particulate Matter and CNS studies 15

1.6 Glial cells at a glance 17

1.7 Astrocyte Reactivity and Neurodegeneration 19

1.8 Air pollution-derived Particulate Matter and Neuroinflammation 23

1.9 Ultrafine Carbon Black: a TRAP-DEP surrogate of air pollution nanoparticles for toxicological modelling 26

1.10 Hypotheses, Aims and Objectives: 29

2. Material and Methods 31

2.1 Cell Culture and Maintenance 31

2.2 Primary Human Cortical Astrocytes 31

2.2.1 Coating solution 31

2.2.2 Culture and maintenance of primary human cortical astrocytes 31

2.3 NTERA-2 cells 33

2.4 NT2 neuronal like cells differentiation 33

2.5 Ultrafine Carbon Black preparation 34

2.5.1 UFCB weighing and suspension 34

2.5.2 UFCB sizing 34

2.6 Cell treatments 35

2.7 Cell Viability (WST-1) Assay 35

2.8 Gene expression analysis 36

2.8.1 RNA extraction 36

2.8.2 Assessment of RNA quality 37

2.8.3 Reverse transcription 37

2.8.4 Primer design and validation 37

2.8.5 qPCR 39

2.9 ELISA 40

2.10 Immunofluorescence 40

2.11 Statistical Analysis 41

3. Results 42

3.1 Assessing UFCB physiochemical properties in different dispersants using Dynamic Light Scattering 42

3.2 Visualising surrogate UFCB nanoparticles in cell culture 44

3.3 Optimising conditions for measurement of cell viability using Human Primary Cortical Astrocytes 46

3.4 Assessing cytotoxicity of surrogate UFCB nanoparticles on Human Primary Cortical Astrocytes viability using the WST-1 assay 48

3.5 Assessing gene expression changes in Human Primary Cortical Astrocytes after UFCB exposure with qRT-PCR 56

3.6 Assessing inflammatory responses with ELISA assay for pro-inflammatory cytokine LCN2 and the anti-inflammatory marker IL-6 64

3.7 Assessing UFCB effects on NT2-derived neuronal-like cell viability 67

3.8 Summary of Results 73

4. Discussion 74

4.1 Physiochemical properties of UFCB 74

4.2 UFCB toxicological dose-response curve and Primary Human Cortical Astrocytes 77

4.3 Astrocyte Reactivity 80

4.3.1 Gene expression analysis 80

4.3.2 Protein secretion levels analysis 84

4.4 Neuronal like cells viability and neurodegeneration 88

5. Conclusion 90

5.1 Concluding remarks and Potential for future directions 90

6. Acknowledgments 92

7. References 93

8. Appendices 114

8.1 Appendix A 114

8.2 Appendix B 116

8.3 Appendix C 117

8.4 Appendix D 118

1. Introduction

1.1 An Introduction to Air Pollution, Particulate Matter and Health

The World Health Organisation (2021) reports that 9 out of 10 people are clinically affected by air pollutants circulating in major cities and consequently, 4.2 million premature deaths are registered each year, an estimate that increases as time passes. Thanks to a study conducted by Prof Sir Stephen Holgate, the London Inner South Coroner's Court concluded that the death of nine-year-old Ella Roberta Adoo Kissi-Debrah in 2013 was the result of air pollution emissions exceeding EU regulations (Cockburn, 2020). This was the first ever registered case in the UK of death due to air pollution, without counting the Great Smog of London of 1952, which opened a broader conversation on how air pollutants and their emission affects public health. Each year, between 28,000 and 36,000 deaths are registered as a consequence of man-made air pollution in the UK alone (Office for Heath Improvement and Disparities, 2022). Many studies report the effects of air pollution on the cardiovascular and pulmonary systems, and these linked exposure of pollutant particles to increased risk of ischaemia, heart attack, Chronic Obstructive Pulmonary Disease (COPD), and other cardiopulmonary co-morbidities (Morris et al.,2021). Air pollution is now one of the greatest environmental risks factors that threatens our wellbeing. Essentially, as reported by the WHO (2021a), 99% of the World population lives in areas where the recommended air pollution threshold is exceeded.

Recent evidence shows that air pollution has detrimental effects on the Central Nervous System (CNS) and might drive premature neurodegenerative decline (Morris et al., 2021). The Lancet Commission on Dementia (2020) estimates that 40% of dementia cases could be prevented if 12 newly identified modifiable risks, including air pollution, were resolved. It also reported that 6.7 million deaths were registered globally from both indoor and outdoor air pollution (Fuller et al., 2022). Additionally, it was estimated that air pollution risk covered 2.3 of the population attributable fraction (PAFs), meaning it contributes to around 2% of the total preventable dementia cases. Recent evidence from epidemiological studies, supported by a recent UK government COMEAP advisory report states that exposure to these particles increases both dementia and Alzheimer's Disease (AD) risk of disease onset (UK Health Security Agency, 2022). A comprehensive

summary of the most recent studies regarding air pollutants and dementia risk, showed that Nitric Oxide (NO), Carbon Monoxide (CO), Ozone (O_3) and Nitrogen dioxide (NO2) were all linked, in eleven different independent studies, to increased risk of dementia (Peters et al.,2019).

Because other neurodegenerative diseases related to the aging brain exist, and neurological decline can start from an early age, research and studies investigating the effects of specific air pollutants particles on brain heath have started to emerge.

1.2 Air Pollution Explained

Air pollutants can either be naturally derived, such as particles and constituents from wildfires and general dust, or they can be artificially produced (Kilian & Kitazawa, 2018). The latter classification includes particles that arise as a result of fossil fuel combustion and mining activities but also every-day activities such as cooking and heating our own homes (Kilian & Kitazawa, 2018). As the United States Environmental Protection Agency (EPA, 2021) reports, there are around six major air pollutant constituents with either clinical or environmental significance. These are Nitrogen Oxides (NOx), Carbon Monoxide (CO), Sulphur Oxides (SOx), Ozone (O_3), Lead - or heavy metals - and **Particulate Matter** (PM).

PM is the result of the agglomeration of different liquefied and semi-solid components that can take up a variety of shapes and sizes. For this reason, there are three main classes of PM; ultrafine or $PM_{0.1}$ - for particles that are up to 0.1 µm in diameter – Fine or $PM_{2.5}$ - for particles that are 2.5 µm in diameter - and Coarse or PM_{10} – for particles that can reach 10 µm in diameter (EPA, 2021; Kilian & Kitazawa, 2018). Particulate matter is comprised of non-biological components and biological ones; these include organic and inorganic carbons – for example black carbons - minerals, metals, sulphates and chlorides, as well as bacteria and viruses (Kilian & Kitazawa, 2018)**.**

Most Coarse and Fine PM particles are produced and distributed into the atmosphere as the indirect product of complex photochemical reactions occurring with SOx and NOx , other waste pollutants deriving from power production plants or cars. Generally, these reactions occur in water droplets and result in ammonium nitrate as a by-product, which then comprises 50% of the total mass of PM (EPA, 2021; Kilian & Kitazawa, 2018). Moreover, these

reactions can occur with organic and inorganic volatile particles, which have at their nucleus either elemental carbon, some type of heavy metals or nitrates and sulphates. These can agglomerate with these secondary sulphates, nitrates and nitrogen oxides found in the atmospheres as a result of engine combustion and form particulate matter. Dusts or “fly ashes”, which derive from fires smokes, fields, or construction sites are also considered as particulate matter particles as well as pollen derivates and plants parts and these are considered as “directly emitted” in the atmosphere (EPA, 2021). Particulate Matter can also be formed as a result of the amalgamation of gaseous products resulting from combustion and from other inorganic ions including ammonium, sodium and chloride (EPA, 2021).

In any case, PMs and particularly ultrafine PMs are extremely dynamic and undergo several physiochemical changes in the atmosphere from the moment they are released until the moment of deposition. Ultrafine PM particles tend to be the most toxic, due to their composite nature and size. These particles which are environmentally dispersed around exposure sites such as busy highways, production plants and power stations can relocate to other sites such as town centres or roads .This means that people can be exposed more easily as air pollution nanoparticles are then present in the environment in which they live(Defra, 2018). Nowadays, it is practically impossible to avoid the release of air pollutants and PM into the environment. Agricultural activities, car exhaust fumes, burning woods, construction and demolition works, among many other activities, all contribute to the increasing number of these particles circulating in the atmosphere (Jayaraj et al.,2017). Therefore, it is imperative to understand the clinical, toxicological, and epidemiological effects that these particles have on human health.

1.3 Global impact of Particulate Matter exposure: a brief statistical report

The concentration of PM particles varies significantly depending on season, weather and even hours of the day. The parameters used to calculate the concentration of these particles in the atmosphere are closely linked to urbanisation levels, industrial emission, and the presence of power plants in the chosen area, as well as distance from highly trafficked roads (Kilian & Kitazawa, 2018). For example, in Northern European cities the concentrations of $PM_{0.1,}$

notoriously very difficult to measure and quantify, was found to be double in winter months compared to mean annual concentrations, but overall, they had an annual concentration of PMs that was 25% lower than Mediterranean cities such as Rome and Barcelona (Schraufnagel, 2020). However, the data relative to these cities, if scaled globally, puts them amongst the countries with the lowest mean annual exposure to bigger sized and easier to quantify air pollution derived particles – specifically for $PM_{2.5}$.

Nine out of ten countries with the highest mean annual exposure to ambient pollution ($PM_{2.5}$) are classed as low income. These include countries such as Niger, Cameroon, Nigeria, and Chad. The latter has a mean annual $PM_{2.5}$ concentration of 66 mg/m^3, 43% more than the World average (Pirlea & Ven-dee Huang, 2019). Overall, 90% of air pollution exposure related deaths occurs in Low- and Medium-Income Countries (LMICs) (Ritchie & Roser, 2017). Additionally, as of 2017, air pollution was linked to 9% of the total global deaths with 15% of these in Asian countries; specifically, the highest death rates were registered in Sub-Saharan and South Asian countries (Ritchie & Roser, 2017a).

Pollutants contributing to these deaths vary depending on the location, but the main ones are non-natural outdoor pollutants derived from metal and fossil fuel combustions, central air conditioning – specifically in Asian countries – but also, naturally-derived compounds such as dusts mainly composed of minerals originating from soil-poor deserts (Ritchie & Roser, 2017a; Querol et al., 2019).

Although, annual deaths caused by indoor household pollution have declined globally over the last 30 years, there are still some significant trends emerging that see specific countries, such as China, to have proportionally, the highest number of people - 416 million - exposed to household air pollution from solid fuel burning (Ritchie & Roser, 2013). Many countries still do not have access to clear fuels for cooking and heating (Ritchie & Roser, 2017a). Overall, in 2019, China alone registered 1.85 million deaths caused directly by either indoor or outdoor air pollution, the highest overall number globally. Additionally, high income countries have a lower annual concentration of air pollutants and PM particles in the atmosphere compared to LMICs. This is likely due to their economies focusing less on heavy industries and having access to cleaner energy sources. Moreover, often developing nations, moving into more industrialised economies, have a lag in public and environmental regulations and controls, a factor that may

influence the type of pollutants they produce and are exposed to. Overall, this difference results in deaths rates per indoor and outdoor air pollution being significantly higher in LMICs- than high-income countries, registering a 1000-fold difference between the two (Ritchie & Roser, 2013; see **Figure 1.1**).

Overall, data gathered in 2019 stated that 11.65% of all the total deaths globally are the result of air pollution and, as such, there is a growing need to start investigating not only the causes of this risk factor but the consequences on human health (Ritchie & Roser 2013: EPA, 2021). Data analysing the type of diseases associated to different pollutants circulating in specific areas of the globe is now slowly emerging. But these statistics change continuously due to the different levels of concentrations of pollutants measured, in relation to both what is measured in terms of particles and to what it is possible to measure technically. Over the last 10 years there have been several improvements to the standards for measurements and nowadays, air pollution microparticles and nanoparticles (NPs) are directly collected straight from the environment, filtered, quantified and their quality assessed (DEFRA, 2018).

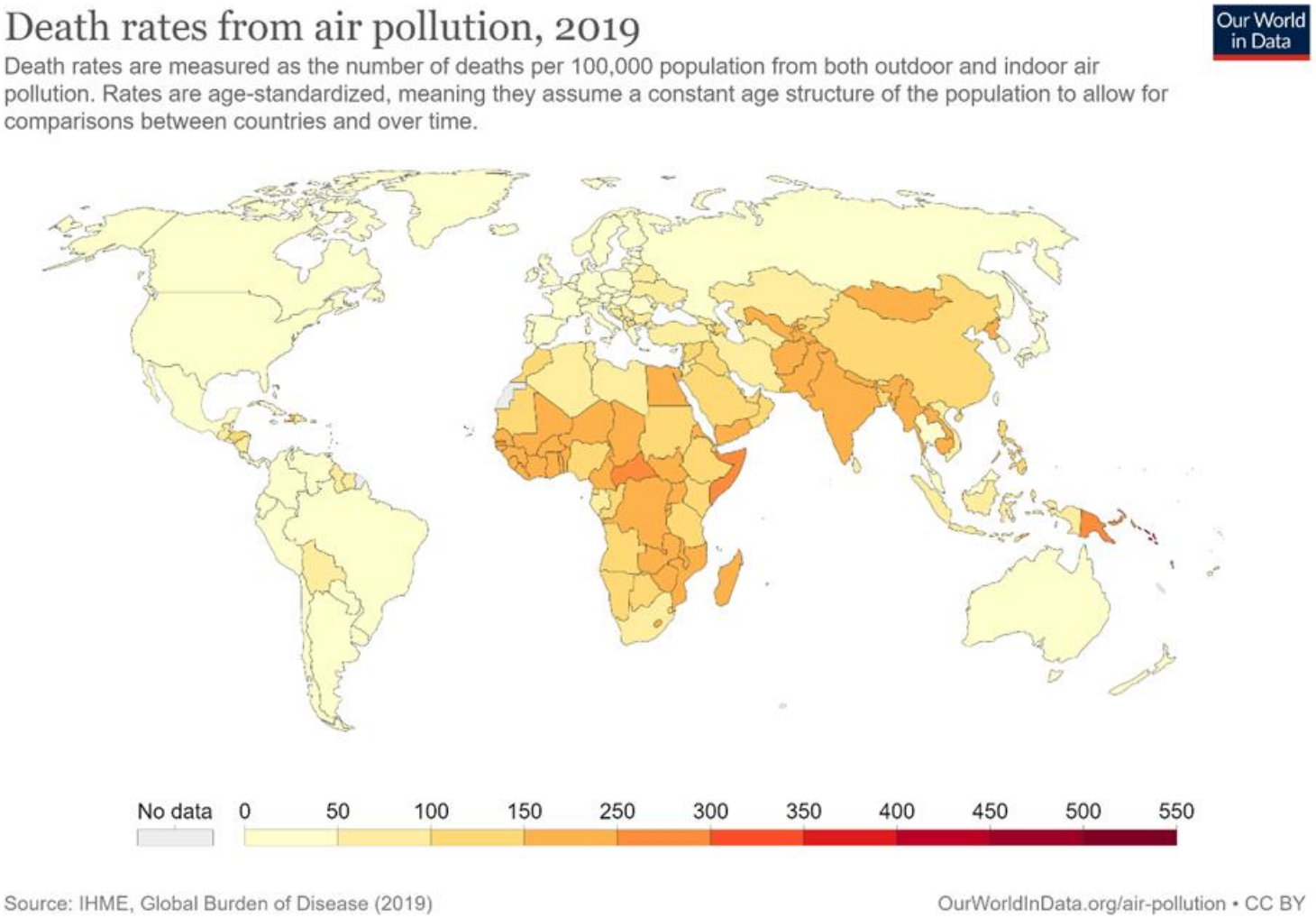

Figure 1.1. Death rates from air pollution map for the year 2019. The heat map presents the number of deaths from both outdoor and indoor air pollution per 100.000 people. Legend for the heat map is at the bottom of the figure. As depicted, countries of both the African and Asian continent seems to have the highest deaths rate, corroborating what reported previously. The graph has been taken from Ritchie & Roser, 2013.

Considering all the statistics mentioned above, as of 2021 Particulate Matter appears to be the main contributor to the increased risks of disease and deaths due to air pollution (Roser, 2021) overall. It is known that these particles tend to accumulate in foci near busy roads, industrial production plants and heavily populated and industrialised cities (Defra, 2018; Kilian & Kitazawa, 2018). Recently, the WHO has revised and published new air quality guidelines that set specific limits for the major components of air pollution including Ozone, Nitrogen Dioxide, Sulphur and Particulate matter. However, while $PM_{2.5}$ and PM_{10} emissions are regulated, **$PM_{0.1}$ emission thresholds are still under review** due to challenges in measuring their total amount as a result of their size (Defra, 2018; Kilian & Kitazawa, 2018).

1.4 Particulate Matter and Mechanisms of Molecular and Cellular Pathophysiology

Because of the extensive variability in size, distinct PM particles can penetrate and are distributed in specific organs in the human body **(Figure 1.2).** PM_{10} tends to reach the upper respiratory tract, depositing mainly in the nasopharyngeal tract (Defra, 2018). Fine and ultrafine PM particles can penetrate deep into the lung tissue (Kilian & Kitazawa, 2018), enter cells, and exerts cytotoxic effects. Ultrafine particles (UFP) can move transcellularly and can cross the lipid bilayer of cells and induce toxicity; (Defra, 2018; Kilian & Kitazawa, 2018; see **Figure 1.2**).

Evidence has previously shown how ultrafine particles that are inhaled, can move away from the pulmonary system, and reach important organs such as the brain. For instance, in a rodent inhalation study, ultrafine Elemental Silver (EAg) particles ranging in size diameter between 4 and 10 nm, were seen to accumulate in the alveoli, then reach heart, kidney, liver, spleen and brain as quantified by ICP–MS analysis and tissue section investigation (Takenaka et al.,2001). In a related study, EAg was retained for up to 7 days in macrophage-like J774A.1 cells and in the rat lung after intratracheal administration, perhaps highlighting how difficult their clearance is once they are stably redistributed and retained by tissues (Takenaka et al., 2000). In fact, evidence links both short-term and long-term PM exposure to increased morbidity and mortality as well as deleterious cardiopulmonary and cardiovascular diseases (Atkinson et al., 2014; Brook et al., 2010; Tamagawa et al., 2008; Hamanaka & Mutlu, 2018).

It was observed that specific components or types of Fine ($PM_{2.5}$) particles cannot be cleared by the lymphatic system (Wang et al., 2017); for example, Polycyclic Aromatic Hydrocarbons (PAHs) present within the PM. PAHs seems to negatively affect both T and B cell suppression of humoral and cell-mediated immunity as well as inhibiting pre-T, pre-B, and myeloid cell development. Moreover, PAHs have been found to induce altered production of cytokines by macrophages as well as an overall toxic effect on the bone marrow structure and function (Burchiel & Luster, 2001).

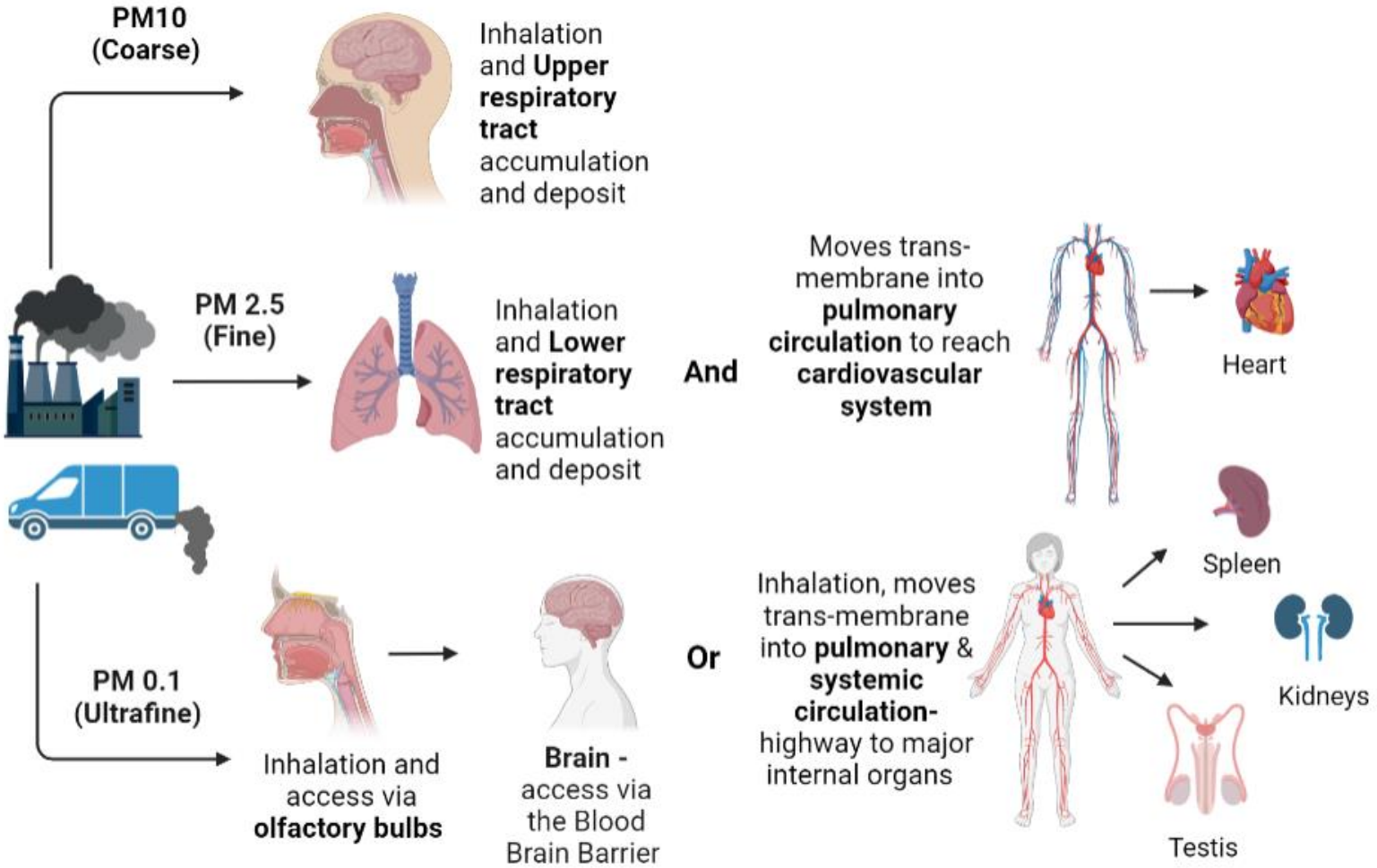

Figure 1.2. Schematic diagram showing different PMs sizes and areas of accumulation in the human body. PMs are emitted from diesel fuelled cars and industrial production plans. PM_{10} and $PM_{2.5,}$ which get inhaled and can reach upper and upper-lower respiratory tract whereas inhaled smaller nano particulate matter particles, $PM_{0.1}$, can penetrate deep into tissues, get access to the bloodstream and reach other internal organs. Graph made with biorender.com.

As shown above (**Figure 1.2**), larger particles – PM_{10} and $PM_{2.5}$ – can only reach and deposit in the upper and upper-lower respiratory tract respectively whereas smaller, nanometer, particles – $PM_{0.1}$ – can penetrate deep into the lower respiratory tract and potentially move. into the bloodstream (Kim et al., 2018; Morris et al., 2021). The systemic circulation, may act as a highway for these particles which can reach major internal organs and cross barriers, such as the blood testis barrier (BTB) or the blood brain barrier (BBB; Morris et al., 2021). They can also reach the kidneys, spleen and pancreas.

They may also have direct or indirect effects on structurally and functionally relevant cells present within these organs, such as microglia and astrocytes in the Central Nervous System (CNS; Costa et al., 2020). Moreover, as their size allows, they can bypass barriers all together and, as it is the case for the brain, use the olfactory system for direct access (Kim et al., 2018; Costa et al., 2020; Morris et al., 2021).

At the molecular level, PM particles exposure tends to cause a general inflammatory response, especially in the lung tissue (Tamagawa et al., 2008). Inflammation that results from oxidative stress isdue to the increased production of reactive oxygen species (ROS) not exclusively in mitochondria and also other cell types such as phagocytic cells (Stone, V., et al., 2007). However, any cells can produce ROS as long as it contains mitochondria or enzymes that are necessary for the redox reactions such as phospholipases and membrane bound oxidases (MacNee, W., & Rahman, I., 2001). Oxidative stress creates an imbalance between oxidants and antioxidants in favours of oxidants (Auten & Davis, 2009; Hameren et al., 2019)It is important to notice that ROS can both be produced by cells or arise, at the surface of nanoparticle, as by-product of their formation (Stone, V., et al., 2007). This is because particulate matter's particles, as well as nanoparticles, all contains ROS and redox-active components that have the potential to lead to ROS generation at the surface (Leni, Z., et al., 2020). Different types of Particulate Matter, of any size, possess different Oxidative Potentials (OP) which is their capacity to induce cellular damage and inflammation via oxidative stress resulting from ROS generation (Leni, Z., et al., 2020).

Increased ROS production in blood lymphocytes taken from healthy volunteers was also linked to both PM_{10} and $PM_{2.5}$ exposure, reaching maximum levels when ultrafine PMs were present (Bhargava et al., 2018). This was attributed to reduced protein expression and overall levels of two antioxidant enzymes, Superoxide dismutase (SOD) and Glutathione Reductase (GR). In peripheral blood lymphocytes taken from healthy volunteers and exposed to PM *in vitro* significant mitochondrial membrane depolarisation was also observed (Bhargava et al., 2018). PM exposure has also been linked to general DNA oxidative damage, activation of the DNA damage repair pathway and therefore, genotoxicity and mutations (Bhargava et al., 2018).

1.5 Particulate Matter and CNS studies

1.5.1 Molecular and cellular causes of PM-induced neuronal damage

Calderon-Gurciduenas & colleagues (2002) were the first to describe deleterious effects of different PM particles on the CNS. Their pre-clinical studies, performed *in vivo* on dogs inhabiting Mexico City, demonstrated that chronic exposure to Ozone led to disruption of the Blood Brain Barrier (BBB) due to increased production of iNOS by endothelial and astrocytic cells. The study also registered the formation of neurofibrillary tangles and increased white matter glial cell apoptosis (Calderon- Gurciduenas et al., 2002). In a set of *in vitro* studies using a human brain microvascular endothelial cell (HBMEC) line, aluminium nanoparticle exposure promoted BBB disruption (Chen et al., 2008) and, in particular, it reduced expression of tight junction proteins. This was confirmed using rat brain tissue where a substantial loss of expression of both claudin 5 and occludin was observed (Chen et al., 2008).

1.5.2 Genetic susceptibility to air pollution-linked neurotoxicity

The apolipoprotein E (APOE) gene is responsible for lipid transport, homeostasis, and general cholesterol maintenance. It exists in three different polymorphic isoforms – e2, e3 and e4, with e4 being strongly associated with Alzheimer's Disease onset and presence in diagnosed patients (Liu et al., 2013).

The e4 allele itself is now considered one of the strongest genetic risks factors for late onset Alzheimer's disease (LOAD) (Liu et al., 2013; Rhea & Banks, 2019; Hyunyoung et al., 2020). Considering this, in an Apo E -/- deficient mice strain (Jackson laboratory, Bar Harbor, ME) it was observed that exposure to fine dust, derived from concentrated ambient particles (CAPs), reduced the number of

dopaminergic neurons by 30% (Veronesi et al., 2004). Moreover, it has been shown that an increased exposure to $PM_{2.5}$, of over 12 ng/m^3, to carriers of one or both alleles of APOE e4 led additively to increased risk of all-cause-dementia onset, registering a Hazard Ratio increase of 295% for carrier of both e4 alleles, 91% for carrier of e3/e4 and 68% for carriers of both e3 alleles (Kilian & Kitazawa, 2018). This might mean that one risk factor – APOE4 – can in turn be influenced by another - air pollutant particles – to collectively increase the risk of disease onset.

1.5.3 Air pollution particulate matter and Cognitive development

Additionally, numerous *in utero* and early life exposure studies working on the effects of different pollutants revealed a general cognitive decline, with an overall decrease in verbal and non-verbal IQ performances, as well as decreased motor skills and memory in young children (Kilian & Kitazawa, 2018). Specifically, increased carbon black exposure, derived from diesel engines, led to a significant decrease in composite intelligence and visual skills (Suglia et al., 2008). In addition to these neurodevelopmental effects, more recent evidence, gathered over the last decade, has revealed air pollution as an environmental risk factor that significantly associates with ageing-related neurodegenerative diseases such as Alzheimer's and Parkinson Diseases (PD; Edwards III et al., 2019; Hyunyoung et al., 2020).

1.5.4 Epidemiological exposure to air pollution toxicants and dementia risk

In a population-based cohort study, Ozone exposure was directly linked to increased risk of AD onset, with data reaching 211% increased risk when the concentration was 10.91 Parts per billion (ppb; Jung et al., 2015). A Swedish study found that exposure to nitric oxide over a 15-year span increased the risk of dementia in a cohort comprising 1,806 participants residing in Umeå, Northern Sweden (Oudin et al., 2016). It was estimated that for every 4 ng/m^3 of $PM_{2.5}$ there is an overall 138% increase in risk of developing AD (Kilian & Kitazawa, 2018). Vascular Dementia, which results from decreased blood flow to the brain, was seen to be exacerbated by NO_2, Ozone and general $PM_{2.5}$ levels in a cohort of around 2 million people residing in Ontario (Chen et al., 2017).

Considering, however, the lack of an arbitrary measurement of PM particles in the studies mentioned above, as well as the immense variability in the parameters

used such as distance from a busy highway, genetic accountability, different air composition as well as other factors, **a causative link between specific types of PM exposure and ageing related brain function has not yet been molecularly confirmed** (Kilian & Kitazawa, 2018); in particular the cell types responsible for mediating neuroinflammation and neurodegeneration warrant further investigation.

1.6 Glial cells

Cells of the CNS include neurons, capable of generating action potentials which propagate a specific message within the brain or between organ systems, and glial cells. Glial cells of the CNS comprise astrocytes, microglia, closely linked to each other, and oligodendrocytes (Ransom, 2012). Astrocytes can be broadly classified into three groups: fibrous, present in white matter-, protoplasmic, present in grey matter, and radial (Matias et al., 2019). They are the most abundant cell-type in the brain, with widespread distribution, as well as heterogeneity, which renders them imperative in supporting a plethora of brain functions (Matias et al., 2019).

Astrocytes present end-feet structures that ensheath and support blood vessels in the BBB and favour many other functions such as transport and movement of nutrients and neurotransmitters from blood to brain (Chiareli et al., 2021). Astrocytes also regulate blood flow within the brain (Chiareli et al., 2021) and have a major role in BBB homeostasis. They do that by maintaining BBB integrity, as a metabolic and physical barrier (Rhea & Banks, 2019), through expression of tetra-spanning membrane proteins such as claudins, occludins, and zonula occludens (1-3) (Persidsky et al., 2006; Rhea & Bank, 2019;). They also aid in fluid exchange for removal of harmful toxins from the brain via aquaporin 4 water channels (Rhea & Banks, 2019).

Although their end-feet structures are not involved in communication with other glial cells, astrocytes can directly communicate and associate with the neuronal presynaptic and postsynaptic membrane, forming what is known as the tripartite synapse. Moreover, if these synapses associate with microglia as well as astrocytes, the complex is known as quadripartite (Perea et al., 2009). Astrocytes possess a star-like conformation, which terminates in peri-synaptic astrocyte processes (PAPs) capable of supporting and interacting with synapses within

brain structures. Astrocytes are also responsible for synaptic formation, maturation, and regulation, as they control the activity and recycling of key neurotransmitters such as ATP, D-Serine and GABA at the synaptic cleft (Matias et al., 2019). Thus**, astrocytes**, play major roles in development, support, maintenance of homeostasis, neurotransmission processes and structural integrity, necessary for **normal brain function**.

Microglia are defined as a CNS-specific and localised macrophage cell type that performs the main brain immune functions (Bachiller et al., 2018). Much like astrocytes, they perform an array of complex and necessary functions to ensure brain homeostasis (Bachiller et al., 2018). For instance, microglia are responsible for clearing dead cells, as well as synapses, that eventually become obsolete. They are responsible for aiding neurons to form newer and stronger connections while eliminating obsolete ones (Thompson & Tsirka, 2017). They are considered as the sensor cells that migrate to sites of damage and release inflammatory and/or anti-inflammatory cytokines, prostaglandins, and chemokines to attract other immune cells, including macrophages (Thompson & Tsirka, 2017). But in many neurodegenerative conditions, overstimulation of these immune responses may also result in phagocytosis of healthy neurons while attempting to restore homeostasis (Bachiller et al., 2018; Thompson & Tsirka, 2017).

Microglia are active cells that also respond to stimuli by becoming reactive. Their reactivity, , and consequent polarisation, marks neuroinflammation. The two most commonly known states are M1 and M2. The first is associated with the release of pro-inflammatory cytokines and other factors such as TNFα and IL-6 (Zhou et al., 2017).The second one seems to be associated with the release of trophic and protective factors that might reduce inflammation at the site of interest (Zhou et al., 2017). In fact, consensus in the field has now accepted that there is a spectrum of polarisation states and that these two represent very specific extremes, which suggests the definition of “M1/M2 microglia activation states” should be reconsidered in both *in vitro* and *in vivo* studies (Martinez & Gordon, 2014).

Microglia cells have always been considered as very different from astrocytes. This is because one originates from the yolk sack and the other from radial cells, one is motile, and the other is not and the only thing that seems they have in common is that neither is electrically active. However, these two very different

types of glial cells are in actuality, closely linked both by their function and in communication (Vainchtein & Molofsky, 2020). They work together in the quadripartite synapses and act together to promote synaptogenesis, support and promote homeostasis and are both associated with onset of many neurodegenerative diseases and progression; the feature, however, that mostly links them together is that they both react and react depending upon specific stimuli (Vainchtein & Molofsky, 2020; Garland et al., 2022).

It is perhaps this feature that allows these very different types of cells to act, as a duo, and respond to stress and other **CNS insults**, in a coordinated way to promote and optimise function and survival of surrounding cells, including neurons (Garland et al., 2022).

1.7 Astrocyte Reactivity and Neurodegeneration

Astrocyte reactivity was originally referred to as a homogenous and passive evolutionary reaction that astrocytes use to protect neuronal tissue and preserve CNS functioning in response to insults, such as traumatic injury, tumours, neurodegenerative disease and environmental exposure to harmful substances (Sofroniew, 2020). Reactivity refers broadly to the ability of astrocytes to change morphological appearance, metabolic activities, gene transcriptional responses and functions, such as influencing BBB tight junction's protein expression or promoting the expression of inflammatory mediators (Liddelow et al., 2017; Liddelow & Barres, 2017; Sofroniew, 2020).

More recent evidence, however, suggests that astrocytes, similarly to microglia, after they have reacted, they can assume two different polarisation states, namely A1 and A2, associated with neurotoxicity and neuroprotection respectively (Escartin et al., 2021). Under stressful conditions a long lasting, and often irreversible change, confers new astrocytic subtypes, whereby measurable effects on morphology, rate of proliferation, interaction with other cells and gene expression are apparent (Sofroniew, 2020). Although dependent on species (Liddelow & Barres, 2017), basal expression levels (Escartin et al., 2021) and cellular proliferation (Escartin et al., 2021), Glial Fibrillary Acid Protein (GFAP) tends to be overexpressed in reactive astrocytes (Chiareli et al., 2017) and this can give an indication of astrocytic responses to stressors, but it cannot state the type of polarisation state they have acquired.

The two main characterised **reactive** astrocytic subtypes, A1 and A2, both express increased GFAP. Both subtypes also appear to be induced by CNS insults, specifically LPS induced-neuroinflammation for A1 and ischaemic stroke for A2 (Escartin et al., 2021; Ting et al., 2019). *In vitro* studies showed that A1 astrocytes are associated with toxicity and neuronal death, as well as upregulating complement cascade genes previously shown to disrupt normal synapse functioning (Liddelow et al., 2017). On the contrary, A2 has been associated with neuroprotection as well as tissue and synapse maintenance and repair (Ting et al., 2019). Astrocyte reactivity can therefore be regarded as both an evolutionary protective response devoted to repairing damage, either to the BBB or neurons, but also as a toxic response to specific CNS insults (Ting et al., 2019).

Indeed, A1 astrocytes have been localised in areas of the brain involved in neurodegenerative diseases such as Alzheimer's, Parkinson's and Huntington's disease (Liddelow et al., 2017). This was assessed by changes in expression of A1-specific transcriptional markers such as Complement Component 3 (C3) (Ting et al., 2019), which was found to be present in 60% of GFAP- overexpressing astrocytic cells (Ting et al., 2019).

It is important to acknowledge that reactive astrogliosis is a complex dynamic process that cannot be explained simplistically as the general consequence of all CNS insults. Consensus in the astrocyte field suggests that reactivity is the result of a combined array of inter and intracellular processes to promote or prevent neuronal health depending on the insult and cellular conditions (Liddelow & Barres, 2017; Sofroniew, 2020: Chiarelli et al., 2017). For instance, A1 and A2 differentiation can be mediated by microglia activation which, via release of specific cytokines, induces reactivity differently with Il-1α, TNF α, and C1q complement protein, released by LPS-activated microglia, promoting A1 conversion but not A2 (Liddelow et al., 2017; Ting et al., 2019). Moreover, both types of reactive astrocytes produce in turn either neurotoxic or neurotrophic factors such as cytokines, ATP, neurotransmitters, and inflammatory signalling molecules (Li et al., 2019), and there are many markers that have been reported to be expressed exclusively by either subtype (Ting et al., 2019; **see Figure 1.3**). These markers have increasingly been used to differentiate between the two reactive states experimentally but, due to the heterogenic nature of reactivity,

caution is now advised in using morphological markers alone to indicate toxicity (Liddelow & Barres, 2017). A range of phenotypes including gene expression, morphology and functional effects on neurodegeneration should, therefore, be used to provide evidence of links between astrocyte reactivity and neurodegeneration or neuroprotection under disease conditions.

Insults on the CNS, such as exposure to Traffic Related Air Pollutants (TRAP), stimulate a cascade of events involving general inflammation and activation of microglia (Gomez-Budia et al., 2020; see **Figure 1.3**). Activated microglia, by releasing specific cytokines and intercellular signalling molecules, can promote astrogliosis and stimulate polarisation of A1 or A2 (see **Figure 1.3**). In turn, either subtype overexpresses exclusively a range of specific markers.

A2 astrocytes preferentially express 150 out of 263 reactive glial genes identified whereas A1 cells express 57 (Ting et al., 2019).
Alongside GFAP, A1 cells express high levels of Complement C3 (C3), Lipocalin 2 (LCN2), involved in promoting selective toxicity and death to neuronal cells (Bi et al., 2017), Complement Factor B (CFB), involved in the homeostasis of blood cellular components during inflammatory responses, and guanylate-binding protein 2 (GBP2) which is strongly upregulated in A1 type astrocytes and responsible for the reduction of GTP via hydrolyzation that during inflammatory responses has anti-viral properties (Liddelow et al., 2017; Kim et al., 2022). A2 astrocytes express S100A10, involved in cell proliferation and tissue repair, TGFβ, important for synapses formation (Matias et al., 2019; Ting et al.,2019) and PTX3,which, after ischaemic stroke, directly stimulates reactivity and polarisation of A2 subtypes, helps regulate BBB integrity and activates the classical complement pathway (Liddelow et al., 2017; Jurga et al., 2021).

The A1 subtype has been seen to promote a neurotoxic profile, leading to neuronal death via release of factors such as C3, TNF-α, IL-1β and IL-6 (John et al., 2003; Sofroniew, 2009; Liddelow et al., 2017). Contrarily, A2 has been seen to promote a neuroprotective profile (Bush et al., 1999), leading to neuronal repair and neurite growth via release of anti-inflammatory factors such as IL-6, Brain-derived-neurotropic factor (BDNF) or Glial cell-derived neurotropic factor (GDNF) (Degos et al., 2013; Liddelow et al., 2017; Fujita et al., 2018).

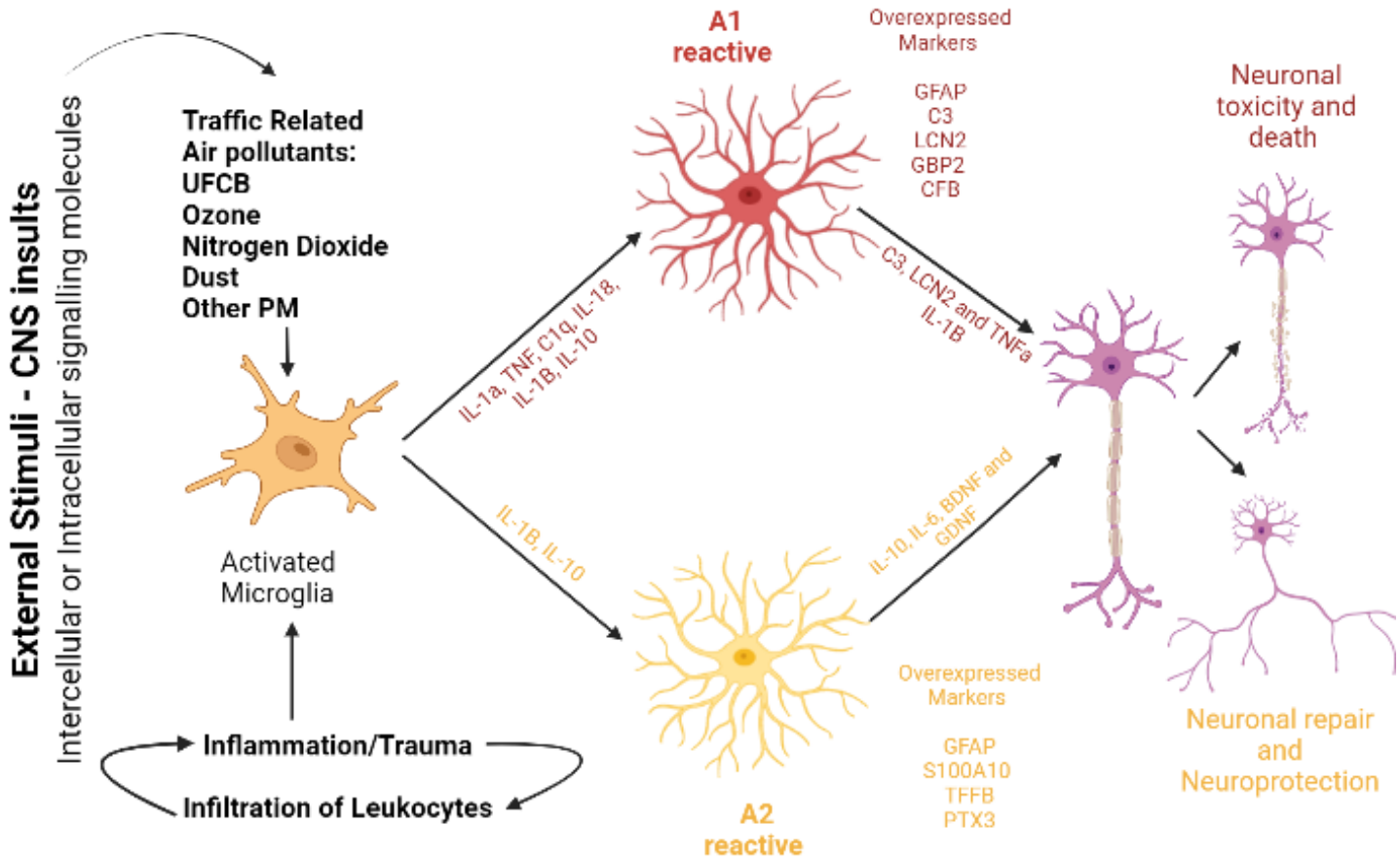

Figure 1.3: Schematic diagram showing the possible cascade of events following CNS insults and consequent microglia activation stimulating A1/A2 subtypes conversion and overexpression of specific markers for either subtype. Traffic related air pollutants, which include Ozone (O_3, a secondary pollutant), Nitrogen dioxide (NO_2), Ultrafine Carbon Black (UFCB) and many more, have been found to stimulate reactivity in microglia by a number of studies. Reactive microglia, in turns, through a cytokine mediated crosstalk, stimulate reactivity in astrocytes. Astrocytes can, simplistically, either assume one of two polarisation subtypes – A1 or A2 – overexpressing subtype-specific markers and secreting proteins, cytokines and other chemical mediators. These will either promote neurotoxicity and death or neuronal survival and protection. Figure made with **biorender.com.**

It is important to acknowledge that this binomial division related to the different polarisation states that astrocytes can assume once having reacted has now been suggested to include many more “in-between” subtypes (Liddelow et al., 2017; Liddelow & Barres, 2017). In fact, although many studies have referred to reactive astrocytes as either A1 and A2 in the past however, recent evidence still suggests moving past this classification or to investigate reactive astrogliosis and polarisation states acknowledging this limitation (Liddelow et al., 2017; Liddelow & Barres, 2017; Sofroniew, 2020).

1.8 Air pollution-derived Particulate Matter and Neuroinflammation

As mentioned, microglia are the main brain immune cells, which contribute to processes such as angiogenesis, neurogenesis, synaptogenesis, and myelination (Harry & Kraft, 2012). Microglia have been the **most-studied** cell type in relation to neuroinflammatory responses to **air-pollution-derived nanomaterials** and particulate matter.

A Diesel Exhaust Particles (DEP) exposure study showed how primary mouse microglia were activated and these cells expressed typical features of activation such as morphology changes, release of pro-inflammatory cytokines and increased production of ROS (Roqué et al., 2016). In another study, DEP led to microglia activation that in turn increased neurotoxicity substantially and decreased neuronal growth. If the activation was prevented by administration of anti-inflammatory drugs, such as minocycline, neuroprotection was favoured due to reduction in pro-inflammatory cytokines (Morris et al., 2021). Other studies have shown that microglia and neuron co-cultures adopt an inflammatory phenotype, alongside promoting ROS production and neurotoxicity, in response to a range of air pollution particles including DEP, $PM_{2.5}$, $PM_{0.1}$ and $_{0.2}$, ultrafine $Particles_{0.18}$ – collected from Los Angeles city – and $PM_{2.5}$ – collected from Wuhan city (Campbell et al., 2014; Roqué et al., 2016).

Fewer studies, however, have specifically investigated the response of astrocytes in mediating neuroinflammatory responses to air-pollution-derived particulate matter (see **Table 1.1**). Calderon-Gurciduenas & colleagues (2002) in their seminal study described a varied intensity of reactive astrocytosis present in subpial areas, olfactory bulbs, and frontal cortex white/grey matter of Southwest

Metropolitan Mexico City dogs' brains after exposure to a series of air pollutants. These included O_3, a variety of PM_{10} and $PM_{2.5}$, SO_2, NO/NO_2 and CO.

PM particles exposed astrocyte and microglia co-cultures registered a decrease in anti-inflammatory cytokines production and release, and an increase in pro-inflammatory cytokines, perhaps leading towards a more neurotoxic profile (Gomez-Budia et al., 2020). This was also assessed *in vivo* where reactive astrocytes themselves were associated with promotion of pro-inflammatory cytokines release, predominantly IL-1β and iNOS, due to p38/JNK/ERK MAPKs and JAK2/STAT3 pathways activation (Gomez-Budia et al., 2020). Morphological changes in the astrocytes were marked by an increase in GFAP *in vivo* (Allen et al., 2014) alongside an increase in expression of cell surface receptor aquaporin 4 (Onoda et al., 2017).

Although astrocytes and microglia co-culture studies have reported astrocytes reactivity *in vitro* and *in vivo (*Allen et al., 2014; Woodward et al., 2017*;* Haghani et al., 2020), when exposed to TRAP or other PM ($PM_{2.5}$ or smaller), these cells were seen to respond differently depending on particle, study design (*in vivo, in vitro*) and localisation area in the brain. For instance, evidence reported that astrocytic cells either did not react at all *in vitro* (Babadjouni et al., 2018) or, contrarily, that the cells assumed a high reactivity profile *in vivo* when localised in both the grey matter of developing brains after UFCB exposure (Onoda et al., 2017a) and fossil fuel ultrafine particles (UFP; not specified; Allen et al., 2015) and when present in the white matter (Calderón-Garcidueñas et al., 2001). As suggested (Babadjouni et al., 2018), white matter and grey matter have different plasticity profiles, with the first type being more susceptible to injuries and the second being more resistant (Babadjouni et al., 2018).

Despite these differences in results, culture conditions and models being tested, what emerged from these studies is the lack of standardised practises to test toxicity of specific NPs on astrocytic cells in isolation and characterisation of their response in terms of reactivity.

Moreover, as reported in **table 1.1**, after 2018, to our knowledge, almost no other studies have investigated astrocyte reactivity linked to air pollution (either as a result of exposure or in co-culture), highlighting a gap in this research area and potential for further studies.

Table 1.1 Adapted table from Gomez-Budia et al. (2020). Summary of studies concerning astrocyte activation after particulate matter exposure. ⬆ (increase) and ⬇ (decrease).

Relevant studies on astrocytes and/or microglia and astrocytes mixed culture			
Reference study	**Model used**	**PM used**	**Phenotype/Inflammatory Response & Signalling Pathway involved**
Cheng et al., 2016.	Mixed Astrocytes and Microglia culture - E18 rat cerebral cortex neurons	10/12 µg/ml of Nanosized, traffic derived PMs (Black Carbon, Organic and Inorganic Carbons, Metals)	⬆TNFα RNA and protein production ⬇Neuronal growth and numbers after conditioned media treatment
Li et al., 2016.	Rat C6 glioma cells	100 µg/ml of PM 2.5 derived from coal combustion and Traffic (carbon core)	⬆Viability of C6 glioma cells →Release of iNOS, IL-1β Activation of MAPK pathway & JAK2/STAT3 pathway → **Astrocytes Activation** Activation of MAPK and JAK inhibitors→ inhibition of iNOS and IL-1β PMs induced
Woodward et al., 2017.	Mixed astrocytes & microglia cultures from rat cerebral cortex	Nanoscale subfraction of TRAP (<200 nm diameter) – 20% $PM_{2.5}$	TLR4 dependent and independent mixed glial response after nPM exposure ⬆ TLR4 mRNA production
Xu et al., 2016.	Mice primary astrocytes from neonatal Nrf2 -/- rats	$PM_{2.5}$ collected from Beijing, China	⬆ TNF-α, IL-6 and IL-1β ⬆ GFAP ⬆ **Astrocytes activation** in $PM_{2.5}$ stimulated mice ⬆ Oxidative stress and inflammation
Jang et al., 2018.	Triple transgenic (3xTg-AD) mice having familial AD mutations	Fine PM (aerodynamic diameter <4µm)	Activation of PARP-1 in neurones (dose-dependent with higher concentration of PM at 30 and 50 µg/ml) ⬆ Aβ in hippocampal tissue sections of ex-vivo rodent model of (3xTg-AD mice) Activation of microglia and astrocytes
Liu et al., 2014.	Kkay mice (modified to be inclined to type II diabetes mellitus)	Concentrated ambient $PM_{2.5}$	⬆ TNFα, IL-6, IKKβ ⬆ Glial activation (astrocytes and microglia)

Within these studies, discordant results were registered including a differential expression of IL-1β, IL-6, COX2 and TNFα (Gomez-Budia et al., 2020), highlighting how culture conditions, time of exposure as well as dosage can influence different astrocytic responses, highlighting how difficult it is to translate much of the previous research. Additionally**, a direct link** between **air pollutant exposure** and **astrocyte reactivity,** favouring either a neurotoxic or neuroprotective phenotype**, has not yet been identified in response to specific air pollution-derived NPs**.

For instance, TRAP promotes astrocyte reactivity, inducing an overall neurotoxic effect (Woodward et al., 2017), however the specific particles responsible were not always elucidated as TRAP is comprised of an array of particles including Ozone, Nitrogen Dioxide, Ultrafine Carbon Black (UFCB), solid particles deriving from unburnt fuel, Carbon Dioxide and DEP.

In addition, it is unclear which component of TRAP particles and ambient air pollution particles might be toxic or lead to degeneration of the CNS (Haghani et al., 2019). Interestingly, Haghani et al. (2019) reports that no study has so far shown either, *in vivo* or *in vitro*, a clear link between air pollution particles and neurotoxicity, explaining how the mixture of TRAP and other PM isolated samples might be too complex to directly link any toxic effect to a single component. Overall, despite the presence of rapidly emerging PM exposure studies on brain derived cells, the specific composition, size and dosage of the particles or surrogate particles used are not clear (Costa et al., 2020). This is because many studies mostly focus on the overall "effects" of PM particles (either $PM_{2.5}$ or PM_{10}) without analysing a single surrogate particle and its toxicological implications on a single cell type (Costa et al., 2020).

Hence there is a need for a full characterisation of astrocytic cells in response to **specific air pollution linked nanoparticle** exposure, to better understand the molecular and cellular links between air pollution and neuroinflammatory mechanisms of neurodegeneration.

1.9 Ultrafine Carbon Black: a TRAP-DEP surrogate of air pollution nanoparticles for toxicological modelling

Nanosized air pollution-derived PMs – also called nanomaterials – have been reported to cause inflammation in the cardiorespiratory system both *in vitro* and

in vivo. The term nanomaterials, refers to particulate matter up to 100 nm in diameter, so ultrafine. This is important as oftentimes DEP, which usually consist of a mixture of fine and ultrafine particulate matter, are referred to as a nanomaterial when, in reality, the size varies as a result of its composite nature (Wichmann 2007).

Ultrafine Carbon Black (UFCB) is a low solubility (Donaldson et al., 2005) and extremely toxic air pollution-derived particle possessing the smallest aerodynamic diameter of all particulate matter (Rui et al., 2019). UFCB is classed as a Combustion Derived NanoParticle (CDNP) resulting from incomplete hydrocarbon thermal decomposition (Donaldson et al., 2005), originating as by-products of industrial production plants and diesel engine combustion.

Alongside this controlled mechanism of production, UFCB is also present, and chemically engineered, in acrylics paints and inks, rubber agents and plastic composed conductive agents (Gao et al., 2021). As evidence has extensively reported, UFCB is more toxic than its fine counterpart Carbon Black (CB; Rui et al., 2019). The research available on UFCB contributed to classifying it as a possible carcinogen to humans as it presents both an increased toxicity and an increased deposition rate (Gao et al., 2021). When originating from diesel engine combustion, UFCB tends to be rich in oils, unburnt fuel and polycyclic aromatic hydrocarbons (Donaldson et al., 2005). Specifically, these aromatic ring structures contribute to UFCB cytotoxicity as they have teratogenic, cancerogenic and immunotoxic effects (Patel et al., 2020). This class of nanoparticles is subjected to Brownian motion movements and its' high dynamicity allows free particles to move down concentration gradients and either coagulate or collide with each other due to the high surface area that UFCB possesses (Kwon et al., 2020).

UFCB has been used for nanotoxicological modelling purposes (Donaldson et al., 2005) however, originally, its fine counterpart, CB, was the one mostly used. CB has been extensively characterised during the last twenty years and has become a "gold standard" for toxicology. This is due to the peculiar characteristics that it possesses: it is a low solubility and low toxicity particle that with difficulty gets contaminated by other by-products, metals, and ions (Heinrich et al., 1995). Conversely, UFCB is a low solubility particle, but as stated, has increased toxicity

due to its size, high surface area and ability to form a protein corona and penetrate biological barriers such as the BBB and the Blood-Lung Barrier (BLB).

Moreover, preliminary evidence has reported that UFCB actively promotes hypertrophy of astrocytic end foot structures and increases GFAP expression in rodent brain tissue culture (Onoda et al., 2014), showing how it might be of interest to study on human derived astrocytic cells cultured in isolation. Additionally, there is not definitive evidence linking UFCB exposure to either neuroprotection or neurotoxicity after reactive astrogliosis which **provides scope** for **investigation.**

These characteristics need to be taken into consideration when trying to design studies that look at its interaction with cells and, possibly, cell specific pathways. Comprehensively, **UFCB** is a relevant particle to study with respect to air pollution toxicants and therefore a reasonable place to start with understanding the molecular and cellular toxicology of air pollution particles with respect to neurodegeneration/inflammation.

1.10 Hypotheses, Aims and Objectives:

This study hypothesised that specific nanoparticle components of air pollution will alter the neuroinflammatory function of astrocytes, to confer either neurotoxic or neuroprotective functions, and that this may depend on the concentration of particulate matter (PM; see **Figure 1.3**). This was investigated using a surrogate air pollution-associated nanoparticle, Ultrafine Carbon Black (**UFCB**) with the aim of determining astrocyte reactivity by examining its' effects on viability and reactivity of astrocytes, and subsequent effects on neuronal-like cells, through the following specific objectives to:

1. Optimise conditions to standardise preparation of UFCB for treatment of brain cells.

Using UFCB nanoparticles (NPs), a toxicological concentration response curve measuring viability of Human Primary Cortical Astrocytes was performed to determine sub-lethal and toxic doses for further investigation of reactivity in Astrocytes.

2. Characterise polarisation and immune function of astrocyte subtypes following treatment with UFCB.

Changes in astrocyte polarisation (differentiation into A1 or A2 subtypes) were measured by qRT-PCR for co-expression of a panel of specific markers including reactive (GFAP), 'neurotoxic' A1 subtype (LCN2/GBP2) or 'neuroprotective' A2 subtypes (S100A10), with data normalised to two housekeepers (GAPDH, RPLPO). Inflammatory responses were assessed by measuring levels of the pro-inflammatory protein LCN2, expressed by A1 specific astrocyte subtypes and the anti-inflammatory marker IL-6.

3. Examine effects of UFCB-stimulated astrocytes on neurodegeneration by measuring neuronal viability.

To determine whether astrocytic responses observed in objective 2 lead to neurodegeneration or neuroprotection, the effects of NP-induced reactive astrocyte conditioned media on neuronal viability was determined using differentiated human NT2-derived neuronal like cells. To confirm differentiation, the NT2 cells were immuno-stained for the neuronal-specific marker TUBβ3 and morphology visualised using a fluorescent microscope.

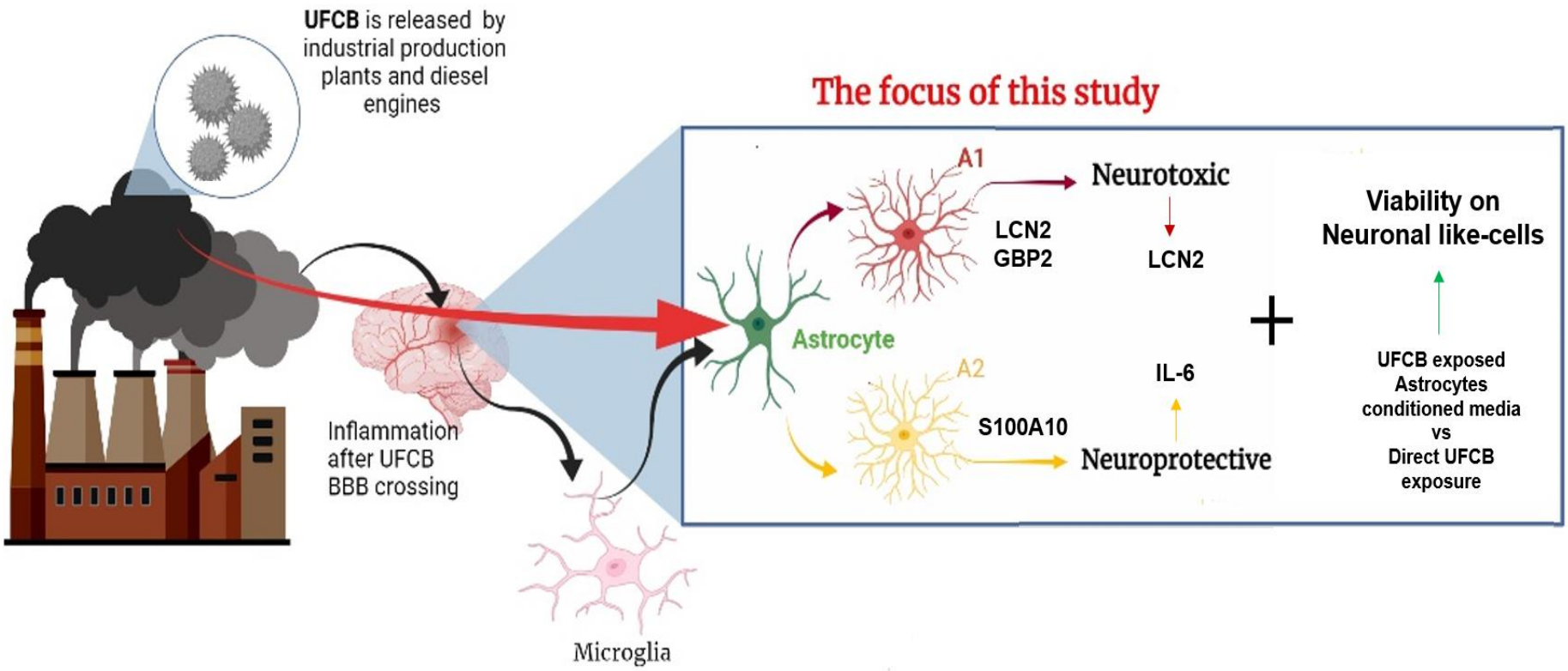

Figure 1.3: Schematic diagram representing the rationale and focus of this project. A UFCB surrogate particle will be used to directly exposed human primary cortical astrocytes, measure polarisation after reactivity and observe any possible effects that might suggest either neurodegeneration or neuroprotection. As previous studies have investigated the role that microglia might play in air-pollution induced neurodegeneration and neuroinflammation, this study focuses on the effects that the surrogate nanoparticle UFCB, might have on astrocyte reactivity after direct exposure, without the presence of a microglia mediated crosstalk.

2. Material and Methods

2.1 Cell Culture and Maintenance

For cell culturing, general laboratory practice (GLP) and correct aseptic technique were used at all times. Moreover, both cell types cultured, NT2 derived cells and Human Primary Cortical Astrocytes, were always handled in a Class II cabinet and maintained at 37°C, with a humidified 5% CO_2 and 95% air atmosphere incubator (Eppendorf,Stevenage, UK). Every 2 months, intra-department mycoplasma testing was performed on all cell types present by the laboratory manager.

2.2 Primary Human Cortical Astrocytes

2.2.1 Coating solution

Prior to Human Primary Cortical Astrocytes cell thawing, a poly-L-ornithine/fibronectin coating solution was made by first dissolving poly-L-ornithine (Sigma Aldrich, Gillingham, UK) in double distilled H_20, to a stock concentration of 1 mg/ml. This was then syringe-filtered and aliquoted for storage at -20°C. Fibronectin from human plasma, lyophilised powder (Sigma/ MilliporeSigma, Gillingham, UK) was dissolved in sterile H_20 to a stock concentration of 1 mg/ml and aliquoted for storage at -20°C. The coating solution was then prepared at a final concentration of 50 µg/ml poly-L-ornithine and 1 µg/ml fibronectin in sterile double distilled H_20. T75 flasks were incubated with approximately 7 mL coating solution, to cover the surface of the flask, for 4 h at 37°C, with a humidified 5% CO_2 and 95% air atmosphere. Coating solution was then removed and stored in the fridge for use up to 3 more times. Flasks were washed with phosphate buffered saline (PBS; Sigma Aldrich, Gillingham, UK) and Astrocyte media (ScienCell, San Diego, California, USA) was added immediately prior to addition of cells.

2.2.2 Culture and maintenance of primary human cortical astrocytes

Adherent Human Primary Cortical Astrocyte p^0 cells (ScienCell, San Diego, California, UK) were cryostored in Liquid Nitrogen (LN_2). Cells were rapidly thawed at 37°C and then added dropwise to a poly-L-ornithine/fibronectin-coated T75 flask containing Astrocyte Media (ScienCell, San Diego, California, USA) supplemented with 2% foetal bovine serum (FBS, ScienCell, UK), 5 mL Astrocyte

Growth Supplement (AGS, ScienCell, San Diego, California, USA) and 5 mL Penicillin/Streptomycin (ScienCell, San Diego, California, USA). Cells were maintained at 37°C, with a humidified 5% CO_2 and 95% air atmosphere. Astrocyte media was refreshed 16 h post-thawing and cells were grown for 2-3 days.

Cells were passaged once 90-95% confluency was reached. Astrocytes medium was aspirated, and the cells were washed with 10 mL PBS. Trypsin-EDTA (diluted to a final concentration of 0.025% in PBS) was added, and the cells were incubated in an incubator (Eppendorf, Stevenage, UK) for 1-2 minutes at 37°C, with a humidified 5% CO_2 and 95% air atmosphere. Following incubation, Trypsin-EDTA was removed and added to a falcon tube containing 5 mL 10% heat-inactivated (hi)FBS (Life Technologies, Carlsbad, California, USA) to de-activate trypsin. The flask was re-incubated for another 2 minutes to allow residual cells to detach. Following incubation, two washes with 5 mL of Trypsin Neutralisation Solution (TNS; 9 mL Astrocyte Media and 1 mL hiFBS) were performed. The remaining cell suspension was collected and added to same falcon tube containing Trypsin-EDTA and hiFBS. The cell suspension was centrifuged using a Universal 320R centrifuge (Hettich U), at 1,000 x g for 6 minutes. The liquid was discarded, and cell pellet was re-suspended in Astrocyte media before seeding at the densities indicated for experiments. The cells were plated at different densities for cell viability assay according to vessel (see **Table 2.1**).

Table 2.1 Human Primary Cortical Astrocytes cell seeding densities expressed in cells/cm^2 and their corresponding values in cells/well.

Seeding density based upon intra-department studies	96 well plate – up to 0.2 ml – 0.32 cm^2	12 well plate – up to 2 ml – 2 cm^2
5000 – 15000 cells / cm^2	1500 – 4800 cells/ well	20000 – 60000 cells/ well

2.3 NTERA-2 cells

Adherent NTERA-2 p^5 (NT2) cells (ATCC, #CRL-1973) were cryostored in LN_2. Cells were rapidly thawed at 37°C, then resuspended using NT2 complete culture/growth media [Dulbecco's Modified Eagle Medium (DMEM; Gibco, Waltham, Massachusetts, USA), supplemented with 10% heat-inactivated foetal bovine serum (hiFBS; Life Technologies, 10270106), 100 units/mL penicillin and 100 µg/mL streptomycin (Gibco, Waltham, Massachusetts, USA) and 2 mM L-Glutamine (Gibco, Waltham, Massachusetts, USA)]. Cell suspension was centrifuged using a Universal 320R centrifuge (Hettich U), at 1,000 x g for 3 minutes at room temperature and the pellet further re-suspended in NT2 complete culture/growth media before seeding into a T25 tissue culture flask (Corning, Corning, New York, USA) for bulking.

Cells were maintained at 37°C, with a humidified 5% CO_2 and 95% air atmosphere, and NT2 complete culture media. Cells were passaged once 70-85% confluency was reached. Growth medium was aspirated, and the cells were washed with 10 mL PBS (Sigma Aldrich, Gillingham, UK). Trypsin-EDTA 0.05% (1x; Gibco, Waltham, Massachusetts, USA) was added, and the cells were incubated at 37°C for 2 minutes. Following incubation, NT2 growth medium was added to inactivate trypsin, and cell suspension was centrifuged at 1,000 x g for 2 minutes at room temperature. Cell pellet was further re-suspended in growth medium before seeding at the densities indicated for individual experiments.

2.4 NT2 neuronal like cells differentiation

For differentiation, NT2 p^{10} cells were thawed and maintained as described above, then at 70-85% confluency re-seeded at a density of 1 x 10^6 cells per T75 flask. Following 24 hrs incubation, the media was changed and substituted with NT2 complete culture/growth media containing 10 µM All-Trans-Retinoic-Acid solution (ATRA; Sigma Aldrich, Gillingham,UK). Stock ATRA was previously prepared by first dissolving powder (Sigma Aldrich, Gillingham, UK) in double distilled H_20, to a concentration of 10 mM, then syringe-filtering and aliquoting for storage in dark Eppendorfs at -20°C. NT2 cells were maintained for four weeks in the same flask and the media changed twice per week. After four weeks, the cells were passaged into experimental vessels and media changed to NT2 culture/growth medium supplemented with two mitotic inhibitors, 1 µM Cytosine

arabinoside (Sigma Aldrich, Gillingham, UK) and 10 µM Fluorodeoxyuridine (Sigma Aldrich, Gillingham, UK)

Cells were plated at 3 x 10^5 cells per cm^2 in a 96 well plate for cell viability assays and 3 x 10^5 cells per cm^2 in 35 mm glass-bottomed dishes for imaging, then maintained for further two weeks until fully differentiated prior to experimentation. Differentiation was monitored via imaging with the Axiocam 208 colour microscope camera (Zeiss, Birmingham, UK) and were considered fully differentiated once morphological changes (presence of axon-like and ganglion-like structures formation) were observed.

2.5 Ultrafine Carbon Black preparation

2.5.1 UFCB weighing and suspension

A stock vial of powdered UFCB, purchased from Printex 90 (Degussa Orion, Frankfurt, Germany) was weighed with a hood isolated (Safetech, London, UK) fine weighing scale (Mettler Toledo, Leicester, UK) with a built antistatic electrode on, measuring 2 mg per tube each time. The weighed UFCB was suspended, in a 2 mg/ml final stock concentration in either NT2 or Astrocyte growth/ complete culture media depending on the cell type for experiments. The suspension prepared each time prior to use, was incubated in a sonicating water bath (Ultrawave, Cardiff, UK) at room temperature for 16 minutes. UFCB stock (2 mg/ml) was used to generate a working concentration range (0-200 µg/ml) by 2-fold serial dilution in the appropriate growth media depending on cell type.

2.5.2 UFCB sizing

UFCB was characterised by dynamic light scattering (DLS). The average hydrodynamic diameter (Z-average) was determined using a Zetasizer NanoZS (Malvern Instruments, Worchestershire, UK) following the manufacturer's instructions. UFCB was weighed and particle suspensions (diluted to 100, 12.5 and 3.125 µg/ml) were prepared as above in different dispersants which included Astrocyte Media, ultrapure distilled water and 10% hiFBS. The measurements were taken at time point 0, 30 mins, 2 hrs, 4 hrs and 24 hrs. The suspensions were transferred to disposable cuvettes and readings were registered. The Zetasizer NanoZS measurement parameters were set as follows: Material: UFCB; RI and Absorption: 1.000; Dispersant: either Water (RI and Viscosity: 1.330) or DMEM (RI: 1.4 and Viscosity: 0.9); 15 seconds of equilibration time;

temperature set at 20°C; Cell: Disposable Cuvette DTS0012; Measurement Angle: 173° Backscatter; Measurement Duration: Manual, 3 run x 15 seconds, 3 measurements with 0 seconds of delay between measurements with Attenuator set at 4.

2.6 Cell treatments

Differentiated NT2 derived neuronal like cells were seeded in 96 well plates at a density of 3 x 10^5 cells per cm^2 in a 96 well cells per cm^2, as indicated, and equilibrated at 37°C, 5% CO_2 and 95% air atmosphere, in NT2 complete culture/growth media for 24 hours before treatment. Human Primary Cortical Astrocytes cells were seeded in 96 well plates at a density of 1.5 x 10^4 cells per cm^2, as indicated, and equilibrated 37°C, 5% CO_2 and 95% air atmosphere, in Astrocyte's media for 24 hours before treatment. Cells were then treated with 100 µl of UFCB concentration in the range of 0-100 µg/ml as indicated for 24 hours, under cell maintenance conditions, prior to analysis.

2.7 Cell Viability (WST-1) Assay

Cell viability was assessed using the Water-Soluble Tetrazolium 1 assay (WST-1; Sigma Aldrich, Gillingham, UK). Following treatment, UFCB suspension was aspirated, and cells were washed using 100 µL NT2 growth media or Astrocyte Media for NT2 or astrocytes respectively. 90 µL of fresh medium and 10 µL of WST-1 reagent were then added to each experimental well. To control for direct reduction of WST-1 reagent by UFCB, WST-1 was added to cell-free wells following incubation with UFCB for 24 hours under the same conditions as described in **section 2.6 above.** To account for the nanoparticle 's large surface area and refractive/adsorption capabilities (Stoeger et al., 2006; Kwon et al., 2020)UFCB NP effects on absorbance were controlled by including wells lacking WST-1, following UFCB treatment under both cell and cell-free conditions. Cells were also treated with Triton-X-100 0.1% V/V (Sigma-Aldrich, Gillingham, UK) which was used as positive control to ensure that WST-1 reagent was not reduced by dead cells.

Plates were then incubated for up to four hours, for optimisation assays, and two hours for measurement of viability in response to UFCB, as indicated in the results section. Subsequently, plates were shaken for 60 seconds and absorbance readings, at 450 nm, measured using a microplate absorbance

reader (Sunrise, Tecan, Zurich, Switzerland). The measurement parameters for plate readings were set as following: Endpoint measurement; Absorbance at 450 nm; Shaking 60 seconds (low) inside & 5 seconds settling time; Absorbance between 420-480 (450); Reference wavelength > 600 nm.

2.8 Gene expression analysis

Human Primary Cortical Astrocytes plated at a density of 15000 cells/ cm^2 in 12 well plates, were exposed to UFCB concentrations corresponding to 0, 3.125 and 12.5 µg/ml to investigate the role of the nanoparticulate matter on astrocytes reactivity. These concentrations were derived following analysis in **section 3.4.** Treatment with, 1 µg/ ml of bacterial lipopolysaccharide (LPS 10 MG from *Escherichia coli* O111;B4, Sigma Aldrich, Gillingham, UK) was used as a positive control for astrocyte reactivity.

2.8.1 RNA extraction

Total RNA from Human Primary Cortical Astrocytes were extracted using an RNeasy Mini Kit (Qiagen Sciences, Venlo, Netherlands) according to the manufacturer's instructions. Cells from 3 wells were scraped and pooled using a total of 350 µL RLT buffer. Subsequently, 700 µl 70% ethanol was added to the lysate and an equal volume of this transferred directly into a RNeasy mini column (within a 2 ml collection tube). The column was then centrifuged for 15 seconds at 8000 x g using a 5215 R centrifuge (Eppendorf, Stevenage, UK) and flow-through discarded. Following this, 700 µl RW1 buffer was added to the spin column and centrifuged again for 15 seconds at 8000 x g, discarding the flow through at the end. Then, 500 µl RPE buffer was added, and samples centrifuged for 15 seconds at 8000 x g. The flow-through was discarded. This last wash step was repeated twice, centrifuging the second time for 2 minutes. To dry the membrane, the spin column was then placed in a sterile 2 ml collection tube and centrifuged for an additional minute at 8000 x g. Lastly, RNA was eluted into a 1.5 mL sterile tube with two elution steps using the same 30 µl of RNAse free H_20 to ensure maximal recovery of RNA.

RNA concentration and purity was quantified using the NanoDrop™ One/One^C Microvolume UV-Vis Spectrophotometer (ThermoFisher Scientific, Waltham, Massachusetts, USA) according to manufacturer's instructions.

2.8.2 Assessment of RNA quality

To analyse RNA quantity and integrity, the Agilent 2100 Bioanalyzer was used (Agilent Technologies, Cheadle, UK). Agilent gel was made fresh (Agilent technologies, Agilent RNA 6000 Nano Gel Reagents Part I, 5067-1511) and 1 µl of each RNA sample, alongside 2 µl of ladder, were loaded onto the RNA Nano Chip (Agilent technologies, Cheadle, UK) according to manufacturer's instructions. Prior to inserting the chip, the machine was cleaned and calibrated with RNAse Zap and RNAse-free H_20 (Sigma Aldrich, Gillingham, UK). RNA quantity and integrity was measured, reporting the RIN numbers for each sample (See **section 3.5** in Results).

2.8.3 Reverse transcription

DNAse treatment of all the RNA samples was performed using Invitrogen DNAse I, Amplification Grade (Thermofisher Scientific, Waltham, Massachusetts, USA), according to manufacturer's protocol (RNA quantity Subsequently, DNAse-treated RNA was reverse-transcribed using the Applied Biosystems high-capacity RNA-to-cDNA synthesis kit (ThermoFisher Scientific, Waltham, Massachusetts, USA) according to manufacturer's protocol.

2.8.4 Primer design and validation

Primer pairs were identified using PrimerBank (https://pga.mgh.harvard.edu/primerbank/), a public resource for PCR primers containing empirically tested primer sets. After having checked annealing temperature, GC content and having ensured that, by matching them to the gene of interest sequence, an amplicon of at least 100 bp was available. No available primers spanned an exon-exon boundary.

Specificity of the primer sets selected was confirmed using BLAST (https://blast.ncbi.nlm.nih.gov/Blast.cgi) and the marked up full genome sequence identified using NCBI accession number. The primer sets sequences for Forward (F) and Reverse (R), are reported below in **table 2.2.**

Table 2.2. Table reporting the primer sets PrimerBank ID and NCBI accession numbers, the amplicon size in bp and F and R sequences (5'-3').
Note that "**HK**" denotes housekeepers, "**RA**" Reactive Astrocyte and **"A1/A2"** are genes specific for either subtype.

Gene	PrimerBank ID	NCBI accession number	Amplicon Size (bp)	Forward Primer (5' - 3')	Reverse primer (5'-3')
GAPDH - **HK**	/	/	200	CTGGGCTACACTGAGCACC	AAGTGGTCGTTGAGGGCAATG
RPLP0 **- HK**	49087144c3	NM_001002.4	97	CAGATTGGCTACCCAACTGTT	GGAAGGTGTAATCCGTCTCCAC
GFAP - **RA**	334688843c1	NM_001363846.2	209	CTGCGGCTCGATCAACTCA	TCCAGCGACTCAATCTTCCTC
S100A10 - **A2**	115298655c1	NM_002966.3	168	GGCTACTTAACAAAGGAGGACC	GAGGCCCGCAATTAGGGAAA
LCN2 - **A1**	108936956c3	NM_005564.5	111	GAAGTGTGACTACTGGATCAGGA	ACCACTCGGACGAGGTAACT
GBP2 - **A1**	38327557c1	NM_004120.5	182	CTATCTGCAATTACGCAGCCT	TGTTCTGGCTTCTTGGGATGA

Primers were purchased from Eurofins Genomics (Eurofins, Livingston, UK) and upon arrival, they were resuspended at a stock concentration of 100 pmol/µl with addition of DNase and RNase -free H_20. Prior to qPCR, all primer sets were optimised using a standard curve - to determine the optimal cDNA concentration, in relation to a standard primer concentration (200 nM for both F and R), correlation coefficients (R^2) and efficiency values for each gene.

A 2-fold serial dilution was made for all primers with the exception of GBP2 and LCN2 primer sets standard curve started from 2x, with 1x being 40 ng/ml, due to the low expression (high Ct value) and low amplification encountered with a trial qPCR melt curve analysis performed for all primers (see **Appendix A**).

2.8.5 qPCR

qPCRs were performed in a total volume of 20 µL. A reaction mastermix for each target transcript was prepared using the 5x HOT FIREPol SolisGreen qPCR mix Plus (ROX) (Solis BioDyne, Tartu, Estonia), 200 nM of forward and reverse primers (except for GAPDH that was 250 nM for both F and R primers), 2 µl of cDNA (+/- RT, either 10-80 ng/µl - this was primer specific) and DNAse/RNAse free H_20.Each reaction was carried out using 96-well BrightWhite real-time PCR plates (PrimerDesign, Z-BW-FAST). Cycling conditions on the StepOnePlus Real-Time PCR System machine (Applied biosystems, Themo Fisher Scientific, Waltham, Massachusetts, USA) were set as follows; Incubation Step (95 ºC for 15 minutes), PCR Stage (95 ºC for 15 seconds followed by 60 ºC for 20 seconds and 72 ºC for 20 seconds repeated for 40 cycles) and Melt Curve Stage (95 ºC for 15 seconds, 60 ºC for 1 minute and then again 95 ºC for 15 seconds).

qPCR data was analysed for gene expression changes using the ΔΔCt method, normalising target gene levels to the geometric mean of the Ct values of the two housekeeper genes (GAPDH and RPLPO). All genes were compared on the same plate, but biologically-independent experiments were analysed using separate plates due to the large number of samples and conditions. To account for plate to plate differences, fold change values were then calculated relative to untreated control cDNA samples within each plate, using the following equation:

$$\text{fold change} = 2^{-\Delta\Delta Ct}$$

ΔΔCt= ΔCt GOI [ΔCt GOI – Geo Mean HKs] – Average* of ΔCt Control [Average* {ΔCt untreated control of GOI – Geo Mean HKs}

2.9 ELISA

Human Primary Cortical Astrocytes were treated with Neurobasal Media [Neurobasal (FisherScientific, Waltham, Massachusetts, USA), 100 units/mL penicillin and 100 µg/mL streptomycin (Gibco, Waltham, Massachusetts, USA) and 2 mM L-Glutamine (Gibco, Waltham, Massachusetts, USA) and 2% B27 (Fisher Scientific, Waltham, Massachusetts, USA)] and then exposed to pre-selected UFCB concentrations (0, 3.125, 12.5 µg/mL) prepared in this media, which was compatible with further treatment of neuronal cell types. Subsequently, the cells were scraped for RNA extraction while the conditioned media from each treatment condition was centrifuged at 2000 g for 30 minutes at 4°C to isolate remaining NPs and collect only NP-free supernatant for the ELISA assay. ELISA assays were performed, using undiluted conditioned media, to measure Human Lipocalin-2 (Abcam, Human Lipocalin-2 ELISA Kit, ab215541, Boston, USA) and Human IL-6 (Abcam, Human IL-6 ELISA Kit, ab178013, Boston, USA) according to manufacturer's protocol and instruction. Absorbance was measured at 450 nm using a microplate absorbance reader (Sunrise, Tecan, Zurich, Switzerland).

2.10 Immunofluorescence

Prior to NT2- neuronal like cells imaging, the cells were grown, differentiated and passaged as explained above in **sections 2.3** & **2.4**. The media was removed, and the cells were fixed for 15 minutes in 4% Paraformaldehyde at room temperature (PFA; Sigma Aldrich, Gillingham, UK). Subsequently, the cells were washed 3 times, for 10 minutes, with 0.3% Triton-X-100 (0.3% V/V; Sigma-Aldrich, Gillingham, UK) diluted in PBS (PBST). The cells were then blocked in 3-5% bovine serum albumin (BSA; Fisher Scientific, Waltham, Massachusetts, USA), diluted in PBST, for 20 minutes at room temperature and the primary antibody purified anti-Tubulin β3 clone TUJ1(1:5000, BioLegend, B2099227, San Diego, California, USA) was added to the blocking solution and incubated overnight at 4ºC. Thereafter, cells were washed 3 times, 10 minutes each time, with PBST. The secondary antibody Goat anti-Mouse IgG (H+L), Superclonal™ Recombinant Secondary Antibody, Alexa Fluor™ 488 (1:2000, Invitrogen,

Waltham, Massachusetts, USA) was added to the blocking solution in the dark for 1 hour. Again, the cells were then washed 3 times as previously described and nuclei stained with DAPI contained mounting media (Vectashield,Vector Labs, California, USA). Cell dishes were then observed under the inverted fluorescent scanning microscope Observer A1 (Zeiss Axio, Birmingham, UK).

2.11 Statistical Analysis

Data were analysed using GraphPad Prism 9 (GraphPad Software, San Diego, CA, USA). All data were expressed as means ± SEM and analysed using either a One-way ANOVA or a Two-way ANOVA, as indicated, followed by Tukey's *post hoc* test for multiple comparisons. LD50/LD10 calculations for toxicological curves were analysed by non-linear curve fitting using GraphPad Prism 9 using a Variable Slope Model and selecting log(dose) response curves analysis.

3. Results

3.1 Assessing UFCB physiochemical properties in different dispersants using Dynamic Light Scattering

Initially, experiments were conducted to determine if the surrogate Ultrafine Carbon Black (UFCB) nanoparticle reflected some of the physiochemical properties of traffic related air pollution (TRAP) and ambient air pollution UFCB. Size was measured via dynamic light scattering (DLS). UFCB was suspended and sonicated in three different dispersants (see **Figure 3.1**), including human astrocyte media, deionised water (dH_20) and 10% FBS. This revealed how the particles present in suspension interact with components of these dispersants, including proteins, as well as to investigate whether the particles coagulated and precipitated over time (Stoeger et al., 2006).

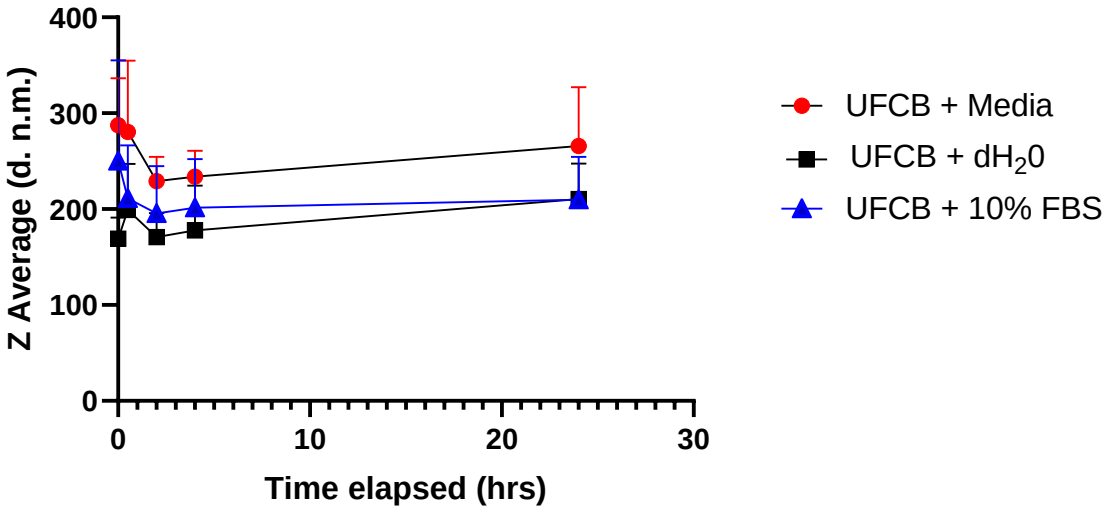

Figure 3.1. Z Average measurement diameter of the UFCB particle in nanometres (d.n.m.) when resuspended in three dispersants. Measurements of Dynamic Light Scattering (DLS) of 100 µg/ml UFCB resuspended in**;** Astrocyte media, dH_20 and 10% FBS were sized immediately (0 hrs), 0.5 hrs, 2 hrs, 4 hrs and 24 hrs post sonication. Polydispersity Indices (PDI), extrapolated from the Zetasizer are presented in **Appendix B.** Data presented as mean ± SEM (n=3) and were analysed by Two-way ANOVA followed by Tukey *post hoc*' s test for multiple comparisons. No statistically significant differences in UFCB size were observed across different dispersants over time.

Importantly, **Figure 3.1**, shows that the diameter of the surrogate UFCB particles measured in nanometres (d.n.m.) prepared in different dispersants, was almost double that expected for a PM 0.1 nanoparticle, which should be in the range of ≤ 100 nm as measured by DLS (Malm & Corbett, 2019).

UFCB size, in fact, was registered to be higher than expected in astrocytes media, however no significant difference in surrogate UFCB size was observed over time, indicating that particle coagulation was minimal. Particle size was also not significantly affected by dispersant type. Overall, despite some intrinsic limitations of DLS measurement (Malm & Corbett, 2019), the measurements obtained were still used in this project to provide an indication of the size of the surrogate UFCB and understand how stable the particle was once sonicated and suspended in media. Due it its' stability, the particle was used for the cell exposure experiments.

3.2 Visualising surrogate UFCB nanoparticles in cell culture

Primary astrocytic cells and differentiated NT2-derived neuronal-like cells were exposed to UFCB for 24 h and imaged. Although it was not possible to determine at a molecular level, the picture provided an indication on whether the nanoparticle coagulated with other factors present in cell culture 24 hrs post sonication. Considering the above physicochemical assessment (**Figure 3.1**), the surrogate UFCB nanoparticle should have not significantly coagulated over time in a suspension made by cell media and containing possible aggregates such as proteins. Consistent with this for both Human Primary Cortical Astrocytes (**Figure 3.2 B**) and NT2 neuronal like cells (**Figure 3.2 D**), the surrogate UFCB nanoparticle appeared uniformly aggregated and distributed across the plate surface; moreover, even if it was not possible to state categorically, the nanoparticle did not seem to associate exclusively with cells present on the plate surface.

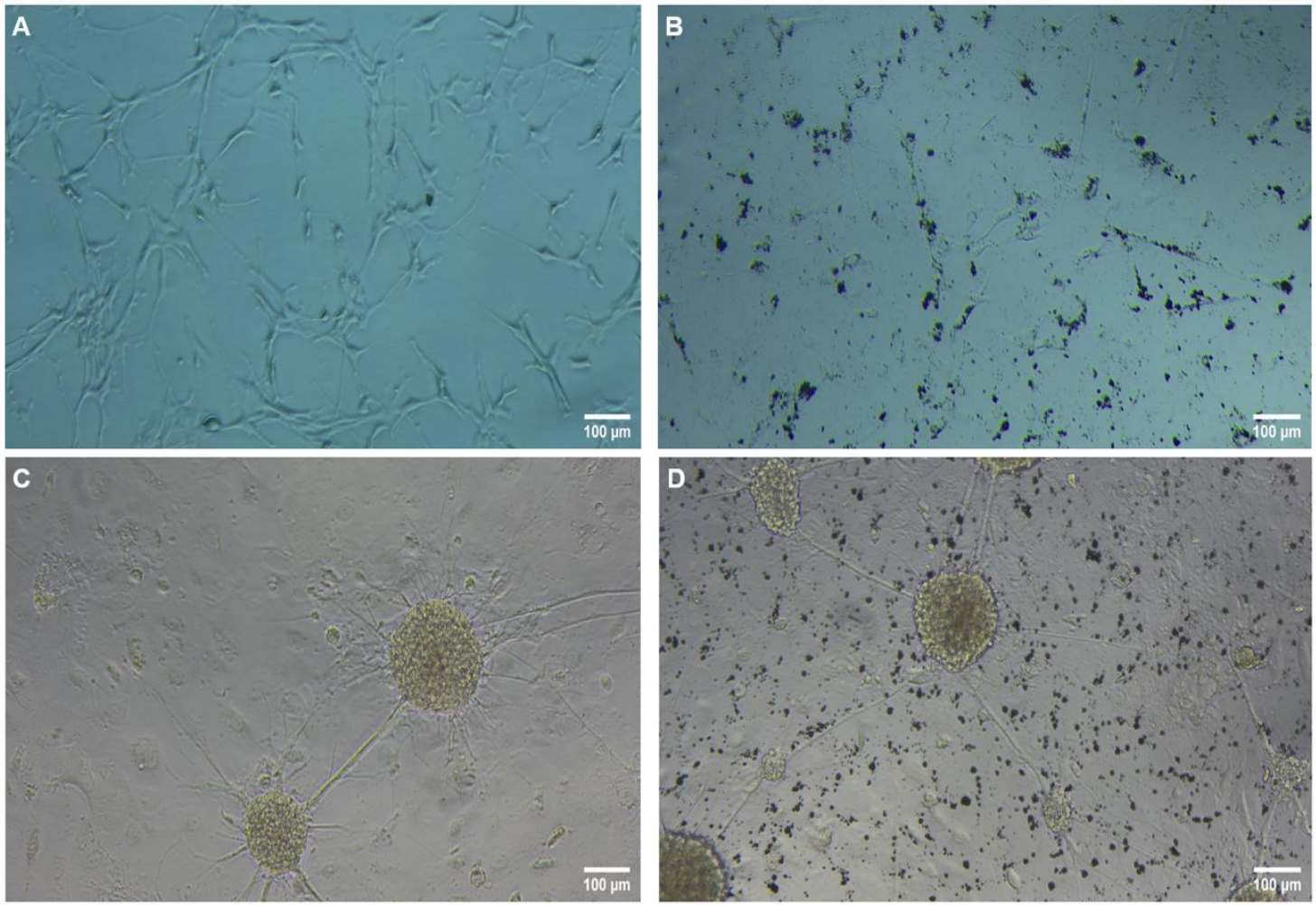

Figure 3.2. Deposition of surrogate UFCB nanoparticles in culture in Human Primary Cortical Astrocytes and NT2 neuronal like cells in culture. Human Primary Cortical Astrocytes in media **(A)** and exposed to 12.5 µg/ml UFCB for 24 hrs **(B)**. Cells were seeded in 12-well plates at a density of 1.5 x 10^4 cells per cm^2, and imaged 48 hrs post seeding. **(C)** Fully differentiated NT2-derived neuronal-like cells in media (C) and exposed to 12.5 µg/ml UFCB for 24 hours **(D)** in 12-well plates. See **section 2.4** for full differentiation and treatment methods and **section 3.7** for assessment of differentiation results. All cells were imaged using an Axiocam 208 colour microscope camera (Zeiss, UK). Magnification 100x. Scale bar added with ImageJ software.

3.3 Optimising conditions for measurement of cell viability using Human Primary Cortical Astrocytes

Following confirmation that UFCB was a suitable nanoparticle for toxicological assessments, the next step was to determine a suitable concentration range of UFCB nanoparticles for cytotoxicity experiments, using the colourimetric WST-1 Cell Viability Assay.

First, it was imperative to determine an appropriate cortical astrocyte cell density, and a suitable incubation time for optimal reduction of WST-1 to obtain absorption values to detect changes in cell viability in response to UFCB treatment (**Figure 3.3**). Cells seeded at three cell densities 6 x 10^4 cells per cm^2, 3 x 10^4 cells per cm^2 and 1 x 10^4 cells per $cm^{2.}$ in 96 well plates, as recommended by ScienCell and as previously optimised by the Kerr group and based on Ratcliffe et al., 2018, then absorbance readings were measured every 30 minutes for 4 hours, the maximum incubation time recommended by the manufacturer.

Previous evidence, from experiments within the Biomedical Sciences department at Edinburgh Napier University, demonstrated that surrogate UFCB, due to its dark colour, interferes with absorbance of WST-1 (data not published). Hence a wash step, using cell culture media, was included prior to addition of WST-1 reagent. As the additional wash may, itself, affect viability of primary cells, we also investigated whether washing significantly altered astrocyte viability compared to unwashed cells.

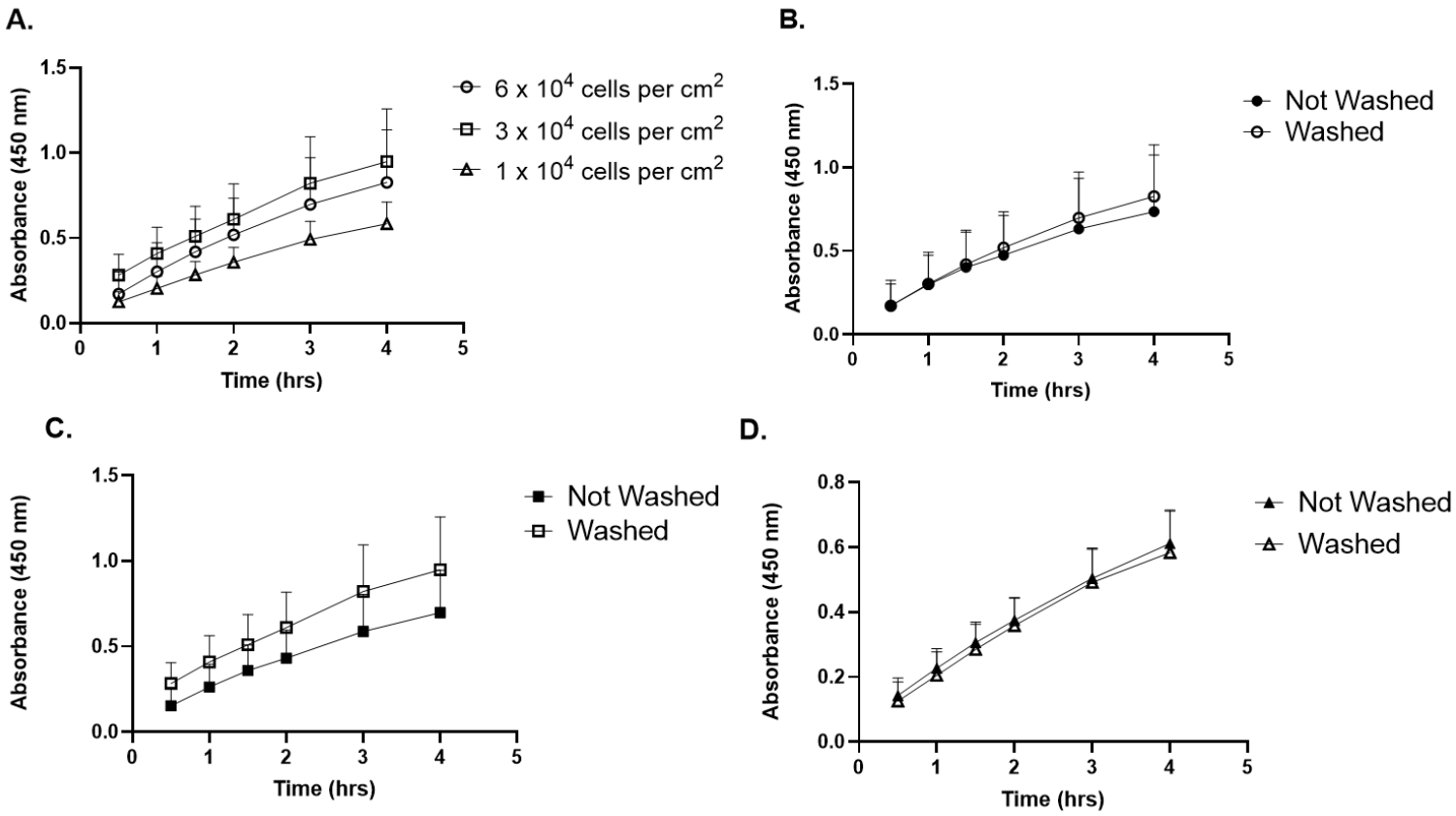

Figure 3.3. Optimisation of human cortical astrocyte seeding density and effect of wash step inclusion for WST-1 cell viability assays. Cell viability was assessed by WST1-assay, as indicated in the **methods section 4.7**, to compare three different cell seeding densities: 6 x 10^4 cells per cm^2, 3 x 10^4 cells per cm^2 and 1 x 10^4 cells per cm^2 in 96 well plates **(A).** The inclusion or exclusion of a wash step at each seeding density was also assessed for 6 x 10^4 cells per cm^2 (**B**), 3 x 10^4 cells per cm^2 (**C**) and 1 x 10^4 cells per cm^2 (**D**). Data presented as mean ± SEM (n=3) and were analysed by Two-way ANOVA followed by Tukey *post hoc*' s test for multiple comparisons. Alterations in absorbance of WST-1 over time were statistically significant only for C ($p= 0.0491$) and D ($p <0.0001$) but, importantly, there were no significant differences in cell viability between different cell densities (**A**) or cells exposed to washing vs. not washing at any density (for all p values and pairwise comparison refer to table 2 in **Appendix C).**

As stated, the only factor that did seem to affect absorbance readings was **time** for cell density 3 x 10^4 cells per cm^2 ($p=0.0491$) and 1 x 10^4 cells per cm^2 ($p<0.0001$) suggesting that over time, cells grew and kept metabolising WST-1. Although the absorbance values did not plateau (Figure **3.3 A-D**), after a 2 h incubation time, at all three cell densities, optimal absorbance values falling in the middle of the slope were produced, therefore, enabling scope for measurement of increases or decreases in viability through reduction of WST-1 reagent. Hence all subsequent incubations for Human Primary Cortical Astrocytes cells were performed with 2 h WST-1 incubation time. As there were no significant differences in cell viability at different cell densities (**Figure 3.3 A**), and all absorbance values were within the manufacturer's recommended range of above 0.2 absorbance units after 2 h, further studies were performed using the lowest cell density (1 x 10^4 cells per cm^2) thus, maximising the number of possible experimental conditions for each experiment from any one flask of human primary cells.

3.4 Assessing cytotoxicity of surrogate UFCB nanoparticles on Human Primary Cortical Astrocytes viability using the WST-1 assay

Once the optimal cell seeding density, incubation time and the size/deposition rate of the surrogate nanoparticle were determined, cytotoxicity of UFCB nanoparticles on Human Primary Cortical Astrocytes was assessed via the WST-1 assay. This aimed to establish sub-lethal concentrations likely to modify astrocyte function and perhaps induce reactivity, without inducing overt cell death, as would be observed in neurodegenerative conditions (Liddelow et al., 2017). Determining a concentration range similar to that of circulating levels of nanoparticles in the air is essential to ensure accurate results and to improve translatability.

Previous intra-department experiments at Edinburgh Napier University have assessed nanoparticle interference in viability assays, thus, three controls were introduced to the WST-1 assay to ensure accuracy and each control was included to monitor a different type of signal interference.

As it is known that UFCB does interfere with viability assay reagents (Monteiller et al., 2007; Monteiro-Riviere et al., 2009;), a “No cells, WST-1” control was designed to capture a possible increase in absorbance even in the absence of cells (**Figure 3.4 A**). In addition, a “Cells and No WST-1” control was used to account for the possible interference between cells and UFCB, present in the cell media suspension, in the absence of the redox reagent WST-1 (**Figure 3.4 B**). Lastly, due to its colour, UFCB alone might have generated an absorbance reading, so a “No cells, No WST-1” control was included (**Figure 3.4 C).**

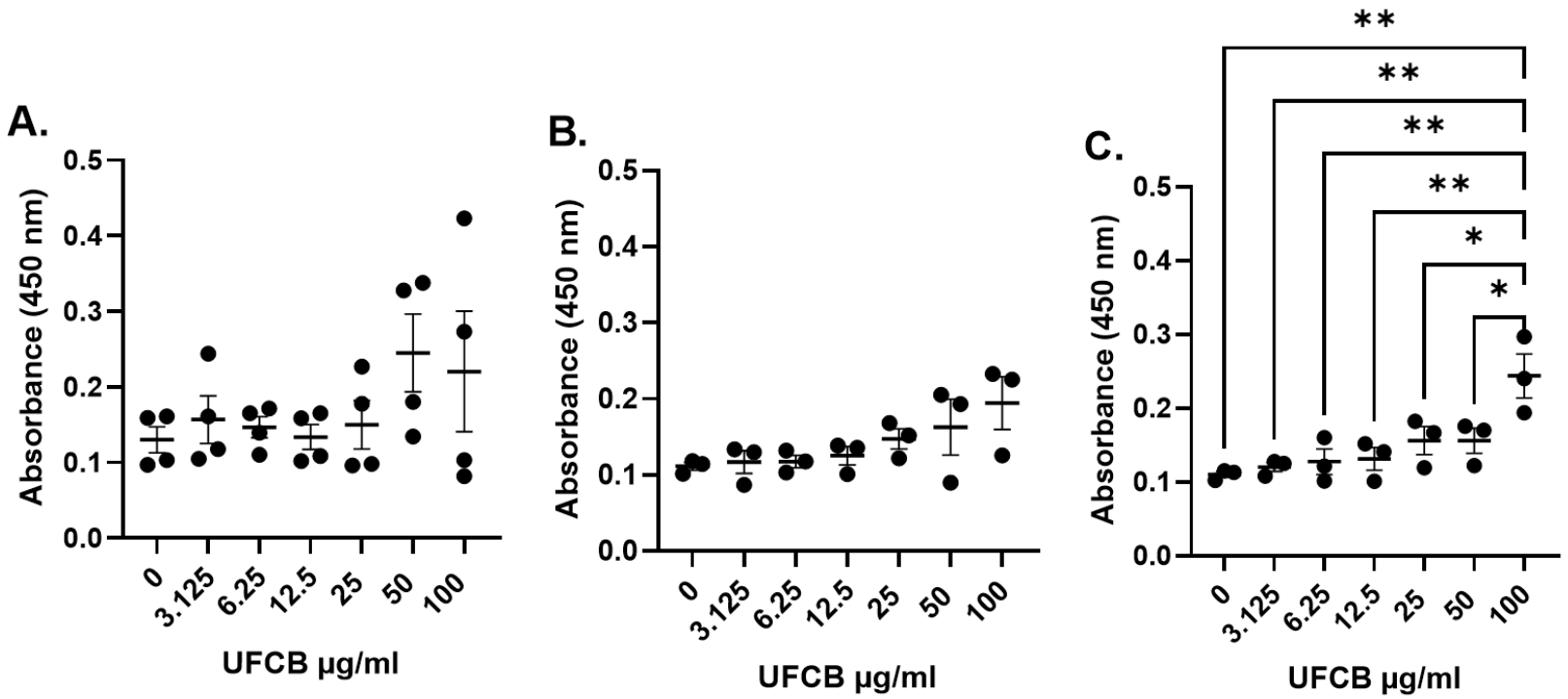

Figure 3.4. Assessment of UFCB Nanoparticle interference in the WST-1 assay. In order to determine if UFCB interfered with signal production in the WST-1 assay, a number of controls were introduced where assays for UFCB-treated Human Primary Cortical Astrocytes cells were conducted in the absence of cells **(A)**, in the absence of WST-1 reagent **(B)**, and in the absence of cells and WST-1 reagent **(C)**. Data presented as means ± SEM and were analysed by One-Way ANOVA followed by Tukey *post hoc*' s test for multiple comparisons (n = 3 except **A**, n=4). In the absence of cells (**A**), although not statistically significant, a slight upward trend in absorbance readings, and so interference, can be seen at 100, 50 and 25 µg/ml UFCB. Although not statistically significant, higher UFCB concentrations (100 and 50 µg/ml), resulted in high absorbance readings independent of WST-1 reduction **(B)**. Conversely, a statistically significant difference in absorbance was registered independently from both WST-1 and cells being present in suspension **(C**; p= 0.0017). In the graph: * = p< 0.05; ** = p <0.01.

Overall, from **Figure 3.4 A-C**, UFCB can interfere with the WST-1 assay, at high concentrations, by interacting with cells without substrate, directly reducing WST-1 and directly through absorption due to the nanoparticle suspension itself in the colorimetric assay. As these factors are all incorporated into the “No cells, WST-1” control (**Figure 3.4 A**), deemed the closest control to experimental conditions, the OD values resulting from this data set were then used to correct the absorbance values from the experimental data, as presented in **Figure 3.5.**

To correct the data, the OD values from the technical replicates of the “No cells, WST-1” control were first averaged for each biological repeat. These values were then subtracted from the average OD of the technical replicates for each experimental condition (0, 3.125, 6.25, 12.5, 25, 50 and 100 µg/ml of UFCB) . Corrected data from biological repeats was then averaged and used to test statistical significance of any differences in viability (see Figure 3.5).

A UFCB nanoparticle concentration range was designed based on previous evidence of physiologically relevant concentration ranges. These were between 0.001 - 400 µg/ml for primary mouse hepatocytes (Zhang et al., 2019) and 5 - 55 µg/ml and 10 - 80 µg/ml for mouse primary splenocytes (Schien et al., 2021). Extrapolating from these published values, the UFCB concentration range used in our study was 0 -100 µg/ml (**Figure 3.5**).

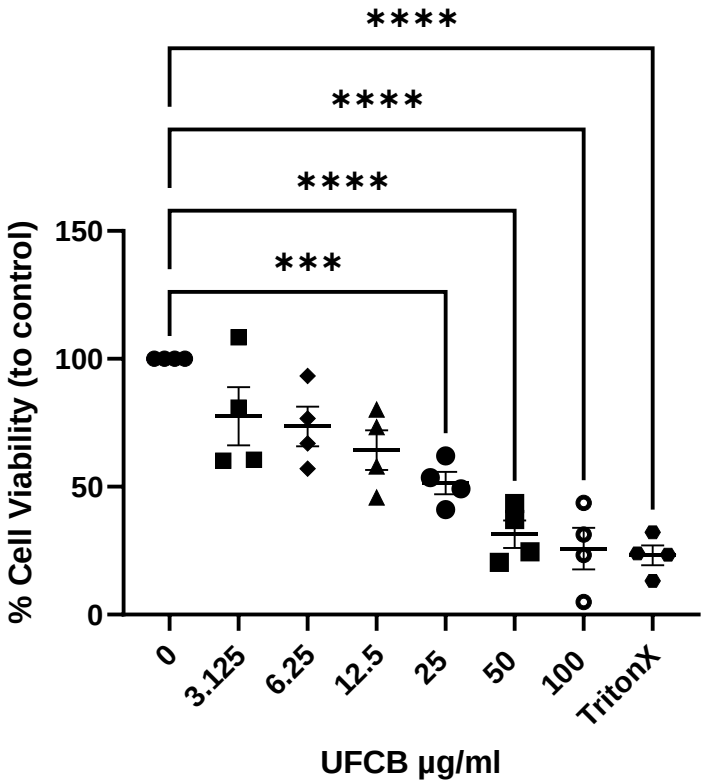

Figure 3.5. Assessment of Human Primary Cortical Astrocyte viability after UFCB exposure via WST-1 cytotoxic assay. Cell viability is expressed as percentages corrected/normalised to the control (whereby 0 µg/ml = 100% viable cells; these data was corrected for the **"No cells WT-1"** control above in **figure 3.4 A).** Data presented as means ± SEM and were analysed by One-Way ANOVA with Tukey *post hoc*' s test used for multiple comparisons test (n=4). Significance differences are shown only in relation to control. In the graph: *** p< 0.01; **** p<0.001 (Tukey's *post-hoc*)**.**

Figure 3.5 clearly shows that astrocyte viability decreases in a dose-dependent manner, inferring that higher concentrations (≥ 25 µg/ml) of the surrogate UFCB nanoparticle are extremely toxic to astrocytic cells, reducing cell viability, compared to control, by 85% (100 µg/ml, p<0.0001), 70% (50 µg/ml, p<0.0001), 49% (25 µg/ml, p= 0.0009) and, although not statistically significant, by 46 % for 12.5 µg/ml (p = 0.0227) respectively.

As depicted by all pair-wise comparisons in Appendix D, no statistically significant difference was measured between the highest UFCB doses (100 and 50 µg/ml) and the positive control TritonX (0.1%) in which negligible viability is detectable suggesting that perhaps UFCB is completely toxic to the cells at those concentrations. No statistically significant difference was also registered in terms of viability between 0, 3.125 and 6.25 µg/ml, suggesting that acute exposure to low concentrations of the surrogate nanoparticle is not necessarily cytotoxic.

To select doses that are more likely to re-capitulate what is observed in the brain, in neurodegenerative disease states, such as astrocyte reactivity, UFCB sublethal doses were determined. Lethal Dose 50 (LD50) and Lethal Dose 25 (LD25), were calculated to then derive concentrations that would not necessarily lead to overt cell death and could provide a starting point for further testing. The LD50 is theoretically higher than the concentration corresponding to the point of departure, which is the point from which cell viability quickly decreases in response to toxins and it corresponds to half of the maximum absorbance of reduced WST-1 in the presence or absence of UFCB. This concentration was determined statistically using a series of calculations performed with GraphPad Prism 9 (**Figure 3.6 A-B**).

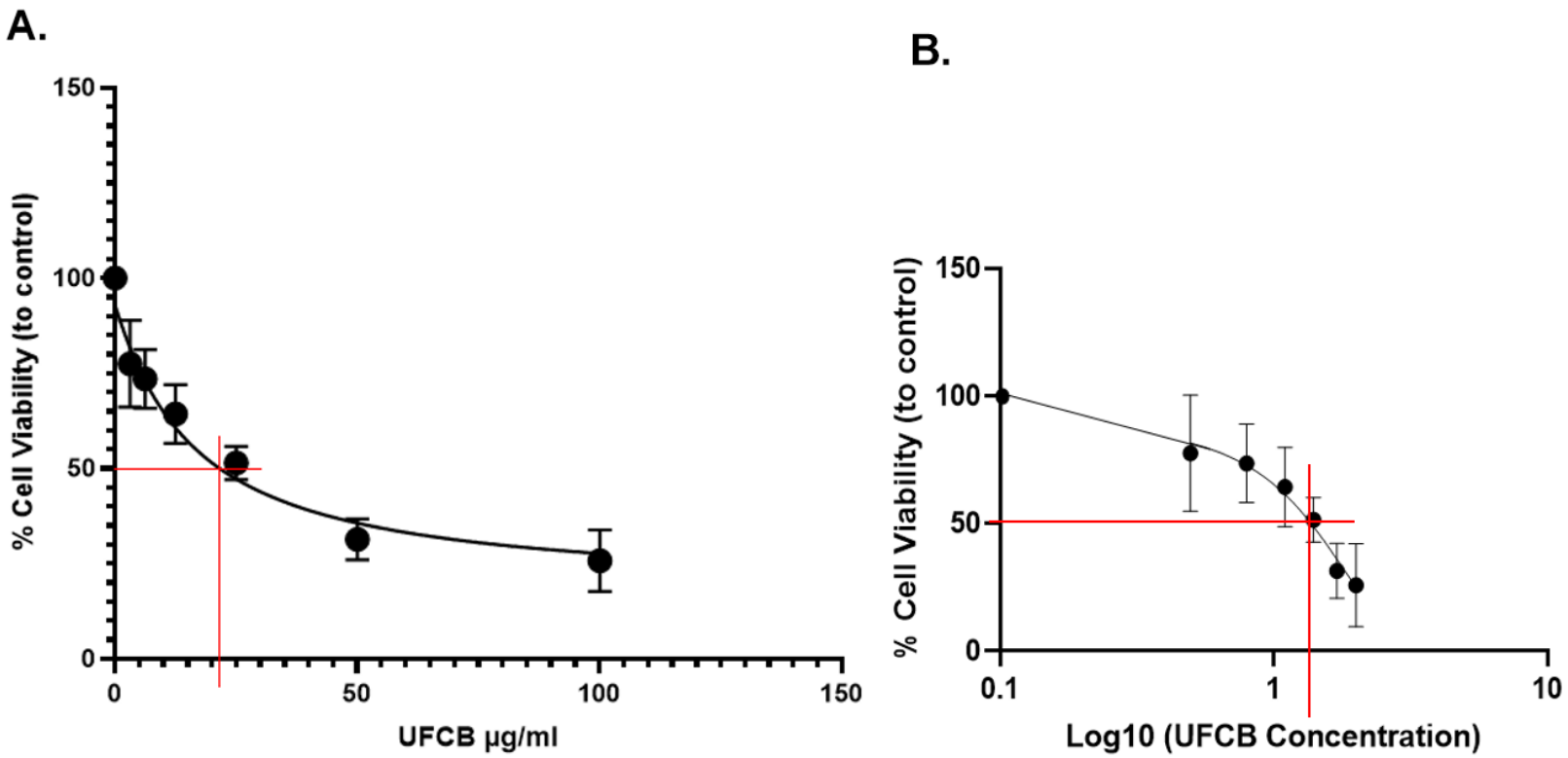

Figure 3.6. Assessment of Lethal Dose 50 after UFCB exposure on Human Primary Cortical Astrocytes derived from viability measurements. (A) Not transformed and (B) transformed and restructured in Log10. GraphPad Prism 9 Curve fitting to determine the **LD50** resulted in two similar – yet – different values: **(A) 16.42 µg/ml,** with a **R^2 of 0.7699 and (B) 24.02 µg/ml** with a **R^2 of 0.7822.** Note that the difference in the two LD50 is due to the transformation of the data. R^2 values indicate how close the data are to the regression line.

As it is possible to see from the graph in **Figure 3.6 A**, the LD50 dose corresponds to circa 25 µg/ml. **As it is standard practice to log transform data to obtain a straight line for more accurate analyses** (Feng et al., 2014), the LD50 chosen was the one with the data re-structured, transformed and expressed in logarithm scale – i.e., **24.02 µg/ml, which appeared to be marginally more accurate than the untransformed data (16.42 µg/ml) due to the slightly higher R^2 value** (Chicco et al., 2021).

This is because oftentimes, if nanoparticles effects on cell viability are graphed, the equation line they produce might almost never yield a perfect sigmoid curve (Dowson et al., 2012) as the result of these particles on cell viability not always result in cell death in a dose dependent manner as interference of the particle might skew the results Hence why most data are usually log transformed. However, in this case, only a small difference in LD50 values was registered.

Nonetheless, 24.02 µg/ml was chosen as the "maximum" concentration to start looking for any observable cell effects. However, considering that half of the cell population is technically dead at 25 µg/ml, the maximum UFCB concentration for exposure was lowered at 12.5 µg/ml – a dose half way between the point of departure and LD50 to ensure cellular responses without overt cell loss. Moreover, even if 12.5 µg/ml was chosen as the maximum concentration to start looking for reactivity**,** the real LD25, although not used, was still determined using GraphPad Prism 9 for comparison. This corresponded to 5.68 µg/ml.

Technically, this concentration determined mathematically, would have not produced any statistically significant difference in terms of viability if compared to the control as the 6.125 µg/ml, a higher and already tested concentration, didn't (**see Figure 3.5**). As stated, the effects of nanoparticles on cell viability are oftentimes very unpredictable, leading to contradictory conclusions. Understanding lethal and sublethal doses with this surrogate particle is necessary for protocol optimisation but also for standardising testing practices for future experiments.

Based upon this set of experiments, the concentrations that were brought forward for further reactivity testing were 0, 3.125 µg/ml, which would have ensured viable cells present, and 12.5 µg/ml, which could have ensured cellular responses and increase the likelihood of observing reactivity and polarisation of astrocytes.

Moreover, as a positive control for astrocyte reactivity, based on previous evidence (Brahmachari et al., 2006; Jurga et al., 2021), cells were also exposed to 1 µg/ml of Bacterial lipopolysaccharides (LPS).

3.5 Assessing gene expression changes in Human Primary Cortical Astrocytes after UFCB exposure with qRT-PCR

To investigate whether UFCB exposure led to reactivity in primary astrocytes, expression of key genes associated with polarisation were analysed via quantitative (q) RT-PCR to determine specific astrocyte subtypes. Well documented housekeeper gene GAPDH was used for normalisation of data (Kreth et al., 2010; Nazet et al., 2019) alongside RPLPO, a gene used for previous experiments with astrocytes within the Biomedical Sciences department at Edinburgh Napier University. To determine if exposure to UFCB nanoparticles induces reactivity in cortical astrocytes, a well-established reactive astrocyte marker, Glial fibrillary acidic protein (GFAP), was included in the expression analysis (Gomez- Budia et al., 2020). Changes in astrocyte polarisation were measured for co-expression of a panel of specific neurotoxic and neuroprotective associated gene markers. The A2 neuroprotective marker S100A10 was chosen as it is a calcium binding protein, proven to be exclusively expressed by A2 reactive astrocytes (Liddelow et al., 2017) and devoted to cell proliferation and tissue repair. LCN2 and GBP2 were both chosen as markers for the A1 neurotoxic types as they were seen to be upregulated exclusively in A1 reactive astrocytes which were seen to promote neuronal death (Bi et al., 2013; Ugalde et al, 2020).

Prior to complementary (c)DNA synthesis, the integrity and quality of RNA isolated from Human Primary Cortical Astrocytes exposed to 0, 3.125 and 12.5 µg/ml UFCB and 1 µg/ml LPS (n=3), was assessed with the Agilent 2100 Bioanalyzer to ensure quality and integrity. During analysis, RNA Integrity Numbers (RINs) (**Table 3.1)** and gel images (**Figure 3.7**) were collected.

Table 3.1. Agilent 2100 Bioanalyzer results including RNA concentration ng/µl and RIN numbers.

Sample	RNA Concentration (ng/µl)	RIN
N=1		
0 µg/ml UFCB	148	10
3.125 µg/ml UFCB	144	10
12.5 µg/ml UFCB	119	10
LPS	153	10
N=2		
0 µg/ml UFCB	202	10
3.125 µg/ml UFCB	159	10
12.5 µg/ml UFCB	153	9.90
LPS	262	9.80
N=3		
0 µg/ml UFCB	106	10
3.125 µg/ml UFCB	370	10
12.5 µg/ml UFCB	185	10
LPS	95	10

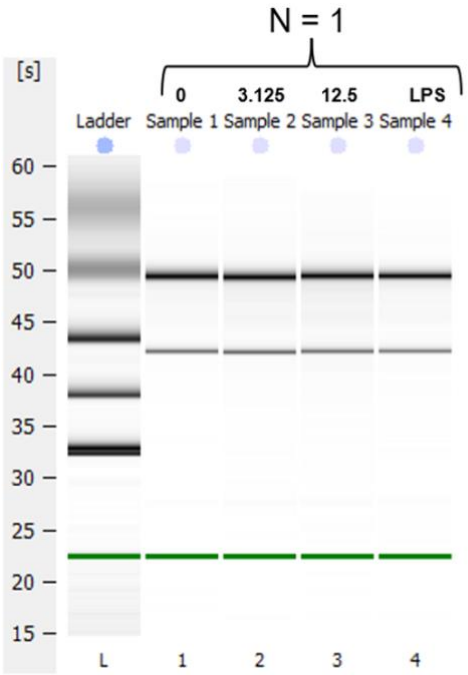

Figure 3.7 Representative gel figure (n=1) obtained with the Agilent 2100 Bioanalyzer. The content of wells is: **(A)** Well 1: 1 µl of Agilent RNA 6000 Nano Ladder; Well 2: 1 µl of sample 0 UFCB; Well 3: 1 µl of sample 3.125 µg/ml UFCB; Well 4: 1 µl of sample 12.5 µg/ml UFCB; Well 5: 1 µl of sample LPS (1 µg/ml).

As per MIQE guidelines (Bustin et al., 2009), to determine correlation coefficients (R^2), slope efficiency values and optimal concentrations of cDNA for gene expression analysis, real-time amplification was performed over a 2-fold standard curve. Starting concentrations varied, as indicated (see **Figure 3.8**), depending on the level of basal expression of each gene in control astrocytes. ROX reference dye was used for the normalisation of well-to-well optical variation.

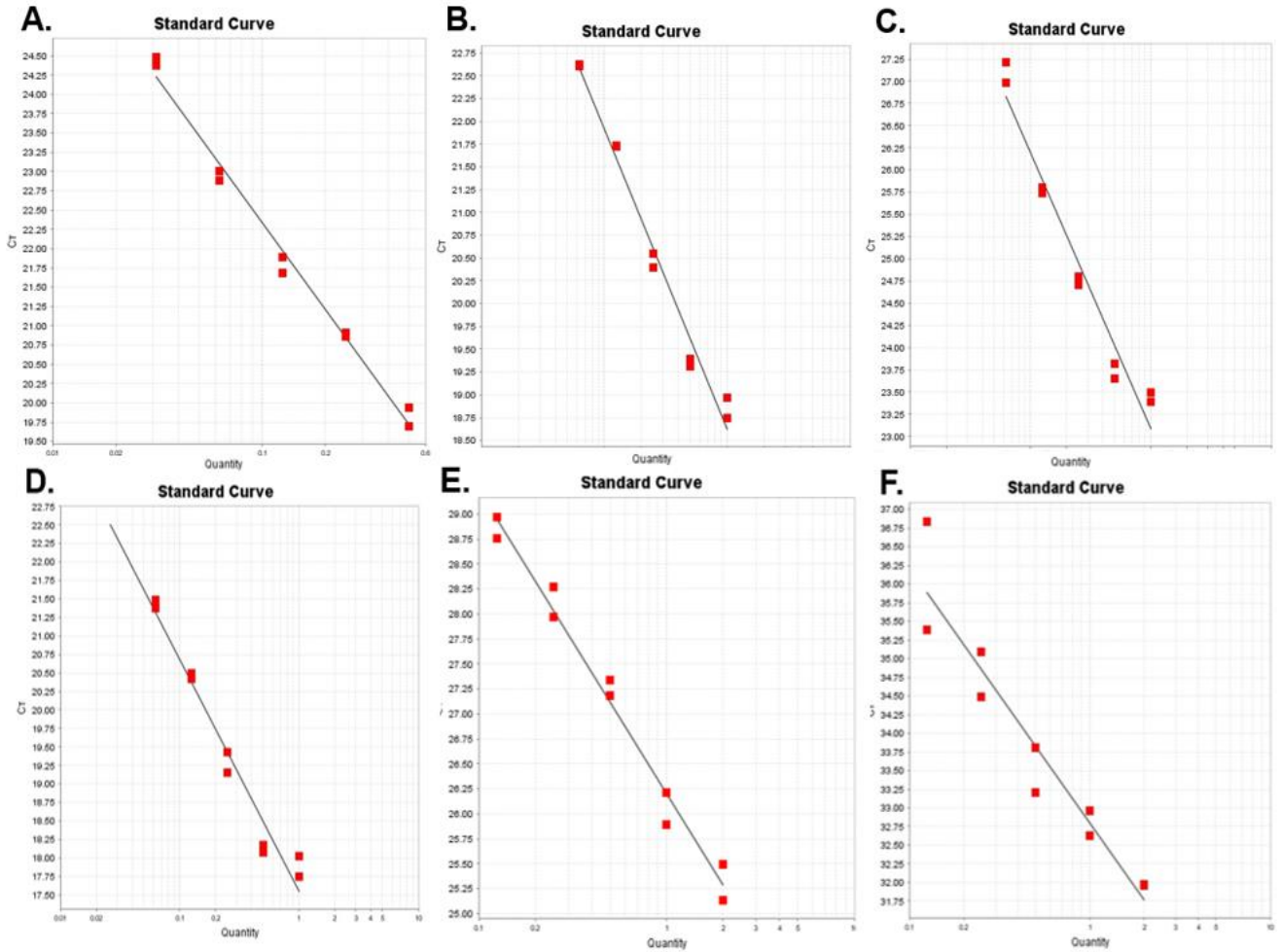

Fi**gure 3.8. Standard Curve optimisation of primers targeting GAPDH (A), RPLPO (B), housekeepers and GFAP (C), S100A1 (D), LCN2 (F) and GBP2 (E) target transcripts.** cDNA from untreated control cortical astrocytes was used to generate 1:2 serial dilutions, whereby each point represents each of the standards**.** All primer concentrations were kept constant at 200 nM for both forward and reverse. The standard curve for GAPDH, RPLPO, GFAP & S100A10 started at 40 ng/µl (n = 2). For GBP2 (n = 3) and LCN2 (n = 2), the standard curve started from 80 ng/µl.

Efficiency (E) values and correlation coefficients derived from the standard curves are reported below in **Table 3.2.**

Table 3.2. Efficiency values and correlation coefficients (R^2) for the primer sets tested with standard curves.

GOI	Efficiency values	R^2
GAPDH	84	0.989
RPLPO	101.6	0.982
GFAP	109.9	0.96
S100A10	108.5	0.96
LCN2	96	0.919
GBP2	113	0.98

All primer sets successfully optimised (aside from GAPDH), as they all registered efficiency values close to 110 with acceptable R^2 values above 0.9 threshold. For each standard curve a No Template Control (NTC) was included and did not show any unspecific amplification.

When the E values are lower than 90%, it normally signifies that the template taken into consideration is not doubling at each replication cycle and the problem might be in primers not being properly designed or their melting temperatures (Tm) not being adequate for those specific primers set or there could be the formation of hairpins or primer dimers (Taylor et al., 2019). This could have resulted in E values lower than 90% for primers such as GAPDH (**Figure 3.8 A**). However, the melt curve for GAPDH (**Appendix A**) did not show the presence of primer dimers as only one amplicon was present, suggesting that perhaps results should be confirmed using a newly designed GAPDH primer set. The primer concentration of GAPDH was, subsequently, increased to 250 nM for both forward and reverse. This concentration had already been tested intra-department and reported as efficient.

Lastly, as it is the case for both LCN2 and GBP2 (**Figure 3.8 E-F**), better care when pipetting should have been applied to avoid repeats on the slope being too far apart. To improve pipetting, the standard curves for both primer sets were repeated multiple times (see **Appendix D**) always obtaining the same result.

Overall, from the standard curve analysis, three different cDNA concentrations were selected for gene expression analysis. These were 10 ng/µl for GAPDH, RPLPO, GFAP and S100A10, 40 ng/µl for GBP2 and 80 ng/µl for LCN2, with all the primer sets, except for GAPDH, being in a final concentration of 200 nM.

Following optimisation of the oligonucleotides and the cDNA concentrations, qPCRs were run to confirm changes in polarisation and to try to determine any specific astrocyte subtypes appearing following UFCB exposure. All data was normalised to the geometric mean of the two housekeepers GAPDH, RPLPO, which were stably expressed across all treatment conditions (**Figure 3.9 A- B**).

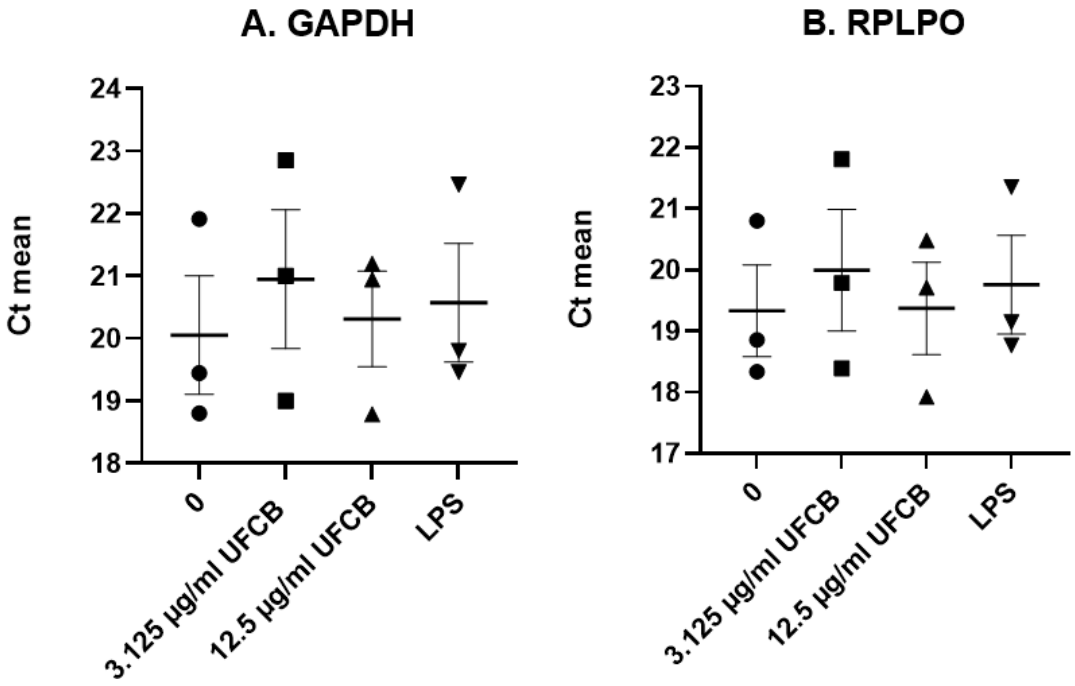

Figure 3.9. Expression analysis of GAPDH (A) and RPLPO (B) in astrocytic cells left untreated (0 – control), exposed to UFCB (3.125 and 12.5 µg/ml) and exposed to LPS (1 µg/ml – positive control for reactivity). Symbols represent biologically independent data-points and horizontal lines the mean +/-SEM and were analysed by One-Way ANOVA followed by Tukey *post hoc*' s test for multiple comparisons (n = 3). Both genes were used as housekeepers as no statistically significant difference (GAPDH, p=0.91900 and RPLPO, p=0.9292) in expression was observed between any of the conditions tested, indicating their stability across experimental samples and conditions**.**

Changes in astrocyte polarisation were measured for co-expression of a panel of specific markers including reactive astrocytes marker GFAP (**Figure 3.10 A**), neuroprotective A2 marker S100A10 (**Figure 3.10 B**) and neurotoxic A1 marker genes GBP2 and LCN2 (**Figure 3.10 C-D)**.

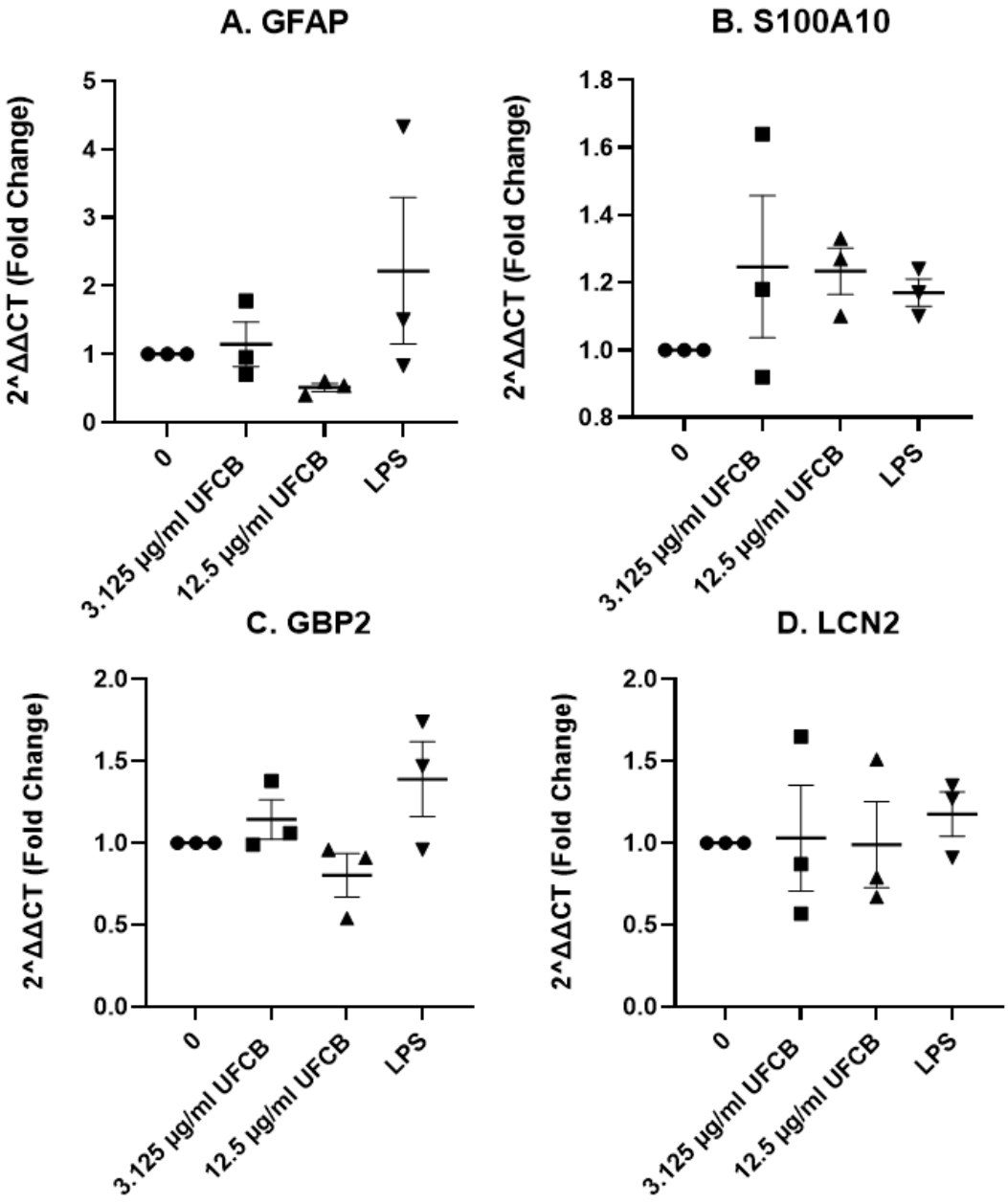

Figure 3.10. Gene Expression analysis of UFCB-treated cells. Transcripts associated with astrocyte reactivity and polarisation were analysed. GFAP (A) to test for general astrocyte reactivity, **S100A10 (B)** to test for neuroprotective reactive astrocytes subtype A2 and **GBP2 (C)** and **LCN2 (D)** to test for neurotoxic reactive astrocyte subtype A1. Data presented as mean ± SEM and were analysed by One-way ANOVA followed by Tukey *post hoc*' s test for multiple comparisons (n = 3).

To investigate differences in expression across samples, fold change – normalised to housekeeper genes – was analysed. Although no statistically significant difference in gene expression has been registered across samples for all genes, some clear upward and downward trends in expression are visible. No statically significant difference in expression was observed across samples for both GAPDH and RPLPO, demonstrating their stability and suitability as housekeeper genes (**Figure 3.9 A-B**).

As stated, for each gene tested, also no significant difference in expression across samples was registered with any statistical tests, yet this can be attributed to a very low sample size. Nonetheless, defined trends can be observed within each gene analysis.

GFAP expression (reported in **Figure 3.10 A**) trended after LPS exposure and after exposure to 3.125 µg/ml of UFCB, GFAP expression increased by 14% compared to the control while, interestingly, it was reduced by 49% compared to the control after exposure to 12.5 µg/ml UFCB (**Figure 3.10 A**). An interesting set of trends was observed with the A2 specific marker gene S100A10 (**Figure 3.10 B**), where a slight increase in expression was seen after exposure to both 3.125 (24% more compared to the control) and 12.5 µg/ml (23% more compared to the control) UFCB. LPS stimulation, although still not significant, also exerted a slight increase in S100A10 gene expression compared to control. Expression of the neurotoxic A1 gene, GBP2, **(Figure 3.10 C)** appeared to trend slightly upward registering a 14% increase compared to the control after exposure to 3.125 µg/ml of UFCB and LPS while 12.5 µg/ml UFCB exposure led to a 20% decrease. Comparatively, the other A1 neurotoxic marker LCN2 **(Figure 3.10 D)** showed negligible expression in all conditions, save for LPS exposure, which led to a marginal 18% increase in expression compared to the control.

Further work is required to repeat these experiments in order to form conclusions. But the these preliminary data may suggest reactive astrocytic cells respond after being exposed to sublethal concentration of UFCB by assuming a more neuroprotective phenotype, thereby increasing S100A10 expression. However, UFCB sublethal dose 3.125 µg/ml also slightly increased in neurotoxic GBP2 levels in some experiments, suggesting that the astrocytic cell population might not uniformly respond to UFCB exposure.

3.6 Assessing inflammatory responses with ELISA assay for pro-inflammatory cytokine LCN2 and the anti-inflammatory marker IL-6

Following qRT-PCR analysis, to try and infer a link between increase expression of neuroprotective or neurotoxic genes and to assess any possible neuroinflammatory response, the protein levels of two pre-selected markers, LCN2, pro-inflammatory and IL-6, anti-inflammatory, were measured in all experimental samples using an enzyme-linked immunosorbent assay (ELISA). LCN2 was selected as its' gene expression and protein secretion are almost always associated with pro-inflammatory stimuli or insults of the CNS (Taklimie et al., 2019). Contrarily, IL-6 was chosen as anti-inflammatory marker, as it has been assessed as neurotrophic factor which has been seen to protect and promote neuronal survival *in vitro* (Hama et al., 1991; Borsini et al., 2020).

Standard Curves were generated for both proteins (**Figure 3.11 A** and **B**) and used to extrapolate protein levels, using equation of the straight line, in astrocyte conditioned media only for IL-6 (**Figure 3.11 C**).

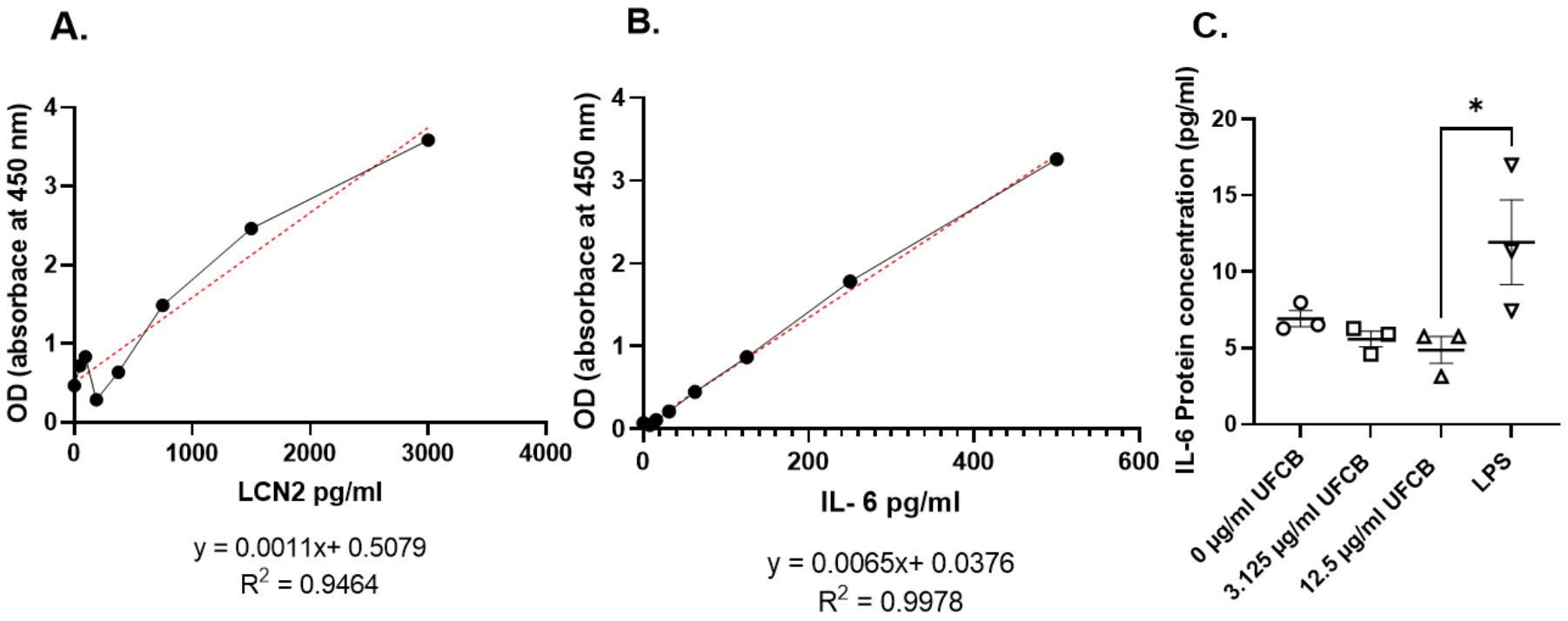

Figure 3.11. ELISA generated Standard curve for LCN2 (A) and IL-6 (B). Equation of the line and R^2 values for each marker tested are specified in each graph. In the graphs, a best fit line (in red) has been added with GraphPad Prism 9 Software. **(C) IL-6 Protein concentration calculated from the equation of the line y=0.0065x + 0.0376 obtained from the IL-6 Standard Curve for all samples (n=3).** Data are presented as means ± SEM and were analysed by One-way ANOVA followed by Tukey *post hoc*' s test for multiple comparisons. *p <0.05

LCN2 levels secreted into conditioned astrocyte media were below the limit of detection of the assay under all treatment conditions. Contrarily, the levels of IL-6 (**Figure 3.11 C)** derived from the standard curve (**Figure 3.11 B**), although very low, were detectable in the astrocyte conditioned media for all samples. LPS samples for all three independent experiments registered the highest levels overall with an average of 11.92 pg/ml. Levels of IL-6 in UFCB conditioned samples were reduced by 1-fold in samples exposed to 3.125 µg/ml and 2- fold in samples exposed 12.5 µg/ml compared to the control ones. A significant difference in IL-6 expression was only registered for the LPS samples compared to the UFCB 12.5 µg/ml ($p= 0.0418$). Although not statistically significant, a net increase in IL-6 expression was observed in the LPS samples compared to both 3.125 µg/ml and the control samples.

3.7 Assessing UFCB effects on NT2-derived neuronal-like cell viability

The last objective of this research was to investigate if the effects of UFCB exposure were likely to be neurotoxic, either directly to neurons or indirectly via neuroinflammatory responses from UFCB-induced astrocytes. Due to resource restrictions, NT2 cells, were differentiated into neuronal-like cells with the use of All-Trans-Retinoic-Acid (ATRA) and mitotic inhibitors (cytosine arabinose, CA, and fluorodeoxyuridine, FUDR) for 6 weeks using published methods already optimised in our department (Martín-Aragón Baudel et al., 2017; Pleasure et al., 1992; **Figure 3.12 A-D**).

Changes in morphology, typical of the differentiation process, can be seen appearing as soon as the second week of ATRA treatment, where the cells tend to first cluster and clump together (circled in blue in **Figure 3.12 B**) and then, between week 4 and week 6, they tend to form round like structures (indicated by the red arrows in **Figure 3.12 C**), developing lastly axon-like and ganglion-like structures (indicated by the black arrows **Figure 3.12 D**).

To determine differentiation, cells were immunostained for the neuronal specific marker β (beta) 3 tubulin, alongside DAPI blue for the cell's nuclei, to then be visualised with fluorescent microscopy (**Figure 3.13 A- B**).

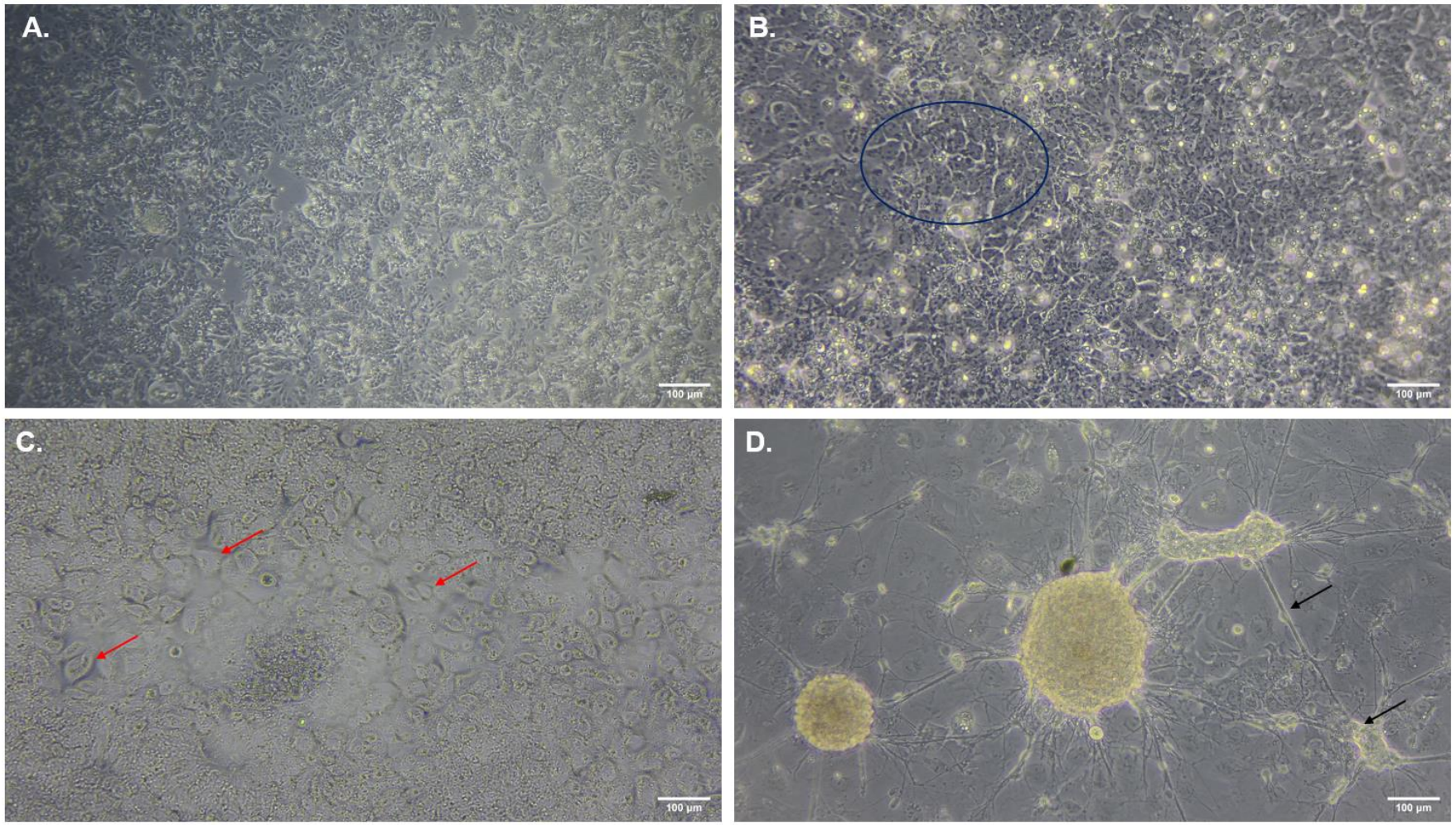

Figure 3.12. Images of different differentiation stages of NT2 neuronal-like cells. (A) NT2 neuronal like cells week 1 of ATRA treatment; Magnification 100x **(B)** NT2 neuronal like cells week 3 of ATRA treatment; Representative cell cluster is circled in blue; Magnification 200x **(C)** NT2 neuronal like cells week 5 of ATRA + CA/FUDR treatment; Representative round-like structure typical of week 4-6 of differentiation are indicated by red arrows; Magnification 200x **(D)** Fully differentiated and seeded in 96 well plates NT2 neuronal like cells week 7; Representative axon and Ganglion-like structures are indicated by black arrows; Magnification 200x. Images taken with the Axiocam 208 colour microscope camera (Zeiss, UK). Scale bar added with ImageJ software.

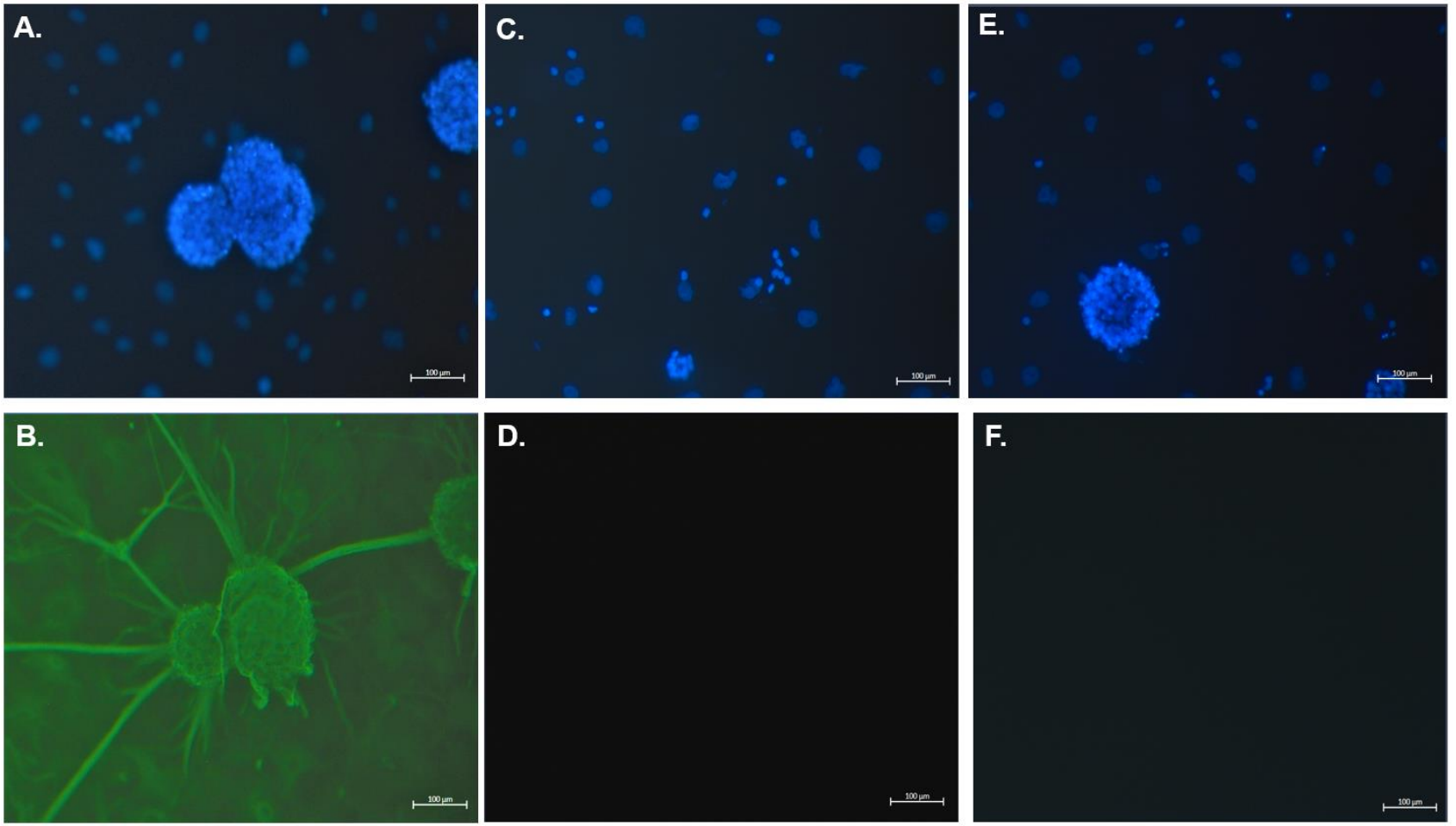

Figure 3.13. Representative Immunofluorescent images of differentiated NT2 cells. Cells were stained with DAPI nuclear stain (**A.** blue) and antitubulin β3 (**B.** green), followed by a fluorescent secondary antibody (goat anti-rabbit). Primary and secondary antibody specificity was determined by looking at different controls/ immunostaining combinations such as Primary and Secondary Antibody (**A- B**), only Secondary Antibody (**C- D**) and No antibody (**E- F**) as well as the general nuclear stain DAPI (blue). Scale bar = 100 μM**.** N= 1.

Although the NT2 derived neuronal-like cells were stained and visualised with the neuron- specific anti-Tubulin β3, some other cells can be seen in the background (**Figure 3.13 B)** suggesting that the staining was not specific. This could have been due to the presence of undifferentiated cells which should have been removed by the mitotic inhibitors cytosine β-D-arabinofuranoside (C-Ara) and FUDR. Overall, the morphology of many cells present resemble the neuronal like, but differentiation may have only been partially successful. Moreover, possibly fresh inhibitors are needed, in the future, to prevent unspecific cell growth.

As NT2 cells were differentiated and validated by immunostaining for neuronal-specific markers, the final objective of this research was to assess whether astrocytic responses previously observed would ultimately lead to neurodegeneration or neuroprotection. Neuronal viability was measured by directly exposing fully differentiated NT2-derived neuronal like cells to the same UFCB concentrations established from the astrocyte experiments (0, 3.125 and 12.5 µg/ml; **Figure 3.14 A**) and to UFCB-induced reactive astrocytes conditioned media (**Figure 3.14 B**) to assess viability with the WST-1 assay.

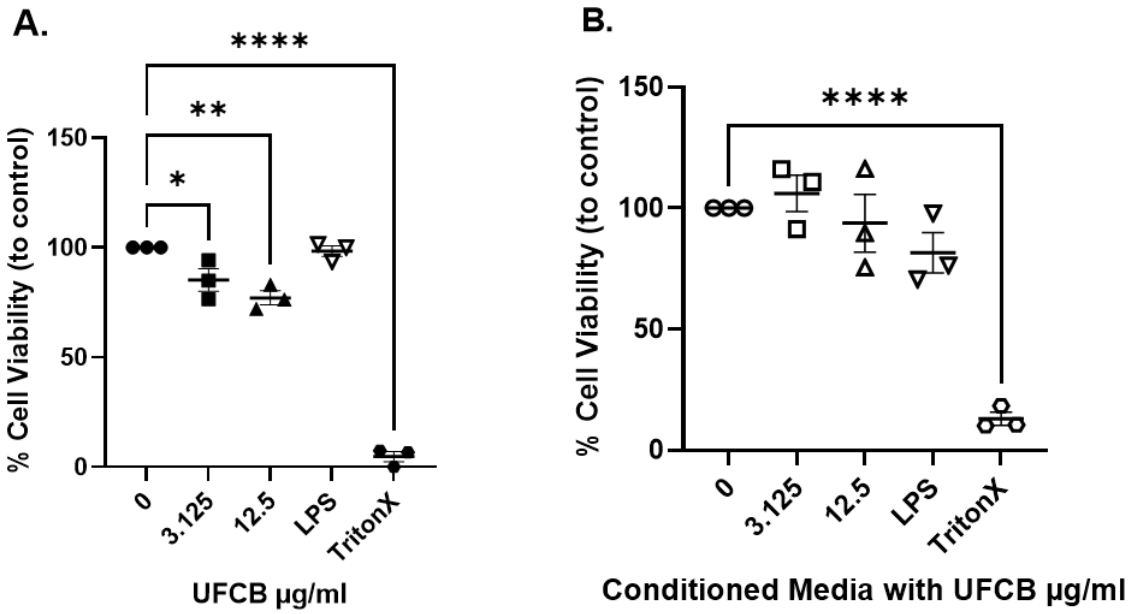

Figure 3.14. Assessment of NT2-derived neuronal-like cell viability following UFCB exposure. Cell viability was assessed using a WST-1 assay following either direct UFCB treatment **(A) or** exposure to UFCB-induced reactive astrocytes conditioned media (**B**) Data are expressed as a percentage of the appropriate control (whereby 0 µg/ml = 100% viable cells), and presented as means ± SEM. One-way ANOVA followed by Tukey *post hoc*' s test for multiple comparisons were performed (n = 3). A statistically significant decrease in cell viability compared to the control was registered after direct exposure to both 3.125 µg/ml (p= 0.0437) and 12.5 µg/ml of UFCB (p=0.0028). Contrarily, no decrease in viability was registered after direct or conditioned media LPS exposure and exposure to UFCB astrocytes conditioned media (**B**). Direct and indirect TritonX exposure significantly decreased viability in both cases (**A-B**): * = p< 0.01; ** = p< 0.01; **** = p<0.001.

Figure 3.14 A shows direct UFCB exposure, at both concentrations, significantly decreased neuronal-like cell viability. Specifically, exposing the cells to 3.125 µg/ml of UFCB decreased viability by 15% (p=0.0437) and by 23% when treating the cells with 12.5 µg/ml (p=0.0028). Conversely, LPS treatment did not affect viability of the neuronal-like cells. In comparison to direct exposure to UFCB, secretions from astrocytes following UFCB exposure had no effect on neuronal-like cells as no significant difference in viability was detectable when cells were exposed to control astrocyte conditioned media with UFCB astrocyte conditioned media (**Figure 3.14 B**).

However, although not statistically significant, LPS-induced astrocyte conditioned media did trend towards reduced viability of the neuronal like cells which might indicate that LPS does work as a positive enhancer of astrocyte reactivity as well as a neuroinflammatory mediator as reported by previous studies (Zhao et al., 2019). Perhaps for this to be significant, in the future, a higher sample number will be needed.

3.8 Summary of Results

This investigation has determined a range of UFCB concentrations that are either sub-lethal or toxic to astrocytic cells over acute (24h) exposure ranges, using WST-1 viability assays. qPCR results suggested that GFAP expression was slightly induced by sublethal, 3.125 µg/ml, and decreased by toxic, 12.5 µg/ml, UFCB doses, but a slight trend towards increased S100A10 expression provides a preliminary indication that astrocytes are more likely to assume a more **neuroprotective role in response to UFCB nanoparticles**. Due to low levels of protein detection, further work is required to confirm the potential effects of any changes in astrocyte polarisation on inflammatory or anti-inflammatory cytokine secretion, despite preliminary indications that UFCB slightly alters IL-6. Both 3.125 and 12.5 ug/ml UFCB were toxic to differentiated NT2 neuronal-like cells, but if exposed to conditioned media from astrocytes treated with UFCB, at both concentrations, no observable effect on neuronal viability was observed. Taken as a whole, the results obtained from this preliminary research don't provide obvious support for any toxic neuro-inflammatory responses to UFCB being astrocyte-mediated. Further studies will need to investigate the direct effects of UFCB on neurons over a wider toxicological response curve designed to establish sublethal and lethal doses for these cells and to determine if UFCB exposed astrocytes release proteins and other markers that can protect against this damage. This means that further work should be focused on determining the neuroprotective mechanisms at play, and to identify specific proteins that might be secreted from astrocytes which can mediate this effect.

4. Discussion

4.1 Physiochemical properties of UFCB

Many of the studies that are currently available on-air pollution nanoparticles lack a thorough investigation into their size, quality and composition of these particles. Chemistry related studies tend to exhaustively analyse the physiochemical properties of some nanoparticles but do not investigate their biological implications. Contrarily, biological-related studies, lack assessment of the particles analysed, so much so that not even the size of the particle under investigation is routinely assessed.

Due to time constraints, this research has only been focused on trying to determine the size of the surrogate UFCB nanoparticle to ensure that it was nanosized. This is because ultrafine nanoparticles, such as UFCB, possess a greater surface area than other particulate matter particles which allows them to absorb and coagulate with others as these are all intrinsically charged (Stoeger et al., 2006). Despite our research showing that Dynamic Light Scattering (DLS) measurements of the diameter of the UFCB particles was more than 100 nm when the particle was suspended in astrocyte media, overall, the surrogate nanoparticle was deemed suitable for toxicological experiments and its size was within literature based and expected ranges. This was not an arbitrary choice as previous evidence (Takenaka et al., 2001) reported the presence of agglomerates of ultrafine particles with a larger-than-normal diameter when present in suspension yet still used them for cell toxicity studies. However, the larger-than-normal diameter could have been due to two reasons: firstly, the high rate of aggregation between single units (single UFCB particles) and secondly, due to coagulation with proteins present in astrocyte media.

DLS measures Brownian Motion and relates it to the size of the particle that it is analysing. The Z Average is a stable parameter that is used for DLS measurement, as it results from averaging all the light intensities detected (Malm & Corbett, 2019). It might not represent the actual size of the nanoparticle, but it provides a measurement that considers the rate of aggregation. As highly charged nanoparticles, such as UFCB, move due to Brownian motion, aggregation – or coagulation – is a factor that greatly influences size over time. To overcome this problem, the Zetasizer has an integrated 173ºC backscatter

feature. This specific angle of detection reduces the effect that might get produced with “multiple scattering”. This might occur if a beam of light scattered on a particle is, in turn, scattered by other particles, altering the reading. Moreover, the 173ºC angle reduces contamination readings resulting from other components being present in suspension (such as dust). These scatter light in a forward direction hence why, with the 173ºC backscatter, they do not get incorporated in the final measurement (Franks et al., 2019; Malm & Corbett, 2019).

Although the Zetasizer has features in place to counteract and account for aggregation, this is only achievable if other parameters and settings are considered. These include, for example, looking at the polydispersity index (PDI) to understand how heterogeneous the suspension might be.

Interestingly, in all three dispersants analysed in this set of experiments, at any given time, the PDI was within a normal range (see **appendix B**) specifically under 0.7 on average. Usually, particles that have a PDI less than 0.2 (out of 1) are regarded as uniform and if they have a PDI lower than 0.7, which is more common, it means that the size reported with DLS mirrors the real particle size. What resulted from this set of experiments, however, does not necessarily mean that the particles were not nanosized, rather it demonstrates that large aggregates formed in suspension as early as the first measurement post sonication (i.e., immediately) which explain the larger than normal diameter, but these aggregates were heterogeneously dispersed in suspension, which might explain why the PDI is within range.

Obviously, as the measurements were taken without cells present, and no proteins – aside from FBS, which was assessed separately – would have been present in the media. Despite that, it is advised to assess interactions between the nanoparticle tested and the media for suspension as issues related to protein corona formation have been reported in other studies looking at the efficacy and toxicological implications of the use of engineered nanoparticles for drug delivery (Guo et al., 2016; Dal Magro et al., 2018; Chakraborty et al., 2019; Hanmei et al., 2021). The protein corona is a structure composed of nanoparticles – the core of the corona – and proteins, phospholipids and other biomolecules that the nanoparticle encounters when entering the human body (Konduru et al., 2017; Lima et al., 2020). This might be of toxicological importance as the nanoparticle,

when reaching secondary organs, such as the brain using the systemic circulation, is not “pure” and unbound but most likely in this form. Moreover, considering the high rate of aggregation and accumulation of ultrafine particles, it could be inferred that what reaches secondary organs is a mixture of many single units – many UFCB particles – which all bound to each other form the core of the protein corona (Lima et al., 2020; Calderón-Garcidueñas & Ayala, 2021). Although this has been reported in previous studies, in this study, the UFCB size in astrocytes media was not significantly different if compared to UFCB suspended in DH_2O or 10% FBS.

Future studies, however, should include cost-effective imaging with a Scanning Electron Microscope (SEM) that might elucidate where the surrogate nanoparticle accumulates and how it interferes with astrocytic cells, as well as elucidate if protein interactions occur in cell media suspension. Moreover, the use of ambient, isolated and filtered air pollution derived nanoparticles might be used to validate results, as those samples could provide a more accurate representation of the real air pollution components that circulate in our cities and might allow for further confirmation of what we observed with this surrogate UFCB nanoparticle. Ideally, to perform a full characterisation of nanoparticles= material, a methodology that has only recently been published should be followed; this is based upon the analysis of the nanoparticle samples via acidic digestion and followed by high resolution mass spectrometry. Organic and Inorganic carbons, including UFCB if present in the samples, could be assessed via Sievers 900 Total Organic Carbon Analyzer and by an aethalometer (Haghani et al., 2020).

4.2 UFCB toxicological dose-response curve and Primary Human Cortical Astrocytes

As previously stated, no studies, to our knowledge, aside from this research, have investigated the effects of a toxicologically-relevant air pollution derived nanoparticle on a specific glial cell type cultured in isolation. This research has developed a robust protocol to establish a suitable concentration range of UFCB nanoparticles for determination of effects on cell viability for human primary cortical astrocytic cells.

Quantitative dose-response data is still very much needed, both *in vitro* and *in vivo*, to assess neurotoxicity of air pollution-derived nanoparticles and to provide evidence to determine a health and safety "threshold" of maximum emissions (Ononda et al., 2017). *In vitro* and *in vivo* studies have previously assessed the effects of particulate matter on neurodegenerative diseases (Calderón-Garcidueñas et al., 2016; 2021; You et al.,2022). However, rather than treating ultrafine particles as compounds that should be toxicologically assessed with a concentration response curve, many of these studies have reported effects on tissues, animals and organs, without stating ranges for toxicity, concentrations or specific chemical components, and thus don't provide a standardised way to effectively investigate what these particles might do to the cells of the CNS. Despite being associated with neurodegenerative decline, it is still unclear, for example, how $PM_{2.5}$ and $PM_{0.1}$ lead to the onset of diseases like Alzheimer's, as the molecular mechanisms have not been elucidated. There is some consensus in the field that microglia activation might be responsible (Campbell et al., 2014; Roqué et al., 2016; Morris et al., 2021) but again, it is not clear whether this is direct or includes other cells such has astrocytes.

Therefore, characterising the response of specific cell types of any newly identified nanoparticle is advised for any further studies investigating their effects on neurodegeneration. In this study, for UFCB and astrocytic cells, the concentration range was set between 0.001 and 100 µg/ml. Despite this concentration range falling mid-way between previously reported concentrations (Schien et al., 2021; Zhang et al., 2019), it still might have been too high to reflect ambient levels of the nanoparticle and investigate reactivity.

This is reflected by our observations that cell viability significantly decrease after exposure to 25 µg/ml UFCB and 12.5 µg/ml UFCB might have already been too high to observe reactivity, based on reducing levels of GFAP observed under this condition compared to control astrocytes. In future studies, the toxicological response curve should be lowered to include concentrations higher than 6.125 µg/ml, that seemingly did not exert any effect on viability, but lower than 12.5 µg/ml, a concentration that was already toxic to the cells as it did induce cell death.

Additionally, several other limitations related to this set of experiments need to be addressed. Firstly, acute exposure to an air pollution derived nanoparticles might only produce limited responses on the cells exposed, meaning the time of exposure should be increased if reactivity is the effect to be observed. Cells of the CNS, especially microglia and astrocytes, act together to promote responses and favour survival of neurons (Matejuk & Ransohoff, 2020). In isolation and acutely exposed, astrocytic cells might have only been able to either survive or die as a response to UFCB exposure, with very few capable of reacting. Despite previous evidence acutely exposing **mixed** microglia- astrocyte cultures for 24 hrs to a mix of ultrafine particles (Campbell et al., 2014; Jang et al., 2018), cells in isolation might need more time than that to react. In fact, rat-derived primary neurons, were exposed for 48 hours to a mixture of ambient collected and filtered TRAP nanoparticles which decreased neurite grown by 40% (Morgan et al., 2011), suggesting that even more delicate cells such as neurons need double the amount of exposure time for effects to be visible. In future studies, exposing samples to UFCB at different time points would avoid missing any possible temporal responses. Moreover, considering that a monoculture does not replicate the intricate interactions present between cells in tissues, using *ex vivo* brain slices might provide an alternative to further confirm the preliminary results obtained with this *in vitro* research.

Secondly, acute exposure to air pollution nanoparticles might be unlikely to often occur in reality. As previously mentioned, UFCB has been extensively used for toxicological modelling purposes. Considering the extensive research available on this particle, it has been classified as a possible carcinogen to humans as it presents both an increased toxicity and an increased aggregation rate compared to particles of a larger size (Shin et al., 2015; Sichen et al., 2021). Previous

studies have demonstrated a cell-specific UFCB concentration-dependent cytotoxicity characterised by substantially **lower levels** of UFCB than the one tested in our study (Zhang et al., 2019; Shien et al., 2021). For mouse primary splenocytes, UFCB was progressively more toxic as concentrations increased and surpassed 15 µg/ml (Sichen et al., 2021). Contrarily, in a human alveolar epithelial type II like cell line, A549, cytotoxic levels were observed at lower concentrations, namely 15, 31 and 62 µg/ml of UFCB (Monteiller et al., 2007). Despite the consistent evidence certifying UFCB toxicity, recruitment of pro-inflammatory mediators and influence on viability of lung epithelial cells (Tamaoki et al., 2004), L-2 - type II epithelial cell lines (Barlow et al., 2005), mouse liver hepatocytes (Zhang et al., 2019) and more, only a few studies have investigated the effects of UFCB on a **brain**-derived cell line or cell type (Wang et al., 2017).

As the overall goal of this project included optimising a concentration of UFCB that leads to astrocyte reactivity, without overt cell death, testing a broad UFCB concentration range in a relevant brain cell type not only allowed for training, protocol development and optimisation, but it facilitated identification of a workable concentration range that, in the future, might also be used as starting point for other analysis of other brain derived cell types.

4.3 Astrocyte Reactivity

4.3.1 Gene expression analysis

Although this study has not found any statistically significant difference in astrocyte reactivity-associated gene expression after direct UFCB exposure on primary astrocytes, several upward and downward trends were observed for each transcript.

For example, GFAP expression increased, especially after LPS was applied to astrocytic cells, which confirms what is already reported that LPS works as an enhancer of astrocyte reactivity and can be used as positive control in experimental settings (Brahmachari et al., 2006; Zhao et al., 219 & Jurga et al., 2021). However, recent evidence warns about the exclusive use of GFAP, a well-known and established marker for astrocyte reactivity itself (Liddelow & Barres., 2017; Chiareli et al., 2017; Li et al., 2019)**.** Several reasons might exist for this, including the fact that increased GFAP proteins and increased mRNA expression might be the result of injury or insults that are not necessarily proportional to the amount of reactivity. If some cells already express higher amounts of GFAP (i.e., higher GFAP basal expression) as is the case for basal levels of GFAP in rodent hippocampal astrocytes, any insults will not render the astrocytes more reactive than others present in different areas (Escartin et al., 2021). Alzheimer's type II astrocytes are metabolically hyperactive in hepatic encephalopathy, a neuropsychiatric disorder caused by hyperammonaemia- and hepatic dysfunction (Agarwal & Mais., 2019). As evidence reported, these astrocytic cells, which react, do not express **GFAP at all**, showing that perhaps although GFAP is a marker for Alzheimer's Disease, it might not cover all disease subtypes and that GFAP might only be present in certain pathological states as a marker of astrocyte reactivity (Simspon et al., 2008; Tatsumi et al., 2018; Xu., 2018; King et al., 2020). Lastly, as a documented reactive astrocytic response includes hyperplasia, GFAP shouldn't be used as marker alone as other alternatives, such as BrdU incorporation, that measure different parameters like cell proliferation, can be combined to GFAP to eventually assess reactivity (Escartin et al., 2021).

Considering all the limitations reported for GFAP and that evidence reports that GFAP might not be the most reliable marker, it still provided a cost-effective, well-documented, method that our laboratory used to assess overall reactivity. GFAP expression in fact, was able to give an indication on whether the astrocytes did

react as a slight increase in transcript expression was reported after LPS exposure compared to the control but as previously mentioned, GFAP could not state the type of polarisation state the cells acquired. Additionally, future studies need to assess baseline levels of GFAP in human cortical primary astrocytic cells prior to stimulation with UFCB and any other positive control as this was not determined. As Szpakowski et al. (2022) have suggested, flow cytometry could be used to determine GFAP levels in untreated cells and use that measure as a comparison for experimental data obtained after exposure, for instance, to UFCB. Moreover, baseline GFAP could also be assessed in untreated primary astrocytic cells via immunostaining first and that data could be used to visualise and compare GFAP expression in the same cells after UFCB treatment (Yin et al., 2019). By taking into consideration baseline GFAP levels, it might be possible to more safely confirm if the cells did react in response to UFCB. However, based upon the resources and results available, to investigate what type of polarisation state the cells might have acquired after a slight increase in GFAP resulting from the qPCR data, specific polarisation gene markers were selected based upon previous evidence.

A1 astrocytes typically express neurotoxic-associated genes, by such as **GBP2** and **LCN2**. GBP2 encodes for the Guanylate binding protein 2 and it has also been found to be responsible for increasing neuronal apoptosis after CNS insults such as Traumatic Brain Injury (TBI; Miao et al., 2017). Moreover, GBP2 is downregulated in reactive astrocytic cells of type 2 (A2; Li et al., 2019) and is usually upregulated alongside Complement 3 (C3) in A1 reactive astrocytes (Liddelow et al., 2017; Ugalde et al., 2020). C3 primers were purchased but, after numerous attempts to improve specificity of amplification, they failed and were not brought forward for further testing. Due to time constraints, it was not possible to design new primers but ideally, in future studies, to investigate neurotoxic astrocytic profile A1, both GBP2 and C3 should be tested.

The second A1 candidate gene, LCN2, was selected as both *in vitro* and *in vivo* testing showed that activated astrocytes promote the increased expression and release of LCN2 to favour morphological changes typical of astrogliosis, apoptosis of surrounding cells and their own cell death (Lee et al., 2015). Moreover, LCN2 is induced in reactive astrocytes in response to neurodegeneration and is capable of promoting neuronal death if applied to

neurones cultured in isolation (Bi et al., 2013) a major reason why this marker was also chosen for ELISA testing.

There was no significant change in GBP2 or LCN2 after exposure to UFCB. However, GBP2 showed a small increase after exposure to sublethal dose 3.125 µg/ml UFCB and following LPS exposure. Perhaps, once again, the exposure time might have not been enough to observe any statistically significant change in expression of either **GFAP** or **GBP2** at this dose. This might also show that the toxicological response curve previously established could be refined with the addition of lower concentrations in between the ones selected or investigating if concentrations lower than 3.125 µg/ml might be able to produce any effects in terms of reactivity. The same can be said for **LCN2**, which also did not increase in expression after exposure to both UFCB doses, but a slight upward trend was registered after LPS exposure.

This might be consistent with evidence which reports that LPS exposure acts an enhancer of LCN2 protein secretion in the brain and the overexpression of the protein is now indicative of neuroinflammatory disorders (Lee et al., 2015; Taklimie et al., 2019). In fact, LCN2 might represent a new marker to be investigated for ischaemic stroke, Alzheimer's disease and spinal cord injury as has been suggested to be actively involved in disease pathogenesis (Taklimie et al., 2019). A note of caution is needed for LCN2; this is a relatively low expression gene which gets secreted by astrocytes only after important stressors –such as hypoxia, which occurs in ischaemic strokes - are applied to astrocytic cells (Taklimie et al., 2019), therefore stimuli of other nature rather than UFCB exposure, might be needed to trigger and increase in expression. In either case, neither GBP2 nor LCN2 seemed substantially and unambiguously overexpressed as result of UFCB exposure, suggesting that UFCB might have not been applied for long enough to favour a net increase in both genes expression. In addition, another possibility that might need to be considered is that UFCB exposure might not lead to increase in expression of either gene and might not favour a neurotoxic profile, inferring that perhaps astrocytes do not assume a A1 profile.

To support this theory is the fact that **S100A10**, a A2 specific gene marker, expression increased because of exposure to both UFCB doses. S100A10, a calcium binding protein, is present in brains of patients who died of ischaemic stroke or infarctions in later life, as well as other neurodegenerative diseases such as Parkinson and Alzheimer's diseases (King et al., 2020). S100A10, surprisingly, was found to be upregulated and co-expressed in specific brain areas (upper frontal cortex, lower frontal cortex and frontal white matter) of post-mortem AD brains where C3, the neurotoxic A1 subtype marker, was also present (King et al., 2020). This suggested that both markers might arise at different times of disease progression, with C3 being increased earlier and then being matched in expression during late disease by S100A10. This finding seems to find endorsement in evidence reporting that between day 1 and day 4 after rat spinal cord injury, there is a net increase in expression of C3 levels which is then surpassed between day 4 and day 7 by a net increase in expression of S100A10 (Li et al., 2021). This may suggest that astrocytes specific markers need longer to substantially increase in expression and co-localise in brain areas associated with neurodegenerative disease, meaning that acute exposure to our nanoparticle, in a single cell type, may only propose a basic understanding of toxicity and indication of whether the response is likely to be more neuroprotective or neurotoxic. Moreover, gene expression profiles in diseases are only temporal, a factor which suggests that future studies should include the investigation of marker genes expression, including GFAP, at different time points.

Overall, based upon the findings of the current study, a more **neuroprotective** state appears to have been acquired by the cells after UFCB exposure, but due to the preliminary nature of these experiments, caution must be taken forming these conclusions. Firstly, a higher number of experimental repeats needs to be included to test whether any of the results reported lead to significance.

Secondly, perhaps increasing the time of exposure to 48 or 72 hrs might lead to a more quantifiable change in gene expression whether that will confirm or not the results reported with this study. Lastly, depending on time availability, more markers, such as C3 for A1 type and Aquaporin-4 or BDNF for A2 (Li et al., 2019) should also be added to the panel of candidate genes to be tested after UFCB exposure, as well as measuring polarisation over a wider range of UFCB concentrations.

This would enable a more accurate analysis of the effects of UFCB exposure on astrocyte polarisation and their potential downstream effects on neurodegeneration.

4.3.2 Protein secretion levels analysis

ELISA kits were purchased before analysing the qRT-PCR data and the choice of protein markers was based on published evidence; however, it was important for this research to try to assess which protein marker would have been better to measure levels of without knowing whether the qPCR would have produced results trending towards neuroprotection or neurodegeneration. For this reason**,** **LCN2**, which as well as being an A1 specific marker, linked to neurodegeneration is also secreted by A1 astrocytes, was chosen as the best candidate to investigate potential links with neurodegeneration. As previous studies reported, A2 subtypes have been less studied (Fujita et al., 2018; Zhou et al., 2020), hence it was more challenging to select a valid marker that would have been overexpressed by the cells but also secreted. For this reason, **IL-6**, was chosen. This Interleukin is released by microglia, astrocytes, and neurons as a result of injury or other CNS insults. Although very important for normal physiological functions, IL-6 seems to possess a dichotomous role in the CNS as it acts as a neuroinflammatory (Erta et al., 2012) but also neuroprotective mediator (Krasovska & Doering, 2018;). IL-6 after CNS insults such as spinal cord injury seems to first act as a pro-inflammatory mediator and later assume a more neuroprotective role (Codeluppi et al., 2014), favouring synapses regeneration as well as axon sprouting (Yang et al., 2012). This might suggest that a more powerful insult, such as traumatic injury, might better show and quantify changes in expression of key mediators. IL-6, however, was chosen as astrocytes are the greatest inductor of IL-6 secretion in the CNS, especially if they acquire specific polarisation states.

IL-6, in the CNS is generally considered anti-inflammatory as it possesses neurotrophic properties and was seen to be released by A2 reactive astrocytes (Degos et al., 2013; Codeluppi et al., 2014; Liddelow et al., 2017; Fujita et al., 2018; Krasovska & Doering, 2018). The media that was analysed via ELISA, was actually the same media that differentiated NT2 neuronal like cells were later exposed to.

As this was conditioned media, in order to completely spin out the nanoparticle suspended, the centrifugation time suggested by the kits' manufacturer was doubled. In fact, by respecting suggested times, the nanoparticle kept coagulating with others as well as probably binding to proteins present in the media. As mentioned above, UFCB tends to form coagulates or form "protein coronas" (Lee et al., 2014). Although it is not possible to state whether UFCB did interact with proteins present in the media, increasing the time seemed a reasonable compromise to ensure that the sample were clear of UFCB and so able to be analysed.

However, this may in part explain why the levels of LCN2 were undetectable, and the levels of IL-6 much lower than expected, in the astrocyte conditioned media under all treatment conditions. Due to time and budget constraints, it was not possible to test whether UFCB interacts with the ELISA assays itself but ideally, in future studies, that should be assessed to determine whether the centrifugation time could be reduced, or protease inhibitors added, to retain and protect proteins from degradation prior to quantitation.

The standard curve for **LCN2** was not as precise as the one for IL-6 and a few reasons might account for this as both were performed following their own manufacturer's protocols. Firstly, it could be due too poor pipetting performance as the pipette sets for the two ELISAs were different. Secondly, it could be that the stock standard for LCN2 was not properly dissolved and in the future, a centrifuge step should be added to mend for this.

LCN2 levels secreted into conditioned astrocyte media were below the limit of detection of the assay under all treatment conditions. Speculatively, however, the absence of LCN2 in all conditions may indicate UFCB exposure did not overtly induce secretion of this protein, which would align with the lack of gene expression changes.

Comparatively, levels of IL-6 significantly increased, compared to control and UFCB exposed samples, after LPS exposure. This agrees with previous studies reporting that LPS, while promoting reactivity, greatly enhanced expression and secretion of IL-6 in astrocytes (Acaz-Fonseca et al., 2019) .

This specific study's experimental settings were similar to the ones chosen for our experiments; they exposed primary astrocytes for 24 hrs to a LPS concentration range varying between 50 to 5000 ng/ml. In our experimental settings, 1000 ng/ml (or 1 µg/ml) was given to the cells for 24 hrs, registering similar results. What differs is the fact that they analysed cell metabolic activity, looked at proliferation with the addition of BrdU and noticed that, surprisingly, a statistically significant increase in IL-6 transcript and secretion was registered after the cells were exposed to only 500 ng/ml of LPS. Hence the LPS concentrations that we used and the observed increase in IL6 compared to controls are in agreement with published data.

Despite reporting these trends in IL-6 levels, it is not possible to infer if there was an effective increase of the protein after UFCB exposure. This is because, in retrospect, the experimental design should have included a step devoted to measure the total amount of protein present in the samples to begin with. In fact, the cells should have been scraped for proteins and a BCA assay, for example, could have been performed to normalise the protein levels registered with the ELISA assay. Perhaps future studies might need to account for the loss of cells under toxic conditions by measuring total protein of cell homogenates and then use that to normalise secreted protein values. For instance, it should be factored in the variability between wells whereby slightly different cell numbers in different wells might not reproduce the same protein content. In addition, variability might have also been generated by the different volumes of conditioned media analysed. Moreover, if time and costs will allow for it, an unbiased highly sensitive proteomic approach could be taken to evaluate the profile of proteins secreted in cell culture media before and after UFCB exposure, perhaps amplifying the number of sublethal doses tested, while understanding how these cells respond by secreting proteins, to a highly dynamic nanoparticle such as UFCB.

Another factor that might have influenced low levels of IL-6 in the conditioned media is related to the possible interference between the nanoparticles and proteins present. Interference was investigated and accounted for in the WST-1 viability assay by introducing three different controls. However, the ELISA experimental design failed to test for interference with either IL-6 or LCN2 and UFCB.

As previously mentioned, nanoparticles do associate with proteins and by binding to them, they might be able to physically “pull them” out of the media during the vortexing step. This might have led to a significant reduction in IL-6 and potentially a false negative, a possibility that we cannot exclude from our results. To corroborate this thesis, interference of specific inflammatory markers such as TNF α and IL-8 has already been reported in relation to nanosized (14 nm) carbon black (Brown et al., 2010). Future experiments should include a step whereby the different ELISA standards are incubated with different concentrations of UFCB to firstly look at interference at all with the specific protein markers and secondly to investigate if higher concentration of the nanoparticles interfere more than lower ones.

4.4 Neuronal like cells viability and neurodegeneration

The brain's cell network and processes are regulated by a complex array of cells working together to promote correct functioning. Although there was some preliminary evidence to indicate that reactive astrocytosis might have occurred but was still, perhaps, in the early stages as a result of UFCB exposure, the polarisation that the astrocytes acquired cannot alone predict neurotoxicity or neurodegeneration. To infer a link with either outcome, the last step of the research project included measuring the effects of UFCB exposed astrocytes conditioned media on neuronal viability using differentiated NT2 neurons. This essential step had the purpose to bring the research aim closer to defining a causative link between air pollution exposure and neurodegeneration despite intrinsic research limitations such as the use of an acute exposure model.

Viability was measured in both UFCB directly exposed neuronal-like cells and cells exposed to astrocyte-conditioned media. Because of this, some of the limitations encountered with ELISA testing might be applied to this set of experiments. Again, these include the fact that no changes in viability encountered with the samples exposed to the conditioned media might have been due to the media being very diluted or due to any possible neuroprotective or neurotoxic factors/proteins present in the media being sedimented during collection.

It could also be that astrocytes did react in a neuroprotective manner and no change in viability has occurred as astrocytes seemed to have reacted assuming more of a "**A2" type of polarisation**.

Considering the qRT-PCR, ELISA and the neuronal viability data, although more repeats are needed and the sample number should be increased, neuroprotective polarisation of astrocytes appears to **trend across** measurements, but further research is needed to prove this hypothesis. Essentially, the brain is made of a complex array of cells that work together to protect themselves and ultimately, to protect neurons. Neurons do not react, rather they die off if the insult they receive is too great for them to bear. This is highly likely what has occurred to the neuronal like cells that have been directly exposed to UFCB. A net decrease in viability, in fact, was registered after the cells were exposed to both UFCB doses. Perhaps, in co-culture with either

astrocytes or microglia, this might have been different and these cells could have provided protection.

Moreover, if time would have allowed it, a different concentration response curve should have been designed for neuronal like cells to test whether their level of toxicity was comparable to the astrocytes. Overall, the incapability of neurons to react might be exploited to work out a UFCB concentration response curve for the primary neurons, which contain neurons and astrocytes, to investigate if they have any level of tolerance to the particle, compared to neurons alone following treatment of cultures with mitotic inhibitors, such as cytosine arabinoside (Bell et al., 2011). Additionally, it would be relevant to look at the differences between primary neuron-enriched cultures made using cytosine arabinose and other mitotic inhibitors and mixed cultures which are generated using standard methods; the comparison might highlight differential responses as well as providing result obtained with a more physiologically relevant culture type (the mixed culture) to address the neuroprotection question. This would help to determine a more direct link between astrocyte responses and neuroprotection following exposure to UFCB.

Lastly, microglia and astrocytes are closely linked to each other as they act together to promote an array of functions including synaptogenesis, communication, and neuronal heath (Vainchtein & Molofsky, 2020; Garland et al., 2022). As mentioned above in section 1.8, several studies have investigated the cytotoxic effects of specific nanoparticles and particulate matter particle's mixture on microglia-astrocytes co-cultures reporting the toxic effects of the compounds tested. However, considering the result obtained with this project and the physiological interactions between these two cell types, it would be relevant to validate results using primary microglia and astrocytes co-cultures after exposure (direct and indirect) to UFCB to investigate these two cell 's types interaction on the overall A1/A2 configuration and then assessing the consequent neuronal toxicity profile.

All of these factors are of extreme importance to understand how many answers are still needed to fulfil gaps in the knowledge regarding both the physiochemical properties of UFCB and their toxic effects on brain derived cell types.

5. Conclusion

5.1 Concluding remarks and Potential for future directions

Despite some available evidence linking air pollution-derived particulate matter (PM) and neurodegeneration (Calderon-Gurciduena et al., 2002), this link is yet to be molecularly confirmed. As air pollution is now a growing concern for governments and populations worldwide, understanding the impact of individual components on biodiversity and human health is imperative. Previous evidence did not provide a starting point for testing a newly identified air pollution-derived nanoparticle on brain-derived cell types and very few studies have focused on analysing the effects of PM particles on specific cells, signalling pathways and receptors. Overall, paucity of research in this field has led to confusion on the type of air pollution components that do cause nerve cell toxicity (Haghani et al., 2019) The intention behind this project was to better understand the molecular and cellular links that might be present between air pollution and neuroinflammatory mechanisms of neurodegeneration. Although this study has its limitations, it still provided useful evidence including protocol design, refinement and optimisation and preliminary results suggesting that UFCB exposed human primary astrocytes react , but cannot clearly explain any pro-inflammatory neurotoxic responses to UFCB nanoparticles. This can, for instance, lay the foundations for further studies that compare the effects of well-studied (heavy metals) and novel (plastics) nanoparticle components of air-pollution on neuroinflammation and neurodegeneration.

Research focused on understanding the molecular pathology of neurodegenerative diseases constantly opens up new avenues for cell response or cell pathways to be investigated. Considering this, testing *in vivo* the effects of physiologically irrelevant concentrations of “mixed” samples of air pollution derived particles should be avoided in favour of firstly, preliminary *in vitro* work that is still very much needed in the toxicology field. *In vitro* work is still required to refine protocol design to standardise practices for testing and investigating the effects of PM on neurodegenerative decline. Therefore, what should be promoted is a cell-based approach whereby the toxicological effects of relevant air pollution nanoparticles are assessed on the main CNS cells to start uncovering cell pathways that might be responsible for neurodegeneration. In the future, *in vivo*

work will be required to encompass the full physiological effects that specific nanoparticles have and will be necessary to validate results. However, as of now, toxicological studies are not at that stage yet for neurodegenerative diseases.

With this study, we propose that astrocyte-mediated inflammation might either cause neurodegeneration or neuroprotection from air pollution-associated nanoparticles, but the differential response might be dependent upon nanoparticle types and dosage as well as time of exposure used. Understanding this variability might be of great toxicological and epidemiological importance. In fact, if astrocytes respond negatively to a specific nanoparticle, leading to neurotoxicity, this might uncover mechanisms that can become targets for new therapeutics and help in assessing toxicity thresholds for legislation changes. Contrarily, it might also be useful to investigate if astrocyte responses lead to a more neuroprotective phenotype in response to specific nanoparticles as that might help to promote neuronal heath by designing ways that mimic those effects and protect the brain from air pollution exposure.

In conclusion, this study proposed, and tested, a preliminary methodology based on the use of accessible systems for the study of nanotoxicity in brain cells and will, in the future, facilitate the investigation of cell-specific mechanisms, as well as comparisons between well-established and novel nanoparticles. The findings from this study might be of interest to researchers in closely related fields such as nanomedicine, environmental science, immunology but also neurodegeneration. Overall, the model proposed in this research requires further refinement to assess if the initial responses observed can be repeated or amplified. Long term research in this area might contribute to provide valuable evidence to scientific advisory committees such as DEFRA to inform policies and regulations devoted to reducing air pollution risk across the world and set specific thresholds for emission. This work could help prevent future illness in both industrialised countries and countries that are in the process of industrialisation and inform policy. Lastly, the findings from this research are necessary to start understanding how and why air pollution causes toxicity in the CNS, with potential to highlight novel ways to prevent or study neurodegenerative diseases.

6. Acknowledgments

Firstly, I would like to express my immense gratitude to **Mr Derek** and **Mrs Maureen Moss** without whom I would have not been able to do this research project. Their support has been much appreciated.

Then, I would like to thank my Director of Studies **Dr Fiona Kerr** for her support, guidance, time dedicated to teaching me and help throughout this year. She is an inspiration for me, and I could not thank her enough for allowing me to become an independent researcher.

Then, I would like to thank the rest of the team, **Professor Gary Hutchinson, Dr Amy Poole** and **Dr Eva Malone**. Their help has been invaluable as they aided me in navigating the world of toxicology and thought me much on how to be a confident in my choices.

Then, I would like to thank those who were with me daily and that made me feel integral part of a thriving scientific community at Edinburgh Napier. The list is long, but it includes **Dr Beatriz Vale De Melo E Oliveira**, **Dr Fern Findlay-Greene, Dr Filipa Henderson Susa, Dr Lesley Young, Robert Wyllie, Bill Surradge,** almost- Dr **Sarah Horgan, Dr Francesco Aiello, Dr Craig Stenton, Dr Ewoma Akpughe, Michael Hinghliffe,** almost-Dr **Raquel Lopera Burgueño, Muna Ali,** almost- Dr **David Hughes, Connan Mason** and many more.

Lastly, I would like to thank my family and friends, the people that were not in the lab nor in university with me and, from close-by or as far as 3000 km away, always supported and helped me: **Martin Green, Benedetta Villani, Anna Lisa Leoni, Mario Leoni, Alessandra Leoni, the entire Green Family**, **Geri, Federica** and **Megan.** Thank you for being kind to me and always pushing me to achieve my goals.

Thank you all for giving me the opportunity and helping me to mature personally, academically, and professionally as an independent researcher.

7. References

Acaz-Fonseca, E., Ortiz-Rodriguez, A., Azcoitia, I., Garcia-Segura, L. M., & Arevalo, M. A. (2019). Notch signaling in astrocytes mediates their morphological response to an inflammatory challenge. *Cell Death Discovery*, *5*(1)https://doi.org/10.1038/s41420-019-0166-6

Agarwal, A. N., & Mais, D. D. (2019). Sensitivity and Specificity of Alzheimer Type II Astrocytes in Hepatic Encephalopathy. *Archives of pathology & laboratory medicine*, *143*(10), 1256–1258. https://doi.org/10.5858/arpa.2018-0455-OA

Allen, J.A., Liu, X., Weston, D., Prince, L., Oberdörster, G., Finkelstein, J.N., Johnston, C. J. & Cory-Slechta, D.A. (2014). Developmental Exposure to Concentrated Ambient Ultrafine Particulate Matter Air Pollution in Mice Results in Persistent and Sex-Dependent Behavioral Neurotoxicity and Glial Activation. *Toxicological Sciences,* 140(1), 160–178. https://doi.org/10.1093/toxsci/kfu059

Atkinson, R.W., Kang, S., Anderson, H.R., Mills, I. C. & Walton, H. A. (2014). Epidemiological time series studies of $PM_{2.5}$ and daily mortality and hospital admissions: a systematic review and meta-analysis. *Thorax, BMJ*, 69(7), 660-665. https://doi:10.1136/thoraxjnl-2013-204492

Auten, R. & Davis, J. (2009). Oxygen Toxicity and Reactive Oxygen Species: The Devil Is in the Details. *Pediatric Research,* 66, 121–127. https://doi.org/10.1203/PDR.0b013e3181a9eafb

Babadjouni, R., Patel, A., Liu, Q., Shkirkova, K., Lamorie-Foote, K., Connor, M., Hodis, D. M., Cheng, H., Sioutas, C., Morgan, T. E., Finch, C. E., & Mack, W. J. (2018). Nanoparticulate matter exposure results in neuroinflammatory changes in the corpus callosum. *PloS one*, *13*(11), e0206934. https://doi.org/10.1371/journal.pone.0206934

Bachiller, S., Jiménez-Ferrer, I., Paulus, A., Yang, Y., Swanberg, M., Deierborg, T., & Boza-Serrano, A. (2018). Microglia in neurological diseases: A road map to brain-disease dependent-inflammatory response. In *Frontiers in Cellular Neuroscience* (Vol. 12). Frontiers Media S.A. https://doi.org/10.3389/fncel.2018.00488

Barlow, P.G., Clouter-Baker, A., Donaldson, K. et al. Carbon black nanoparticles induce type II epithelial cells to release chemotaxins for alveolar macrophages. Part Fibre Toxicol 2, 11 (2005). https://doi.org/10.1186/1743-8977-2-11

Bell, K. F., Al-Mubarak, B., Fowler, J. H., Baxter, P. S., Gupta, K., Tsujita, T., Chowdhry, S., Patani, R., Chandran, S., Horsburgh, K., Hayes, J. D., & Hardingham, G. E. (2011). Mild oxidative stress activates Nrf2 in astrocytes, which contributes to neuroprotective ischemic preconditioning. *Proceedings of the National Academy of Sciences of the United States of America*, *108*(1), E1–E4. https://doi.org/10.1073/iti0111108

Bhargava, A., Tamrakar, S., Aglawe, A., Lad, H., Srivastava, R. K., Mishra, D. K., Tiwari, R., Chaudhury, K., Goryacheva, I. Y., & Mishra, P. K. (2018). Ultrafine particulate matter impairs mitochondrial redox homeostasis and activates phosphatidylinositol 3-kinase mediated DNA damage responses in lymphocytes. *Environmental pollution*, 234, 406–419. https://doi.org/10.1016/j.envpol.2017.11.093

Bi, F., Huang, C., Tong, J., Huang, G., Wu, Q., Li, F., Xu, Z., Bowser, R., Xia, X-G. & Zhou, H. (2013). Reactive astrocytes secrete lcn2 to promote neuron death. *Proceedings of the National Academy of Sciences,* 110 (10) 4069-4074; https://doi.org/10.1073/pnas.1218497110

Brahmachari, S., Fung, Y. K., & Pahan, K. (2006). Induction of glial fibrillary acidic protein expression in astrocytes by nitric oxide. *The Journal of neuroscience: the official journal of the Society for Neuroscience*, *26*(18), 4930–4939. https://doi.org/10.1523/JNEUROSCI.5480-05.2006

Brook, R.D., MD, Rajagopalan, S., Pope III, A., Brook, J.R., Bhatnagar, A., Diez-Roux, A.V., Holguin, F., Hong, Y., Luepker, R. V., Mittleman, M. A., Peters, A., Siscovick, D., Smith, S. C., Whitsel, L., Kaufman, J.D., and on behalf of the American Heart Association Council on Epidemiology and Prevention, Council on the Kidney in Cardiovascular Disease, and Council on Nutrition, Physical Activity and Metabolism (2010). Particulate Matter Air Pollution and Cardiovascular Disease: An Update to the Scientific Statement From the American Heart Association. *Circulation,* 121(21), 2331-2378. https://doi.org/10.1161/CIR.0b013e3181dbece1

Burchiel, S. W., & Luster, M. I. (2001). Signaling by environmental polycyclic aromatic hydrocarbons in human lymphocytes. *Clinical Immunology*, *98*(1), 2–10. https://doi.org/10.1006/clim.2000.4934

Bush, T. G., Puvanachandra, N., Horner, C. H., Polito, A., Ostenfeld, T., Svendsen, C. N., Mucke, L., Johnson, M. H., & Sofroniew, M. V. (1999). Leukocyte infiltration, neuronal degeneration, and neurite outgrowth after ablation of scar-forming, reactive astrocytes in adult transgenic mice. *Neuron*, *23*(2), 297–308. https://doi.org/10.1016/s0896-6273(00)80781-3

Bustin, S. A., Benes, V., Garson, J. A., Hellemans, J., Huggett, J., Kubista, M., Mueller, R., Nolan, T., Pfaffl, M. W., Shipley, G. L., Vandesompele, J., & Wittwer, C. T. (2009). The MIQE guidelines: minimum information for publication of quantitative real-time PCR experiments. *Clinical chemistry*, *55*(4), 611–622. https://doi.org/10.1373/clinchem.2008.112797

Calderón-Garcidueñas, L., Azzarelli, B., Acuna, H., Garcia, R., Gambling, T. M., Osnaya, N., Monroy, S., Del Rosario Tizapantzi, M., Carson, J. L., Villarreal-Calderon, A., & Rewcastle, B. (2002). Air Pollution and Brain Damage. *Toxicologic Pathology*, 30(3), 373–389. https://doi.org/10.1080/01926230252929954

Calderón-Garcidueñas, L., & Ayala, A. (2021). Air Pollution, Ultrafine Particles, and Your Brain: Are Combustion Nanoparticle Emissions and Engineered Nanoparticles Causing Preventable Fatal Neurodegenerative Diseases and Common Neuropsychiatric Outcomes? *Environmental Science and Technology*. https://doi.org/10.1021/acs.est.1c04706

Calderón-Garcidueñas, L., Leray, E., Heydarpour, P., Torres-Jardón, R., & Reis, J. (2016). Air pollution, a rising environmental risk factor for cognition, neuroinflammation and neurodegeneration: The clinical impact on children and beyond. *Revue neurologique*, *172*(1), 69–80. https://doi.org/10.1016/j.neurol.2015.10.008

Campbell, A., Daher, N., Solaimani, P., Mendoza, K., & Sioutas, C. (2014). Human brain derived cells respond in a type-specific manner after exposure to urban particulate matter (PM). *Toxicology in Vitro*, *28*(7), 1290–1295. https://doi.org/10.1016/j.tiv.2014.06.015

Chakraborty, D., Chauhn, P., Kumar, S., & Chaundhary, S., Utilizing corona on functionalized selenium nanoparticles for loading and release of doxorubicin payload. Journal of molecular liquids, 296, 111864. https://doi.org/10.1016/j.molliq.2019.111864

Chen, H., Kwong, J. C., Copes, R., Hystad, P., van Donkelaar, A., Tu, K., Brook, J. R., Goldberg, M. S., Martin, R. V., Murray, B. J., Wilton, A. S., Kopp, A., & Burnett, R. T. (2017). Exposure to ambient air pollution and the incidence of dementia: A population-based cohort study. *Environment international*, 108, 271–277. https://doi.org/10.1016/j.envint.2017.08.020

Chen, L., Yokel, R.A., Hennig, B. & Toborek, M. (2008). Manufactured Aluminum Oxide Nanoparticles Decrease Expression of Tight Junction Proteins in Brain Vasculature. *Journal of Neuroimmune Pharmacology,* 3, 286–295. https://doi.org/10.1007/s11481-008-9131-5

Chiareli, R.A., Carvalho,G.A., Marques, B.L.,, Mota, L.S., Oliveira-Lima, O. C., Gomes, R.M.,Birbrair, A., Gomez, R.S., Simão, F.K.F, Leist, M. & Pinto, M. C. X. (2021). The Role of Astrocytes in the Neurorepair Process. *Frontiers in Cell and Developmental Biology*, 9. https://doi.org/10.3389/fcell.2021.665795.

Chicco, D., Warrens, M. J., & Jurman, G. (2021). The coefficient of determination R-squared is more informative than SMAPE, MAE, MAPE, MSE and RMSE in regression analysis evaluation. *PeerJ. Computer science*, *7*, e623. https://doi.org/10.7717/peerj-cs.623

Cockburn, H. (2020, December, 16). Ella Kissi-Debrah inquest: Coroner says air pollution contributed to death of nine-year-old in landmark ruling. *Independent*. https://www.independent.co.uk/climate-change/news/ella-kissi-debrah-inquest-result-pollution-b1774841.html

Codeluppi, S., Fernandez-Zafra, T., Sandor, K., Kjell, J., Liu, Q., Abrams, M., Olson, L., Gray, N. S., Svensson, C. I., & Uhlén, P. (2014). Interleukin-6 secretion by astrocytes is dynamically regulated by PI3K-mTOR-calcium signaling. *PloS one*, *9*(3), e92649. https://doi.org/10.1371/journal.pone.0092649

Degos, V., Charpentier, T. L., Chhor, V., Brissaud, O., Lebon, S., Schwendimann, L., Bednareck, N., Passemard, S., Mantz, J., & Gressens, P. (2013). Neuroprotective effects of dexmedetomidine against glutamate agonist-

induced neuronal cell death are related to increased astrocyte brain-derived neurotrophic factor expression. *Anesthesiology*, *118*(5), 1123–1132. https://doi.org/10.1097/ALN.0b013e318286cf36

Department for Environment, Food and Rural Affairs (DEFRA) and AIR QUALITY EXPERT GROUP (2018). Ultrafine particles (UFP) in the UK. https://uk-air.defra.gov.uk/assets/documents/reports/cat09/1807261113_180703_UFP_Report_FINAL_for_publication.pdf and https://uk-air.defra.gov.uk/

Donaldson, K., Tran, L., Jimenez, L. A., Duffin, R., Newby, D. E., Mills, N., MacNee, W., & Stone, V. (2005). Combustion-derived nanoparticles: A review of their toxicology following inhalation exposure. In *Particle and Fibre Toxicology* (Vol. 2). https://doi.org/10.1186/1743-8977-2-10

Dawson, D. A., Genco, N., Bensinger, H. M., Guinn, D., Il'giovine, Z. J., Wayne Schultz, T., & Pöch, G. (2012). Evaluation of an asymmetry parameter for curve-fitting in single-chemical and mixture toxicity assessment. *Toxicology*, *292*(2-3), 156–161. https://doi.org/10.1016/j.tox.2011.12.006

Edwards III, G.A., Gamez, N. E. G.,Calderon, O., Moreno-Gonzalez, I., (2019). Modifiable Risk Factors for Alzheimer's Disease. *Frontiers in Aging Neuroscience,* 11. https://doi.org/10.3389/fnagi.2019.00146

Erta, M., Quintana, A., & Hidalgo, J. (2012). Interleukin-6, a major cytokine in the central nervous system. *International journal of biological sciences*, *8*(9), 1254–1266. https://doi.org/10.7150/ijbs.4679

Escartin, C., Galea, E., Lakatos, A. et al. (2021). Reactive astrocyte nomenclature, definitions, and future directions. *Nature Neuroscience*, 24, 312–325. https://doi.org/10.1038/s41593-020-00783-4

European Environmental Agency (EEA). (2021). Health impacts of air pollution in Europe, 2021. *Air quality in Europe 2021*. EEA.com. https://www.eea.europa.eu/publications/air-quality-in-europe-2021/health-impacts-of-air-pollution

Feng, C., Wang, H., Lu, N., Chen, T., He, H., Lu, Y., & Tu, X. M. (2014). Log-transformation and its implications for data analysis. *Shanghai archives of*

psychiatry, *26*(2), 105–109. https://doi.org/10.3969/j.issn.1002-0829.2014.02.009

Franks, K., Kestens, V., Braun, A., Roebben, G., & Linsinger, T. P. J. (2019). Non-equivalence of different evaluation algorithms to derive mean particle size from dynamic light scattering data. *Journal of Nanoparticle Research*, *21*(9). https://doi.org/10.1007/s11051-019-4630-2

Fuller, R., Landrigan, P. J., Balakrishnan, K., Bathan, G., Bose-O'Reilly, S., Brauer, M., Caravanos, J., Chiles, T., Cohen, A., Corra, L., Cropper, M., Ferraro, G., Hanna, J., Hanrahan, D., Hu, H., Hunter, D., Janata, G., Kupka, R., Lanphear, B., … Yan, C. (2022). Pollution and health: a progress update. In *The Lancet Planetary Health* (Vol. 6, Issue 6, pp. e535–e547). Elsevier B.V. https://doi.org/10.1016/S2542-5196(22)00090-0

Fujita, A., Yamaguchi, H., Yamasaki, R., Cui, Y., Matsuoka, Y., Yamada, K. I., & Kira, J. I. (2018). Connexin 30 deficiency attenuates A2 astrocyte responses and induces severe neurodegeneration in a 1-methyl-4-phenyl-1,2,3,6-tetrahydropyridine hydrochloride Parkinson's disease animal model. *Journal of neuroinflammation*, *15*(1), 227. https://doi.org/10.1186/s12974-018-1251-0

Gao, S., Li, T., Pan, J., Han, D., Lin, J., Niu, Q., & Liu, R. (2021). Toxic effect and mechanism of ultrafine carbon black on mouse primary splenocytes and two digestive enzymes. *Ecotoxicology and Environmental Safety*, *212*. https://doi.org/10.1016/j.ecoenv.2021.111980

Garland, E. F., Hartnell, I. J., & Boche, D. (2022). Microglia and Astrocyte Function and Communication: What Do We Know in Humans? In *Frontiers in Neuroscience* (Vol. 16). Frontiers Media S.A. https://doi.org/10.3389/fnins.2022.824888

Girouard, M. P., Simas, T., Hua, L., Morquette, B., Khazaei, M. R., Unsain, N., Johnstone, A. D., Rambaldi, I., Sanz, R. L., Di Raddo, M. E., Gamage, K. K., Yong, Y., Willis, D. E., Verge, V., Barker, P. A., Deppmann, C., & Fournier, A. E. (2020). Collapsin Response Mediator Protein 4 (CRMP4) Facilitates Wallerian Degeneration and Axon Regeneration following Sciatic Nerve Injury. *eNeuro*, *7*(2), ENEURO.0479-19.2020. https://doi.org/10.1523/ENEURO.0479-19.2020

Gómez-Budia, M., Konttinen, H., Saveleva, L., Korhonen, P., Jalava,P.I., Kanninen, K.M. & Malm,T. (2020). Glial smog: Interplay between air pollution and astrocyte-microglia interactions. *Neurochemistry International*, 136. https://doi.org/10.1016/j.neuint.2020.104715

Guo, J., O'Driscoll, C.M., Holmes, J. D., & Rahme, K. (2016).Bioconjugated gold nanoparticles enhance cellular uptake: a proof of concept study for siRNA delivery in prostate cancer cells. *International journal of pharmaceutics* , 509 (1-2), 16-27. https://doi.org/10.1016/j.ijpham/.2016.05.027

Haghani, A., Cacciottolo, M., Doty, K. R., D'Agostino, C., Thorwald, M., Safi, N., Levine, M. E., Sioutas, C., Town, T. C., Forman, H. J., Zhang, H., Morgan, T. E., & Finch, C. E. (2020). Mouse brain transcriptome responses to inhaled nanoparticulate matter differed by sex and *APOE* in *Nrf2-Nfkb* interactions. *eLife*, *9*, e54822. https://doi.org/10.7554/eLife.54822

Haghani, A., Dalton, H. M., Safi, N., Shirmohammadi, F., Sioutas, C., Morgan, T. E., Finch, C. E., & Curran, S. P. (2019). Air Pollution Alters Caenorhabditis elegans Development and Lifespan: Responses to Traffic-Related Nanoparticulate Matter. *The journals of gerontology. Series A, Biological sciences and medical sciences*, *74*(8), 1189–1197. https://doi.org/10.1093/gerona/glz063

Hama, T., Kushima, Y., Miyamoto, M., Kubota, M., Takei, N., & Hatanaka, H. (1991). Interleukin-6 improves the survival of mesencephalic catecholaminergic and septal cholinergic neurons from postnatal, two-week-old rats in cultures. *Neuroscience*, *40*(2), 445–452. https://doi.org/10.1016/0306-4522(91)90132-8

Hamanaka, R. B. & Mutlu, G.M. (2018). Particulate Matter Air Pollution: Effects on the Cardiovascular System. *Frontiers in Endocrinology*, 9, 680. https://doi.org/10.3389/fendo.2018.00680

Hameren, G., Campbell, G., Deck, M., Berthelot, J., Gautier, B., Quintana, P.,Chrast, R. & Tricaud, N. (2019). In vivo real-time dynamics of ATP and ROS production in axonal mitochondria show decoupling in mouse models of peripheral neuropathies. *Acta Neuropathologica Communications*, 7 (86). https://doi.org/10.1186/s40478-019-0740-4

Hanmei, L., Yao, W., Tang, Q., Yin, D., Tang, C., He, E., Zou, L., Peng, Q. (2021). The protein corona and its effects on nanoparticle-based drug delivery systems, *Acta Biomaterialia,*129, 57-72, https://www.sciencedirect.com/science/article/pii/S1742706121003299

Harry, G. J., & Kraft, A. D. (2012). Microglia in the developing brain: a potential target with lifetime effects. *Neurotoxicology*, 33(2), 191–206. https://doi.org/10.1016/j.neuro.2012.01.012

Heinrich, U., Fuhst, R., Rittinghausen, S., Creutzenberg, O., Bellmann, B., Koch W., & Levsen , K.. (1995). Chronic Inhalation Exposure of Wistar Rats and two Different Strains of Mice to Diesel Engine Exhaust, Carbon Black, and Titanium Dioxide, *Inhalation Toxicology*, 7:4, 533-556, https://www.tandfonline.com/doi/abs/10.3109/08958379509015211

Hofman, J., Staelens, J., Cordell, R., Stroobants, C., Zikova, N., Hama, S.M.L., Wyche, K.P., Kos, G.P.A., Van Der Zee, S., Smallbone, K.L., Weijers, E.P., Monks, P.S. & Roekens, E. (2016). Ultrafine particles in four European urban environments: Results from a new continuous long-term monitoring network, *Atmospheric Environment*, 136, 68-81. Ultrafine particles in four European urban environments: Results from a new continuous long-term monitoring network - ScienceDirect

Hyunyoung, K., Won-Ho, K., Young-Youl ,K. & Hyun-Young, P., (2020). Air Pollution and Central Nervous System Disease: A Review of the Impact of Fine Particulate Matter on Neurological Disorders. *Frontiers in Public Heath*, 8. https://doi.org/10.3389/fpubh.2020.575330

Jang, S., Kim, E. W., Zhang, Y., Lee, J., Cho, S. Y., Ha, J., Kim, H., & Kim, E. (2018). Particulate matter increases beta-amyloid and activated glial cells in hippocampal tissues of transgenic Alzheimer's mouse: Involvement of PARP-1. *Biochemical and biophysical research communications*, 500(2), 333–338. https://doi.org/10.1016/j.bbrc.2018.04.068

Jayaraj, R.L., Rodriguez, E.A., Wang, Y. & Block, M.L. (2017). Outdoor Ambient Air Pollution and Neurodegenerative Diseases: the Neuroinflammation Hypothesis. *Current Environmental Health Reports 4*, 166–179. https://doi-org.ezproxy.napier.ac.uk/10.1007/s40572-017-0142-3

John, G. R., Lee, S. C., & Brosnan, C. F. (2003). Cytokines: powerful regulators of glial cell activation. *The Neuroscientist : a review journal bringing neurobiology, neurology and psychiatry*, *9*(1), 10–22. https://doi.org/10.1177/1073858402239587

Jurga, A. M., Paleczna, M., Kadluczka, J., & Kuter, K. Z. (2021). Beyond the GFAP-Astrocyte Protein Markers in the Brain. *Biomolecules*, *11*(9), 1361. https://doi.org/10.3390/biom11091361

Jung, C. R., Lin, Y. T., & Hwang, B. F. (2015). Ozone, particulate matter, and newly diagnosed Alzheimer's disease: a population-based cohort study in Taiwan. *Journal of Alzheimer's disease : JAD*, 44(2), 573–584. https://doi.org/10.3233/JAD-140855

Kilian, J., & Kitazawa, M. (2018). The emerging risk of exposure to air pollution on cognitive decline and Alzheimer's disease - Evidence from epidemiological and animal studies. *Biomedical journal*, 41(3), 141–162. https://doi.org/10.1016/j.bj.2018.06.001

Kim, D., Chen, Z., Zhou, L. F., & Huang, S. X. (2018). Air pollutants and early origins of respiratory diseases. *Chronic diseases and translational medicine*, *4*(2), 75–94. https://doi.org/10.1016/j.cdtm.2018.03.003

Kim, H., Leng, K., Park, J., Sorets, A. G., Kim, S., Shostak, A., Sturgeon, S. M., Neal, E. H., McMahon, D. G., Schrag, M. S., Kampmann, M., Lippmann, E. S., Zuckerberg Biohub, C., Lippmann, E., & Professor, A. (n.d.). *Reactive astrocytes transduce blood-brain barrier dysfunction through a TNFα-STAT3 signaling axis and secretion of alpha 1-antichymotrypsin*. https://doi.org/10.1101/2022.02.21.481336

King, A., Szekely, B., Calapkulu, E., Ali, H., Rios, F., Jones, S., & Troakes, C. (2020). The Increased Densities, But Different Distributions, of Both C3 and S100A10 Immunopositive Astrocyte-Like Cells in Alzheimer's Disease Brains Suggest Possible Roles for Both A1 and A2 Astrocytes in the Disease Pathogenesis. *Brain sciences*, *10*(8), 503. https://doi.org/10.3390/brainsci10080503

Konduru, N. v., MJurgaolina, R. M., Swami, A., Damiani, F., Pyrgiotakis, G., Lin, P., Andreozzi, P., Donaghey, T. C., Demokritou, P., Krol, S., Kreyling, W., &

Brain, J. D. (2017). Protein corona: Implications for nanoparticle interactions with pulmonary cells. *Particle and Fibre Toxicology*, *14*(1). https://doi.org/10.1186/s12989-017-0223-3

Krasovska, V., & Doering, L. C. (2018). Regulation of IL-6 secretion by astrocytes via TLR4 in the fragile X mouse model. *Frontiers in Molecular Neuroscience*, *11*. https://doi.org/10.3389/fnmol.2018.00272

Kreth, S., Heyn, J., Grau, S., Kretzschmar, H. A., Egensperger, R., & Kreth, F. W. (2010). Identification of valid endogenous control genes for determining gene expression in human glioma. *Neuro-oncology*, *12*(6), 570–579. https://doi.org/10.1093/neuonc/nop072

Kwon, H. S., Ryu, M. H., & Carlsten, C. (2020). Ultrafine particles: unique physicochemical properties relevant to health and disease. In *Experimental and Molecular Medicine* (Vol. 52, Issue 3, pp. 318–328). Springer Nature. https://doi.org/10.1038/s12276-020-0405-1

Lee, S., Jha, M. K., & Suk, K. (2015). Lipocalin-2 in the Inflammatory Activation of Brain Astrocytes. *Critical reviews in immunology*, *35*(1), 77–84. https://doi.org/10.1615/critrevimmunol.2015012127

Lee, Y. K., Choi, E. J., Webster, T. J., Kim, S. H., & Khang, D. (2014). Effect of the protein corona on nanoparticles for modulating cytotoxicity and immunotoxicity. In *International Journal of Nanomedicine* (Vol. 10, pp. 97–113). Dove Medical Press Ltd. https://doi.org/10.2147/IJN.S72998

Leni, Z., Kunzi, L., Geiser, M. (2020). Air pollution causing oxidative stress. Current Opinion in Toxicology (Vol. 20-21, pp. 1-8). https://doi.org/10.1016/j.cotox.2020.02.006

Li, T., Chen, X., Zhang, C., Zhang, Y., & Yao, W. (2019). An update on reactive astrocytes in chronic pain. In *Journal of Neuroinflammation* (Vol. 16, Issue 1). BioMed Central Ltd. https://doi.org/10.1186/s12974-019-1524-2

Li, K., Li, J., Zheng, J., & Qin, S. (2019). Reactive Astrocytes in Neurodegenerative Diseases. *Aging and disease*, 10(3), 664–675. https://doi.org/10.14336/AD.2018.0720

Li, L., Li, Y., He, B., Li, H., Ji, H., Wang, Y., Zhu, Z., Hu, Y., Zhou, Y., Yang, T., Sun, C., Yuan, Y., & Wang, Y. (2021). HSF1 is involved in suppressing A1 phenotype conversion of astrocytes following spinal cord injury in rats. *Journal of Neuroinflammation*, *18*(1). https://doi.org/10.1186/s12974-021-02271-3

Li, T., Zhao, J., Ge, J., Yang, J., Song, X., Wang, C., Mao, J., Zhang, Y., Zou, Y., Liu, Y., & Chen, G. (2016). Particulate Matter Facilitates C6 Glioma Cells Activation and the Release of Inflammatory Factors Through MAPK and JAK2/STAT3 Pathways. *Neurochemical research*, 41(8), 1969–1981. https://doi.org/10.1007/s11064-016-1908-y

Liddelow, S. A. & Barres, B. A. (2017). Reactive Astrocytes: Production, Function, and Therapeutic Potential. *Immunity*, 46(6), 957–967. https://doi.org/10.1016/j.immuni.2017.06.006

Liddelow, S.h., Guttenplan, K.A., Clarke, L.E., Bennett, F.C., Bohlen, C., Schirmer, L., Bennett, M., Münch, A., Chung, W.S., Peterson, T.C., Wilton, .K., Frouin, A., Napier, B.A., Panicker, N., Kumar, M., Buckwalter,M.S., Rowitch, D.H., Dawson, V., Dawson, T., StevenS, B. & Barres, B. (2017). Neurotoxic reactive astrocytes are induced by activated microglia. *Nature,*541, 481–487. https://doi.org/10.1038/nature21029

Lima, T., Bernfur, L., Vilanova, M et al. Understanding the Lipid and protein corona formation on different sized polymeric nanoparticles. Sci Rep 10, 1129 (2020). https://doi.org/10.1038/s41598-020-57943-6

Livingston, G., Huntley, J., Sommerlad, A., Ames, D., Ballard, C., Banerjee, S. et al. (2020). Dementia prevention, intervention, and care: 2020 report of the Lancet Commission. *THE LANCET COMMISSIONS,* 396 (10248), 413-446. https://doi.org/10.1016/S0140-6736(20)30367-6

Liu, C. C., Liu, C. C., Kanekiyo, T., Xu, H., & Bu, G. (2013). Apolipoprotein E and Alzheimer disease: risk, mechanisms and therapy. *Nature reviews. Neurology*, *9*(2), 106–118. https://doi.org/10.1038/nrneurol.2012.263

MacNee, W., & Rahman, I. (2001). Is oxidative stress central to the pathogenesis of chronic obstructive pulmonary disease? *Trends in molecular medicine, 7 2*, 55-62 .

Malm, A. v., & Corbett, J. C. W. (2019). Improved Dynamic Light Scattering using an adaptive and statistically driven time resolved treatment of correlation data. *Scientific Reports*, *9*(1). https://doi.org/10.1038/s41598-019-50077-4

Matias, I., Morgado, J. & Carvalho Alcantara Gomes, F. (2019). Astrocyte Heterogeneity: Impact to Brain Aging and Disease. *Frontiers in Aging Neuroscience* , 11. https://doi.org/10.3389/fnagi.2019.00059

Martín-Aragón Baudel MAS, Rae MT, Darlison MG, Poole AV, Fraser JA (2017) Preferential activation of HIF-2α adaptive signalling in neuronal-like cells in response to acute hypoxia. *PLoS ONE* 12(10): e0185664. https://doi.org/10.1371/journal.pone.0185664

Martinez, F. O., & Gordon, S. (2014). The M1 and M2 paradigm of macrophage activation: Time for reassessment. *F1000Prime Reports*, *6*. https://doi.org/10.12703/P6-13

Matejuk, A., & Ransohoff, R. M. (2020). Crosstalk Between Astrocytes and Microglia: An Overview. In *Frontiers in Immunology* (Vol. 11). Frontiers Media S.A. https://doi.org/10.3389/fimmu.2020.01416

Miao, Q., Ge, M., & Huang, L. (2017). Up-regulation of GBP2 is Associated with Neuronal Apoptosis in Rat Brain Cortex Following Traumatic Brain Injury. *Neurochemical research*, *42*(5), 1515–1523. https://doi.org/10.1007/s11064-017-2208-x

Monteiller, C., Tran, L., MacNee, W., Faux, S., Jones, A., Miller, B., & Donaldson, K. (2007). The pro-inflammatory effects of low-toxicity low-solubility particles, nanoparticles and fine particles, on epithelial cells in vitro: the role of surface area. Occupational and environmental medicine, 64(9), 609– 615. https://doi.org/10.1136/oem.2005.024802

Monteiro-Riviere, N. A., Inman, A. O., & Zhang, L. W. (2009). Limitations and relative utility of screening assays to assess engineered nanoparticle toxicity in a human cell line. Toxicology and applied pharmacology, 234(2), 222–235. https://doi.org/10.1016/j.taap.2008.09.030

Mosser, D. M. (2003). The many faces of macrophage activation. *Journal of Leukocyte Biology*, *73*(2), 209–212. https://doi.org/10.1189/jlb.0602325

Morgan, T. E., Davis, D. A., Iwata, N., Tanner, J. A., Snyder, D., Ning, Z., Kam, W., Hsu, Y. T., Winkler, J. W., Chen, J. C., Petasis, N. A., Baudry, M., Sioutas, C., & Finch, C. E. (2011). Glutamatergic neurons in rodent models respond to nanoscale particulate urban air pollutants in vivo and in vitro. *Environmental health perspectives*, *119*(7), 1003–1009. https://doi.org/10.1289/ehp.1002973

Morris, R. H., Counsell, S. J., McGonnell, I. M., & Thornton, C. (2021). Early life exposure to air pollution impacts neuronal and glial cell function leading to impaired neurodevelopment. *BioEssays.* 43, e2000288. https://doi.org/10.1002/bies.202000288

Mueller, O., Lightfoot, S., & Schroeder, A. (n.d.). *RNA Integrity Number (RIN)-Standardization of RNA Quality Control Application*. https://www.agilent.com/cs/library/applications/5989-1165EN.pdf

Nazet, U., Schröder, A., Grässel, S., Muschter, D., Proff, P., & Kirschneck, C. (2019). Housekeeping gene validation for RT-qPCR studies on synovial fibroblasts derived from healthy and osteoarthritic patients with focus on mechanical loading. *PloS one*, *14*(12), e0225790. https://doi.org/10.1371/journal.pone.0225790

Onoda, A., Takeda, K., & Umezawa, M. (2017a). Dose-dependent induction of astrocyte activation and reactive astrogliosis in mouse brain following maternal exposure to carbon black nanoparticle. *Particle and fibre toxicology*, *14*(1), 4. https://doi.org/10.1186/s12989-017-0184-6

Onoda, A., Takeda, K., & Umezawa, M. (2017). Pretreatment with N-acetyl cysteine suppresses chronic reactive astrogliosis following maternal nanoparticle exposure during gestational period. *Nanotoxicology,* 11(8), 1012–1025. https://doi.org/10.1080/17435390.2017.1388864

Onoda, A., Umezawa, M., Takeda, K., Ihara, T., & Sugamata, M. (2014). Effects of maternal exposure to ultrafine carbon black on brain perivascular macrophages and surrounding astrocytes in offspring mice. *PloS one*, 9(4), e94336. https://doi.org/10.1371/journal.pone.0094336

Oudin, A., Forsberg, B., Adolfsson, A. N., Lind, N., Modig, L., Nordin, M., Nordin, S., Adolfsson, R., & Nilsson, L. G. (2016). Traffic-Related Air Pollution and Dementia Incidence in Northern Sweden: A Longitudinal Study.

Environmental health perspectives, 124(3), 306–312. https://doi.org/10.1289/ehp.1408322

Patel, A. B., Shaikh, S., Jain, K. R., Desai, C., & Madamwar, D. (2020). Polycyclic Aromatic Hydrocarbons: Sources, Toxicity, and Remediation Approaches. *Frontiers in microbiology*, 11, 562813. https://doi.org/10.3389/fmicb.2020.562813

Perea, G., Navarrete, M., & Araque, A. (2009). Tripartite synapses: astrocytes process and control synaptic information. *Trends in neurosciences*, *32*(8), 421–431. https://doi.org/10.1016/j.tins.2009.05.001

Persidsky, Y., Ramirez, S. H., Haorah, J., & Kanmogne, G. D. (2006). Blood-brain barrier: structural components and function under physiologic and pathologic conditions. *Journal of neuroimmune pharmacology: the official journal of the Society on NeuroImmune Pharmacology*, 1(3), 223–236. https://doi.org/10.1007/s1148bi1-006-9025-3

Peters, R., Ee, N., Peters, J., Booth, A., Mudway, I., & Anstey, K. J. (2019). Air Pollution and Dementia: A Systematic Review. *Journal of Alzheimer's disease: JAD*, 70(s1), S145–S163. https://doi.org/10.3233/JAD-180631

Pirlea, F. & Ven-dee Huang, W. -The World Bank (2019). *The global distribution of air pollution.* The World Bank. https://datatopics.worldbank.org/world-development-indicators/stories/the-global-distribution-of-air-pollution.html

Pleasure, S. J., Page, C., & Lee, V. M. (1992). Pure, postmitotic, polarized human neurons derived from NTera 2 cells provide a system for expressing exogenous proteins in terminally differentiated neurons. *The Journal of neuroscience : the official journal of the Society for Neuroscience*, *12*(5), 1802–1815. https://doi.org/10.1523/JNEUROSCI.12-05-01802.1992

Querol, X., Tobías, A., Pérez, N., Karanasiou, A., Amato, F., Stafoggia, M., Pérez García-Pando, C., Ginoux, P., Forastiere, F., Gumy, S., Mudu, P. & Alastuey, A. (2019). Monitoring the impact of desert dust outbreaks for air quality for health studies,*Environment International,* V 130, 104867. https://www.sciencedirect.com/science/article/pii/S016041201930604X

Ransom, B. R. (2012). *Neuroglia* (3rd edition). United States: Oxford University Press.

https://books.google.co.uk/books?hl=en&lr=&id=y40NAwAAQBAJ&oi=fnd&pg=PA35&ots=VFn6G8lbUz&sig=FjEF6yIazN7MOB75EFkiEA-

Ratcliffe, L. E., Vázquez Villaseñor, I., Jennings, L., Heath, P. R., Mortiboys, H., Schwartzentruber, A., Karyka, E., Simpson, J. E., Ince, P. G., Garwood, C. J., & Wharton, S. B. (2018). Loss of IGF1R in Human Astrocytes Alters Complex I Activity and Support for Neurons. *Neuroscience*, *390*, 46–59. https://doi.org/10.1016/j.neuroscience.2018.07.029

Rhea, E. M. & Banks, W.A. (2019). Role of the Blood-Brain Barrier in Central Nervous System Insulin Resistance. *Frontiers in Neuroscience* , 13. https://doi.org/10.3389/fnins.2019.00521

Ritchie, H. & Roser, M (2013). Indoor Air Pollution. *OurWorldInData.org.* https://ourworldindata.org/indoor-air-pollution

Ritchie, H. & Roser, M. (2017). Air Pollution. *OurWorldInData.org.* https://ourworldindata.org/air-pollution#citation

Ritchie, H. & Roser, M. (2017a). Outdoor Air Pollution. *OurWorldInData.org.* https://ourworldindata.org/outdoor-air-pollution?country

Roser, M (2021). Data Review: How many people die from air pollution? *OurWorldInData.org. https://ourworldindata.org/data-review-air-pollution-deaths#the-pollutant-that-is-responsible-for-most-air-pollution-deaths-is-particulate-matter*

Roqué, P.J., Dao, K. & Costa, L.G. (2016). Microglia mediate diesel exhaust particle-induced cerebellar neuronal toxicity through neuroinflammatory mechanisms. *NeuroToxicology.* 56,204-214. https://www.sciencedirect.com/science/article/abs/pii/S0013935121002036

Rui, Z., Xun, Z., Sichen, G. & Rutao L. (2019). Assessing the in vitro and in vivo toxicity of ultrafine carbon black to mouse liver, *Science of The Total Environment,* 655, 1334-1341. Assessing the in vitro and in vivo toxicity of ultrafine carbon black to mouse liver - ScienceDirect

Schraufnagel, D.E. (2020). The health effects of ultrafine particles. *Experimental & Molecular Medicine*, 52, 311–317. https://doi.org/10.1038/s12276-020-0403-3

Simpson, J. E., Ince, P. G., Lace, G., Forster, G., Shaw, P. J., Matthews, F., Savva, G., Brayne, C., Wharton, S. B., & MRC Cognitive Function and Ageing Neuropathology Study Group (2010). Astrocyte phenotype in relation to Alzheimer-type pathology in the ageing brain. *Neurobiology of aging*, *31*(4), 578–590. https://doi.org/10.1016/j.neurobiolaging.2008.05.015

Shin, S. W., Song, I. H., & Um, S. H. (2015). Role of physicochemical properties in nanoparticle toxicity. In *Nanomaterials* (Vol. 5, Issue 3, pp. 1351–1365). MDPI AG. https://doi.org/10.3390/nano5031351

Sofroniew M. V. (2009). Molecular dissection of reactive astrogliosis and glial scar formation. *Trends in neurosciences*, *32*(12), 638–647. https://doi.org/10.1016/j.tins.2009.08.002

Sofroniew, M. (2020). Astrocyte Reactivity: Subtypes, States, and Functions in CNS Innate Immunity. *Trends in Immunology*, 41(9), 758-770. https://doi.org/10.1016/j.it.2020.07.004

Sei, K., Wang,Q., Tokumura,M., Hossain, A., Raknuzzaman,M., Miyake,Y. & Amagai,T. (2021). Occurrence, potential source, and cancer risk of PM2.5-bound polycyclic aromatic hydrocarbons and their halogenated derivatives in Shizuoka, Japan, and Dhaka, Bangladesh. *Environmental Research,* V.196, 110909. *https://www.sciencedirect.com/science/article/abs/pii/S0013935121002036*

Sichen, G., Tong, L., Jie, P., Dengcheng, H., Jing, L., Qigui, N. and Rutao, L. (2021). Toxic effect and mechanism of ultrafine carbon black on mouse primary splenocytes and two digestive enzymes. Ecotoxicology and Environmental Safety, 212, - 111980. https://www.sciencedirect.com/science/article/pii/S0147651321000919

Stoeger, T., Reinhard, C., Takenaka, S., Schroeppel, A., Karg, E., Ritter, B., Heyder, J., & Schulz, H. (2006). Instillation of six different ultrafine carbon particles indicates a surface area threshold dose for acute lung inflammation in mice. *Environmental Health Perspectives*, *114*(3), 328–333. https://doi.org/10.1289/ehp.8266

Stone, V., Johnston, H., & Clift, M. J. (2007). Air pollution, ultrafine and nanoparticle toxicology: cellular and molecular interactions. *IEEE transactions on nanobioscience*, *6*(4), 331–340. https://doi.org/10.1109/tnb.2007.909005

Suglia, S. F., Gryparis, A., Wright, R. O., Schwartz, J., & Wright, R. J. (2008). Association of black carbon with cognition among children in a prospective birth cohort study. *American journal of epidemiology,* 167(3), 280–286. https://doi.org/10.1093/aje/kwm308

Szpakowski, P., Ksiazek-Winiarek, D., Turniak-Kusy, M., Pacan, I., & Glabinski, A. (2022). Human Primary Astrocytes Differently Respond to Pro- and Anti-Inflammatory Stimuli. *Biomedicines*, *10*(8), 1769. https://doi.org/10.3390/biomedicines10081769

Takenaka, S., Karg, E., Möller, W., Roth, C., Ziesenis, A., Heinzmann, U., Schramel, P., & Heyder, J. (2000). A Morphologic Study on the Fate of Ultrafine Silver Particles: Distribution Pattern of Phagocytized Metallic Silver in Vitro and in Vivo. *Inhalation toxicology*, *12 Suppl 3*, 291–299. https://doi.org/10.1080/08958378.2000.11463225

Takenaka, S., Karg, E., Roth, C., Schulz, H., Ziesenis, A., Heinzmann, U., Schramel, P. and Heyder, J. (2001). Pulmonary and systemic distribution of inhaled ultrafine silver particles in rats. *Environmental Heath Perspective*, 109:suppl 4. https://doi.org/10.1289/ehp.01109s4547

Taklimie, F. R., Gasterich, N., Scheld, M., Weiskirchen, R., Beyer, C., Clarner, T., & Zendedel, A. (2019). Hypoxia induces astrocyte-derived lipocalin-2 in ischemic stroke. *International Journal of Molecular Sciences*, *20*(6). https://doi.org/10.3390/ijms20061271

Tamagawa, E., Bai, N., Morimoto, K., Gray, C., Mui, T., Yatera, K., Zhang, X., Xing, L., Li, Y., Laher, I., Sin, D. D., Man, S. F., & van Eeden, S. F. (2008). Particulate matter exposure induces persistent lung inflammation and endothelial dysfunction. *American journal of physiology*, *Lung cellular and molecular physiology*, 295(1), L79–L85. https://doi.org/10.1152/ajplung.00048.2007

Tamaoki, J., Isono, K., Takeyama, K., Tagaya, E., Nakata, J., & Nagai, A. (2004). Ultrafine carbon black particles stimulate proliferation of human airway

epithelium via EGF receptor-mediated signaling pathway. American journal of physiology. Lung cellular and molecular physiology, 287(6), L1127–L1133. https://doi.org/10.1152/ajplung.00241.2004

Tatsumi, K., Isonishi, A., Yamasaki, M., Kawabe, Y., Morita-Takemura, S., Nakahara, K., Terada, Y., Shinjo, T., Okuda, H., Tanaka, T., & Wanaka, A. (2018). Olig2-Lineage Astrocytes: A Distinct Subtype of Astrocytes That Differs from GFAP Astrocytes. *Frontiers in neuroanatomy*, *12*, 8. https://doi.org/10.3389/fnana.2018.00008

Taylor, S. C., Nadeau, K., Abbasi, M., Lachance, C., Nguyen, M., & Fenrich, J. (2019). The Ultimate qPCR Experiment: Producing Publication Quality, Reproducible Data the First Time. *Trends in biotechnology*, *37*(7), 761–774. https://doi.org/10.1016/j.tibtech.2018.12.002

Thompson, K. K., & Tsirka, S. E. (2017). The diverse roles of microglia in the neurodegenerative aspects of central nervous system (CNS) autoimmunity. In *International Journal of Molecular Sciences* (Vol. 18, Issue 3). MDPI AG. https://doi.org/10.3390/ijms18030504

Ting, L., Xuhui, C.,Chuanhan, Z., Yue, Z., & Wenlong Y. (2019). An update on reactive astrocytes in chronic pain. *Journal of Neuroinflammation*, 16 (140). https://doi.org/10.1186/s12974-019-1524-2

Ugalde, C. L., Lewis, V., Stehmann, C., McLean, C. A., Lawson, V. A., Collins, S. J., & Hill, A. F. (2020). Markers of A1 astrocytes stratify to molecular sub-types in sporadic Creutzfeldt–Jakob disease brain. *Brain Communications*, *2*(2). https://doi.org/10.1093/braincomms/fcaa029

United Kingdom Office for Health Improvement & Disparities (2022, February 02). Air pollution: applying All Our Health. Gov.uk. https://www.gov.uk/government/publications/air-pollution-applying-all-our-health/air-pollution-applying-all-our-health#:~:text=In%20the%20UK%2C%20air%20pollution,and%2036%2C000%20deaths%20every%20year

United Kingdom Health Security Agency (2022, July 25). Air pollution: cognitive decline and dementia - A report by the Committee on the Medical Effects of Air

Pollutants (COMEAP). Gov.uk. Air pollution: cognitive decline and dementia - GOV.UK (www.gov.uk)

United States Environmental Protection Agency (EPA) (2021, July 16). Particulate Matter (PM) Pollution - *Particulate Matter (PM) Basics*. https://www.epa.gov/pm-pollution/particulate-matter-pm-basics#PM

Vainchtein, I. D., & Molofsky, A. v. (2020). Astrocytes and Microglia: In Sickness and in Health. In *Trends in Neurosciences* (Vol. 43, Issue 3, pp. 144–154). Elsevier Ltd. https://doi.org/10.1016/j.tins.2020.01.003

Veronesi, B., Makwana, O., Pooler, M., & Chen, L. (2005). Effects of Subchronic Exposures to Concentrated Ambient Particles: VII. Degeneration of Dopaminergic Neurons in Apo E−/− Mice. *Inhalation Toxicology, 17*, 235 - 241. https://www.tandfonline.com/doi/citedby/10.1080/08958370590912888?scroll=top&needAccess=true

Wang, H., Peng, X., Cao, F., Wang, Y., Shi, H., Lin, S., Zhong, W., & Sun, J. (2017). Cardiotoxicity and Mechanism of Particulate Matter 2.5 (PM2.5) Exposure in Offspring Rats During Pregnancy. *Medical science monitor: international medical journal of experimental and clinical research*, 23, 3890–3896. https://doi.org/10.12659/msm.903006

Wang, J., Ma, T., Ma, D., Li, H., Hua, L., He, Q., & Deng, X. (2021). The Impact of Air Pollution on Neurodegenerative Diseases. *Therapeutic drug monitoring*, *43*(1), 69–78. https://doi.org/10.1097/FTD.0000000000000818

Wang, Y., Liu, D., Zhang, H., Wang, Y., Wei, L., Liu, Y., Liao, J., Gao, H. M., & Zhou, H. (2017). Ultrafine carbon particles promote rotenone-induced dopamine neuronal loss through activating microglial NADPH oxidase. *Toxicology and applied pharmacology*, *322*, 51–59. https://doi.org/10.1016/j.taap.2017.03.005

Wichmann H. E. (2007). Diesel exhaust particles. *Inhalation toxicology*, *19 Suppl 1*, 241–244. https://doi.org/10.1080/08958370701498075

Woodward, N. C., Levine, M. C., Haghani, A., Shirmohammadi, F., Saffari, A., Sioutas, C., Morgan, T. E., & Finch, C. E. (2017). Toll-like receptor 4 in glial inflammatory responses to air pollution in vitro and in vivo. *Journal of Neuroinflammation*, *14*(1). https://doi.org/10.1186/s12974-017-0858-x

World Health Organisation (WHO). (2021). *Air pollution.* https://www.who.int/data/gho/data/themes/theme-details/GHO/air-pollution

World Heath Organisation (Who). (2021ad). *Ambient (outdoor) Air Pollution.* https://www.who.int/news-room/fact-sheets/detail/ambient-(outdoor)-air-quality-and-health

Xu, H., Wang, Z., Li, J., Wu, H., Peng, Y., Fan, L., Chen, J., Gu, C., Yan, F., Wang, L., & Chen, G. (2017). The polarization states of microglia in TBI: A new paradigm for pharmacological intervention. In *Neural Plasticity* (Vol. 2017). Hindawi Limited. https://doi.org/10.1155/2017/5405104

Xu J. (2018). New Insights into GFAP Negative Astrocytes in Calbindin D28k Immunoreactive Astrocytes. *Brain sciences*, *8*(8), 143. https://doi.org/10.3390/brainsci8080143

Xu, M. X., Zhu, Y. F., Chang, H. F., & Liang, Y. (2016). Nanoceria restrains PM2.5-induced metabolic disorder and hypothalamus inflammation by inhibition of astrocytes activation related NF-κB pathway in Nrf2 deficient mice. *Free radical biology & medicine*, 99, 259–272. https://doi.org/10.1016/j.freeradbiomed.2016.08.021

Yang, P., Wen, H., Ou, S., Cui, J., & Fan, D. (2012). IL-6 promotes regeneration and functional recovery after cortical spinal tract injury by reactivating intrinsic growth program of neurons and enhancing synapse formation. *Experimental neurology*, *236*(1), 19–27. https://doi.org/10.1016/j.expneurol.2012.03.019

Yin, J. C., Zhang, L., Ma, N. X., Wang, Y., Lee, G., Hou, X. Y., Lei, Z. F., Zhang, F. Y., Dong, F. P., Wu, G. Y., & Chen, G. (2019). Chemical Conversion of Human Fetal Astrocytes into Neurons through Modulation of Multiple Signaling Pathways. *Stem cell reports*, *12*(3), 488–501. https://doi.org/10.1016/j.stemcr.2019.01.003

You, R., Ho, Y. S., & Chang, R. C. C. (2022). The pathogenic effects of particulate matter on neurodegeneration: a review. In *Journal of Biomedical Science* (Vol. 29, Issue 1). BioMed Central Ltd. https://doi.org/10.1186/s12929-022-00799-x

Zhang, R., Zhang, X., Gao, S., & Liu, R. (2019). Assessing the in vitro and in vivo toxicity of ultrafine carbon black to mouse liver. The Science of the total environment, 655, 1334–1341. https://doi.org/10.1016/j.scitotenv.2018.11.295

Zhao, J., Bi, W., Xiao, S., Lan, X., Cheng, X., Zhang, J., Lu, D., Wei, W., Wang, Y., Li, H., Fu, Y., & Zhu, L. (2019). Neuroinflammation induced by lipopolysaccharide causes cognitive impairment in mice. *Scientific Reports*, *9*(1). https://doi.org/10.1038/s41598-019-42286-8

Zhou, T., Huang, Z., Sun, X., Zhu, X., Zhou, L., Li, M., Cheng, B., Liu, X., & He, C. (2017). Microglia polarization with M1/M2 phenotype changes in rd1 mouse model of retinal degeneration. *Frontiers in Neuroanatomy*, *11*. https://doi.org/10.3389/fnana.2017.00077

Zhou, Y., Shao, A., Yao, Y., Tu, S., Deng, Y., & Zhang, J. (2020). Dual roles of astrocytes in plasticity and reconstruction after traumatic brain injury. *Cell communication and signaling : CCS*, *18*(1), 62. https://doi.org/10.1186/s12964-020-00549-2

8. Appendices

8.1 Appendix A

Representative Melt curve Analysis

Melt curve analysis for each primer of untreated sample 0 showing +RT, -RT and Not Template Control (NTC; all indicated on each graph).

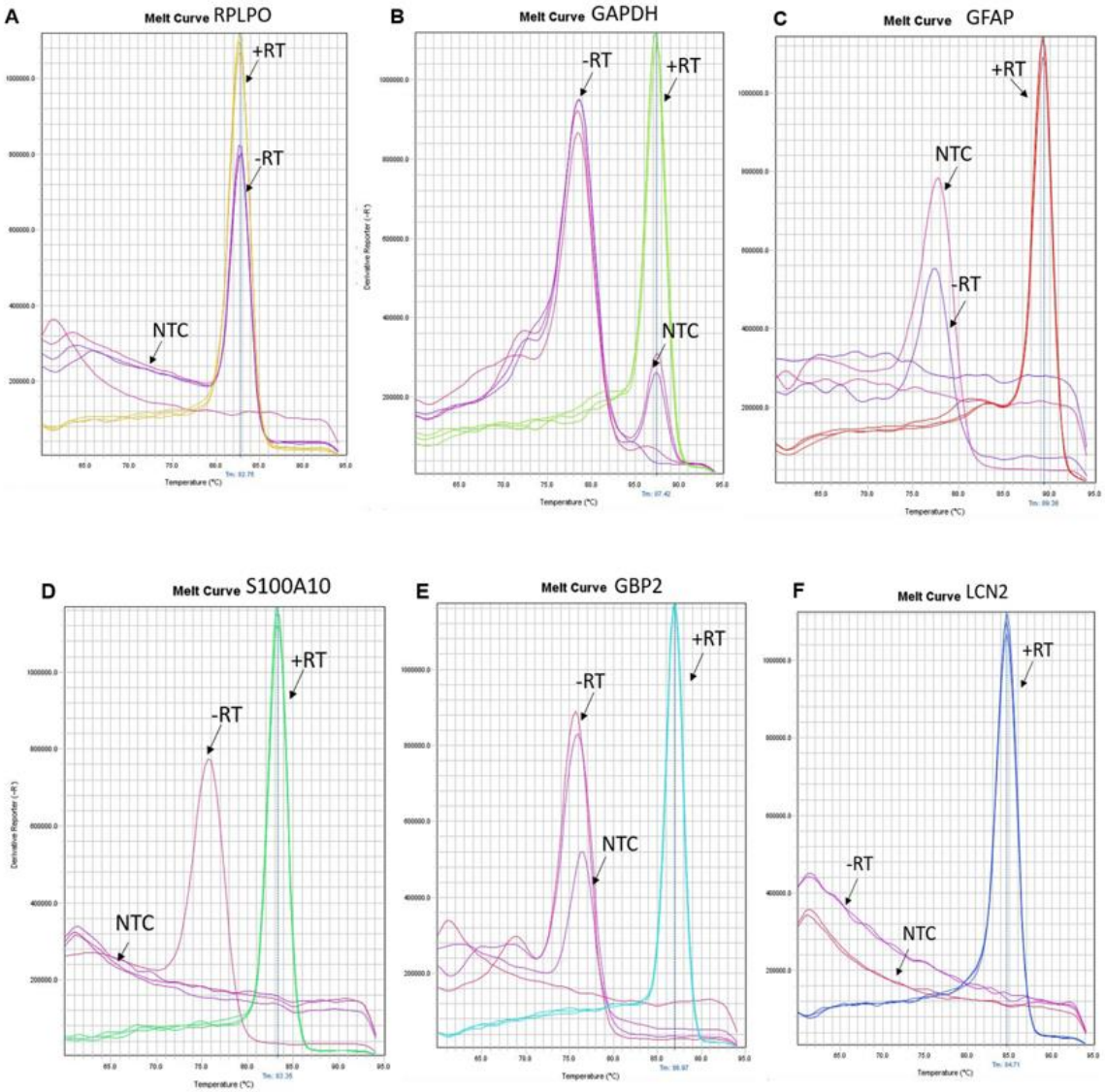

Figure 8.1. Melt Curves for RPLPO Primer set (A), GAPDH Primer set (B), GFAP primer set (C), S100A10 primer set (D), GBP2 primer set (E) and LCN2 primer set (F), all showing +RT (Untreated cDNA), -RT and NTC.

To verify whether or not -RT of RPLPO was also amplified, the **amplification plot (below in Figure 8.2)** was also reported, showing clearly that +RT and -RT were amplified at different Ct cycles.

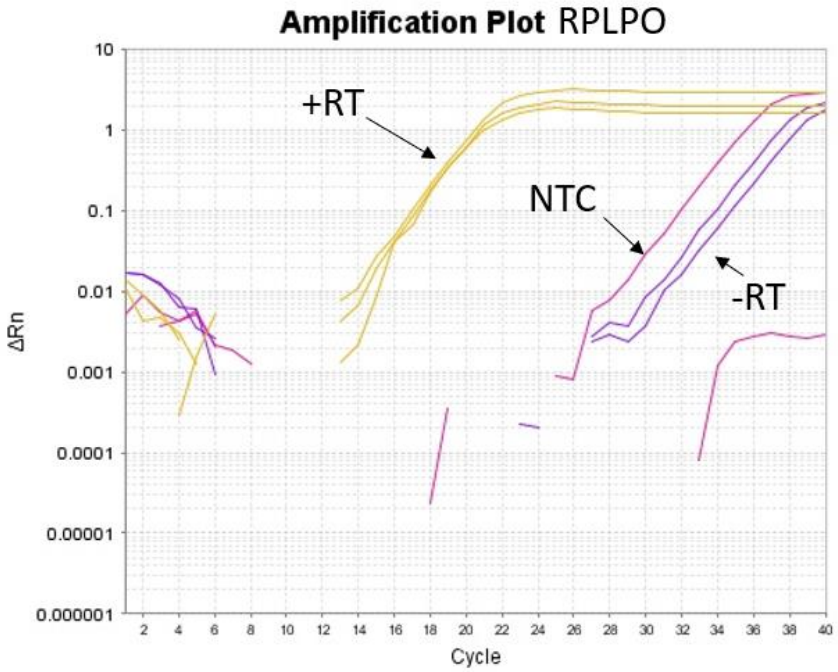

Figure 8.2. RPLPO amplification plot related to Melt Curve in 8.1. As it possible to see, the +RT and -RT registered different Ct cycles (as the NTC).

8.2 Appendix B

Polydispersity Indices for Zetasizer Measurements

Table 8.1. Polydispersity Index (PDI) for 100 µg/ml of UFCB in Astrocytes Media, dH20 and 10% FBS registered at time: immediately, 30 minutes, 2 hrs, 4 hrs and 24 hrs post sonication.

PDI	**100 µg/ml UFCB A. Media**			**100 µg/ml UFCB dH20**			**100 µg/ml UFCB 10% FBS**		
	N=1	N=2	N=3	N=1	N=2	N=3	N=1	N=2	N=3
Immediate	0.746	0.407	0.255	0.271	0.836	0.265	0.578	0.268	0.630
30 minutes	0.805	0.225	0.216	0.222	0.579	0.236	0.416	0.390	0.569
2 hrs	0.592	0.330	0.161	0.271	0.292	0.212	0.451	0.607	0.895
4 hrs	0.517	0.354	0.187	0.389	0.225	0.279	0.414	0.605	0.553
24 hrs	0.436	0.253	0.219	0.375	0.322	0.275	0.405	0.747	0.593

8.3 Appendix C

All pairwise comparison table from figure 3.3.

Table 8.2. All pairwise comparison for Two Way Anova from figure 3.3 “Optimisation of human cortical astrocyte density and wash steps for WST-1 cell viability assays”.

Graph/ Experiment	**P values**		
	Interaction	**Time of incubation**	**Cell density**
A – all three densities* compared	>0.9999	0.0039**	0.0725
			Washed vs Not Washed
B - 6.25 x 10^4 cells per cm^2	>0.9999	0.1443	0.7886
C - 3.12 x 10^4 cells per cm^2	0.9994	0.0491**	0.1244
D - 1.56 x 10^4 cells per cm^2	>0.9999	< 0.0001**	0.6867

*the three densities are: 6.25 x 10^4 cells per cm^2 , 3.12 x 10^4 cells per cm^2 and 1.56 x 10^4 cells per cm^2 .

** = significance

8.4 Appendix D

GBP2 and LCN2 standard curve trials plots.

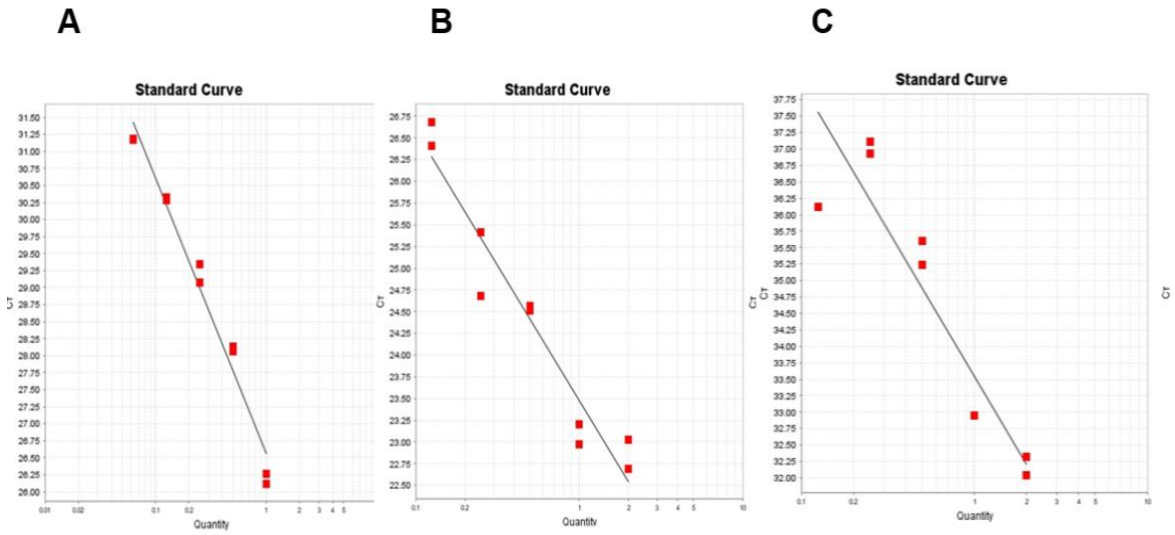

Figure 8.3. Standard Curves for primers GBP2 (A, second trial and B, third trial) and LCN2 (C, second trial) showing the relationship between threshold (Ct) and log copy number of the target genes. In the above graphs, 1:2 serial dilutions of neat cDNA, whereby each point represents each of the standards. All primers concentrations were kept constant at 200 nM for both Forward and Reverse oligos. The standard curve settings started from 80 ng/µl. The cDNA used for the curves was from untreated control cells. Each point was done in duplicate. **Note that A-B refers to GBP2 standard curve other two trials which did not worked, and C is the second LCN2 stand curve trial, which also did not work.** Efficiency/ R2 values are reported below in table 8.3.

Table 8.3 Efficiency values and correlation coefficients (R^2) for the primer set tested with standard curves.

GOI	**Efficiency values**	**R^2**
GBP2 trial 2 - A	76.7	0.97
GBP2 trial 3 - B	110	0.93
LCN2 trial 2 - C	95	0.95